Technical University of Denmark

DTU

Microfluidic devices for investigation of biomimetic membranes for sensor and separation applications

Pszon-Bartosz, Kamila Justyna; Emnéus, Jenny; Geschke, Oliver; Hélix-Nielsen, Claus

[Link back to DTU Orbit](#)

DTU Library
Technical Information Center of Denmark

Microfluidic devices for investigation of biomimetic membranes for sensor and separation applications

Kamila Pszon-Bartosz
PhD thesis

Supervisors
Professor Jenny Emnéus, DTU Nanotech 2010-2011
Associate Professor Oliver Geschke, DTU Nanotech 2008-2010
Associate Professor Claus Hélix-Nielsen, DTU Physics and CSO at Aquaporin A/S

Contents

Abstract

The term biomimetic membrane denotes membrane that mimics biological cell membrane. Artificially made membranes are powerful tools for the fundamental biophysical studies of membrane proteins. Moreover, they may be used in biomedicine, serving as biosensors in high-throughput screening of potential drug candidates and in separation technologies, where an exciting example is water purification device based on biomimetic membranes containing aquaporins (highly water selective proteins). However, there are many challenges that must be overcome in order to build biomimetic membrane-based devices for industrial applications. Among them are the inherent fragility of lipid membranes, the challenge of up-scaling the effective membrane area and the quantification of the protein delivery to the lipid membrane which may determined the biomimetic membrane application. This PhD thesis addresses the above mentioned difficulties. First, a device that facilitates atomic force microscopy (AFM) measurements of biomimetic membranes is presented. The microfluidic device was specifically designed and fabricated to accommodate the AFM probes that were used to study micrometer-sized fluid polymeric membranes. Second, membrane arrays stability was increased by two ways; surface modification of support partitions and by involving fully closed and automated microfluidic device. The surface was covalently modified by plasma resulting in a hydrophobic coating and thus greatly improved the average membrane array lifetimes (up to 6 days) with a bilayer membrane area ~50% of the available aperture area. Highly stable membranes (up to 2 days) with a bilayer membrane area ~24% of the available aperture area were created in the developed microfluidic device. Further, reconstitution of α-hemolysin (α-HL) membrane proteins in the biomimetic membranes was performed. Third, an outer membrane porin (OMP) fusion efficacy assay was established and used to quantify protein delivery to an array of planar membranes. Incorporation was established as a process with either first order or exponential kinetics. This may be of interest to microfluidic designs involving protein delivery to biomimetic membranes developed for sensor and separation applications. Finally, an OMP functionality modulation with β-cyclodextrin (β-CD) was shown and revealed the protein potential application as a sensor. Moreover, the β-CD blocker may be used to prevent human dental plaque formation and the development of periodontitis.

Resumé

Termen biomimetisk membran betegner en membran, der imiterer en biologisk cellemembran. Kunstigt skabte membraner er stærke redskaber i fundamentale biofysiske studier af membranproteiner. Desuden finder de anvendelse i biomedicin, hvor de tjener som biosensorer i high-throughput screening af potentielle lægemiddelkandidater og i separationsteknologier, hvor et interessant eksempel er vandrensningsenheder baseret på biomimetiske membraner indeholdende aquaporiner (specifikt vandselektive proteiner). Der er imidlertid en del udfordringer at overkomme, før man vil kunne bygge biomimetiske enheder til industrielle formål. Blandt andet er lipidmembraners iboende skrøbelighed, udfordringen i opskalering af det effektive membranareal og kvantificering af systemer til inkorporering af protein i lipidmembranen, som kan være afgørende for den biomimetiske membranapplikation. Denne Ph. D. afhandling adresserer disse vanskeligheder. For det første præsenteres en enhed, der faciliterer målinger ved hjælp af atomic force mikroskopi (AFM) af biomimetiske membraner. Den mikrofluide enhed blev specifikt designet og fremstillet til at kunne huse AFM proberne, der anvendtes til at studere polymer-væskemembraner i mikrometerskala. For det andet blev stabiliteten af membranarrays forøget på to måder; overflademodifikation af support partitioner og ved involvering af en fuldt lukket og automatiseret mikrofluid-enhed. I den fremstillede mikrofluide enhed blev overfladen kovalent plasmamodificeret, hvilket resulterede i en hydrofob coating, og dermed blev de gennemsnitlige array-levetider (op til 6 dage) af et bilagsmembranareal på ca. 50% af det tilgængelige aperturareal betydeligt forøget. Det var muligt at fremstille højtstabile membraner (op til 2 dage) med et bilagsmembranareal på ca. 24% af det tilgængelige aperturareal i den udviklede mikrofluid-enhed. Desuden kunne rekonstitution af α-hemolysin (α-HL) membranproteiner udføres i de biomimetiske membraner. For det tredje etableredes et assay til fastlæggelse af fusionsvirkningsgraden af outer membrane porin (OMP), og dette blev anvendt til at kvantificere proteininkorporering i et array af plane membraner. Inkorporering blev etableret som en proces med enten førsteordens- eller eksponentiel kinetik. Dette kan have interesse for mikrofluid-design, der involverer proteininkorporering i biomimetiske membraner, der udvikles til sensor- og separationsapplikationer. Endelig vistes modulering af en OMP-funktionalitet med β-cyclodextrin (β-CD), hvilket understøtter proteinets applikationspotentiale i en biosensor. Herudover kan en β-CD blocker anvendes til forebyggelse af dannelsen af dentalplaque og udvikling af periodontitis hos mennesker.

Acknowledgments

This thesis is the summary of work that has been done for obtaining the PhD degree at the Technical University of Denmark. The work was conducted at the Department of Micro- and Nanotechnology (DTU Nanotech), the Department of Physics (DTU Physics) and Aquaporin A/S in the period from January 2008 to November 2011. This project has been filled with lots of new experiences and would not have been possible without the support of many people who I want to say thank you to.

First, I want to thank my supervisors, Oliver, Claus and Jenny for leading me through the project, giving me the freedom to follow my own ideas and always having the ability to push me in the right direction.

Second a big thank you to all members of Aquaporin A/S for the good and inspiring working atmosphere. For the great time as well as for the help and support I would like to thank you to Mark, Thomas, Karin, Jesper S, Marianne, Dorthe, Jesper G, Dorte and Peter. A special thank you to PhD students at Aquaporin A/S and DTU Nanotech: Sania, Jörg, Maciej, Jan and Christian. It has been a pleasure to share offices, laughs and daily life with you. I have highly appreciated your help and support you have given me throughout the project – thank you!

I would also like to acknowledge everybody at the BIOMICS and POLYMIC sections at DTU Nanotech and the Danish Polymer Centre for motivating discussions and help.

Thank you for funding for my work from The Technical University of Denmark and funding from the Danish National Advanced Technology Foundation (023-2007- 1).

Finally, I thank my family and friends for their encouragement and help for these years. A special thank you goes to my husband Artur and my son Emil for your love, patience and support.

Whoever I have failed to mention – forgive me and thank you.

Abbreviations

AFM	Atomic force microscopy
AFM device	Microfluidic device for AFM imaging of biomimetic membranes
ATP	Adenosine triphosphate
α-HL	α-hemolysin
Badan	6-bromoacetyl-2-dimethylaminonaphthalene
BFS	Bilayer Forming Solution
BLM	Black lipid membrane
BPM	Black polymer membrane
C_m	Membrane capacitance
C_s	Specific membrane capacitance
CD	Cyclodextrin
CymA	Outer membrane protein of *Klebsiella oxytoca*
DOPC	1,2-dioleoyl-sn-glycero-3-phosphocholine
DPhPC	1,2-diphytanoyl-sn-glycero-3-phosphocholine
ETFE	Ethylene tetrafluoroethylene
FEP	Fluorinated ethylene propylene
FomA	Major outer membrane protein of *Fusobacterium nucleatum*
g	Single ion channel conductance
G	Membrane conductance after ion channels incorporation
G_m	Membrane conductance
gA	Gramicidin A
GUV	Giant unilamellar vesicles
HMDSO	Hexamethyldisiloxane
LB	Langmuir-Blodgett
LDAO	N-lauryl-N,Ndimethylammonium-N-oxide
LPR	Lipid to protein molar ratio
LS	Langmuir-Schaefer
LUV	Large unilamellar vesicles
MF device	Closed and automated microfluidic device
MLV	Multilamellar vesicles
NBD	4-nitrobenzo-2-oxa-1,3-diazole
NBD-PC	1-Oleoyl-2-[6-[(7-nitro-2–1,3-benzoxadiazol-4-yl)amino]hexanoyl]-sn-glycero-3-phosphocholine
NTA	Nanoparticle tracking analysis
OMP	Outer membrane porin
OmpA	Outer membrane porin A
OmpF	Outer membrane porin F
OmpG	Outer membrane porin G
OG	Octyl-β-D-glycopyranoside
Parylene	Poly(p-xylylene)
PBS	Phosphate buffered saline
PC	Phosphatidylcholine
PDMS	Polydimethylsiloxane
PE	Phosphatidylethanolamine

PEO-PEE	Polyethyleneoxide-polyethylethylene
PET	Poly(ethylene terephthalate)
PI	Phosphatidylinositol
PMMA	Poly(methyl methacrylate)
PMOXA-PDMS-PMOXA	Poly(2-methyloxazoline)-block-poly(dimethylsiloxane)-block-poly(2-methyloxazoline)
PS	Phosphatidylserine
PTFE	Polytetrafluoroethylene
SNAP	Soluble N-ethylmaleimide-sensitive factor attachment protein
SNARE	SNAP receptor protein
SUV	Small unilamellar vesicles
Texas Red®	Sulforhodamine 101 acid chloride
UV	Unilamellar vesicles
VDAC	Mitochondrial voltage dependent anion channel
Viton®	Dipolymer of hexafluoropropylene and vinylidene fluoride

List of publications

Paper I **Free-standing biomimetic polymer membrane imaged with Atomic Force Microscopy**
Christian Rein, **Kamila Pszon-Bartosz**, Karin B. Stibius, Thomas Bjørnholm and Claus Hélix-Nielsen
Langmuir, 2011, 27 (2), 499–503

Paper II **Surface modifications of support partitions for stabilizing biomimetic membrane arrays**
Mark Perry, Jesper S. Hansen, Karin Stibius, Thomas Vissing,
Kamila Pszon-Bartosz, Christian Rein, Bahram Eshtehardi, Maike Benter and Claus Hélix-Nielsen,
Journal of Membrane Science & Technology, 2011, (in press)

Paper III **Microfluidic formation and regeneration of highly stable biomimetic membrane arrays**
Kamila Pszon-Bartosz, Mark Perry, Jesper S. Hansen, Jörg Vogel, Claus Hélix-Nielsen, Jenny Emnéus and Oliver Geschke,
Journal of Micromechanics and Microengineering, *to be submitted*

Paper IV **Assessing the efficacy of vesicle fusion with planar membrane arrays using a mitochondrial porin as reporter**
Kamila Pszon-Bartosz, Jesper S. Hansen, Karin B. Stibius, Jesper S. Groth, Jenny Emnéus, Oliver Geschke and Claus Hélix-Nielsen,
Biochemical and Biophysical Research Communications, 2011, 406 (1), 96–100

Book chapter **Biomimetic Membrane for Sensor and Separation Applications. Book chapter - Strategies for integrating membrane proteins in biomembranes.**
Jesper S. Hansen, Inés Plasencia and **Kamila Pszon-Bartosz**,
Springer Verlag, *2011, p. 251-271, ISBN 978-94-007-2183-8*

The story of the papers

This doctoral thesis includes four scientific publications and one book chapter. They reflect the work that was done during my PhD study. Paper I and II (co-author) and Paper III and IV (first-author) are listed in the order they appear in the experimental part of the thesis. Papers I and III present the investigation, formation and stabilization of biomimetic membranes in a microfluidic system. Paper I discuss a microfluidic device for biomimetic membrane investigation by AFM and this device was an inspiration for the generation of the device described in Paper III. Paper II describes surface modification of the partition for stabilizing biomimetic membrane arrays and Paper IV shows the quantification of protein delivery to the lipid bilayer that can be used in developing biomimetic membrane applications. The book chapter presents strategies for integrating membrane proteins in biomembranes and some of it is used in the thesis.

Paper I

The aim of this paper was to investigate fluid polymeric biomimetic membranes made in the microfluidic device with AFM, using probes with both normal tetrahedrally shaped tips and nanoneedle-shaped Ag_2Ga rods. When using nanoneedle probes, the collected force volume data show three distinct membrane regions which match the expected membrane structure when spanning an aperture in a hydrophobic scaffold. The method used provides a general method for mapping fluid surfaces. In particular, the nanoneedle probing allows for characterization of free-standing biomimetic membranes with thickness on the nanometer scale suspended over 300-µm-wide apertures and significantly reduces the amount of measurement artefacts and increases the precision of the probing comparing to the conventional tetrahedrally shaped tip.

Paper II

The paper studies the effect of covalently modifying the partition substrate using surface plasma polymerization with hydrophobic n-hexen (mixture of isomers), 1-decene and hexamethyldisiloxane (HMDSO) as modification groups on BLM (Black lipid membrane) array stability. The average lifetime of membranes formed across single-sided HMDSO modified partitions and 1-decene modified partitions were similar, but significantly lower than for arrays formed using untreated ethylene tetrafluoroethylene (ETFE) partitions. For single side n-hexene modification the average membrane array lifetime was comparable to untreated ETFE. Double-sided n-hexene modification greatly improved average membrane array lifetimes compared to membrane arrays formed across untreated ETFE partitions. n-hexene modifications resulted in BLM membrane arrays which over time developed significantly lower conductance and higher capacitance values compared to the other membranes with the strongest effect for double-sided modification. The improvement in membrane array lifetime, signal to noise ratio and reconstituting gramicidin A (gA) and α-HL into BLM arrays demonstrate that surface plasma polymerization of the supporting partition can be used to increase the stability of biomimetic membrane arrays.

Paper III

Paper III utilized microfluidics for BLMs formation. Here a microfluidic system was implemented on both sides of a perforated (8×8 array of 300 μm wide apertures) ETFE partition for inducing the membrane thinning process. A fully automated and closed microfluidic device for the formation, regeneration and investigation of an array of planar lipid membranes by electrical measurements was developed. Highly stable membranes (lifetime of ~42 h), constituting ~24 % of the total area of the array were created. To evaluate whether the functional lipid bilayers were established in the microfluidic device the pore-forming heptameric α-HL membrane protein was incorporated into the membranes.

Paper IV

This paper addresses reconstitution of functionally active membrane proteins into artificially made membranes. Here, a novel assay for quantifying protein incorporation into lipid membranes was developed and presented. The protein incorporation efficacy assay uses the major non-specific porin of *Fusobacterium nucleatum* (FomA) as reporter. The efficacy of FomA proteoliposome fusion with planar membrane arrays was calculated using electrical conductance and fluorescence microscopy. It was shown that protein reconstitution in the biomimetic membrane arrays can be quantified using the developed FomA assay. Specifically, it was shown that FomA vesicles are inherently fusigenic. Optimal FomA incorporation was obtained with a proteoliposome lipid to protein molar ratio (LPR) of 50 resulting in that more than 10^5 FomA proteins could be incorporated into a bilayer array with a total membrane area of 2 mm^2 within 20 min.

Book chapter

This chapter gives a detailed overview of available and novel membrane protein reconstitution strategies in both vesicular and planar model membrane designs.

My contribution to the papers

Paper I

I designed and fabricated the microfluidic device that can be used for biomimetic membrane formation and investigation by AFM. I had a small part in writing the manuscript.

Paper II

I was involved in designing and performing the experiments concerning biomimetic membrane formation and characterization using the voltage clamp method. I had a small part in writing the manuscript.

Paper III

I designed and fabricated the microfluidic device, formed and characterized biomimetic membranes using the voltage clamp method, and incorporated protein in the membranes. I analysed the results and drafted the manuscript.

Paper IV

I designed and performed the experiments. I analysed the results and drafted the manuscript.

Book chapter

I had a part in writing the subsection about protein reconstitution in planar membranes.

1. Introduction

Scientists and engineers are increasingly trying to find ways to "imitate nature" to solve complex problems. This is known as a biomimetic approach, where some guiding principles from nature are extracted in order to provide a basis for creating new "nature inspired" technological devices. These devices can be used in many areas, e.g. in biomedicine, replicating failing human organs, as well as replace unethical, costly and time-consuming animal studies that currently hamper drug development. Studying the navigational systems and locomotive strategies of insects can help to design the next generation of autonomous robots and vehicles. Another exciting example is the water industry, where an aquaporin proteins based membranes can be used for separating and purifying water from all other compounds, as these proteins are capable of highly selective water transport, which can go up to ~10^9 molecules of H_2O per second per channel[1, 2]. Aquaporins and other specialized proteins incorporated in naturally occurring lipid bilayers may be utilized in sensor and separation devices[3]. Replication of lipid bilayers with incorporated proteins and their utilization in technological device development will be discussed further in this thesis.

Nature utilizes the lipid bilayer as a cell defining membrane, selectively permeable to ions and organic molecules, which controls the movement of electrolytes and other compounds in and out of cells. The movement of electrolytes is crucial for many life-supporting reactions, e.g. generating and transmitting electrical signals by nerve and muscle cells, generating electrochemical potentials in response to external cellular stimuli by specialized sensing cells, maintaining volume control in cells, and in secreting fluids as saliva and tears. Transport, sensing and transduction proteins incorporated into lipid membranes, selectively control the flow of electrolytes, therefore, providing a system with combined sensing and separation elements[4]. Therefore, there is a major interest in trying to replicate naturally occurring lipid bilayers and utilize them in sensor and separation devices.

In order to mimic what nature has developed through billions of years of trial and error, a lot of scientific effort has to be invested, and interdisciplinary fields of research needs to be combined. Scientists in biology, biophysical chemistry, membrane technology and micro- and nanotechnology have already put a lot of effort to reach this goal, but still many challenges remain to be solved. This project shows development of some steps in creating a biomimetic device for sensor and separation applications.

A lipid bilayer is the main component of biomimetic membrane-based device[3, 5, 6]. Strategies for lipid membranes formation and investigation have been studied for many years[7-9]; even so these membranes cannot be widely used due to their fragility and bad reproducibility. Therefore searching for new ways of forming lipid membrane may be beneficial in increasing their lifetime and reproducibility, as well as overcoming the challenge of up-scaling the effective membrane area, which may be required for some applications. One way of doing this could be by the use of microfluidics[10, 11] and this will be discussed in this thesis.

The second component of a biomimetic membrane-based device, and its "heart", is associated membrane protein, which depending on the device application may be a membrane spanning channel or carrier protein[3, 6]. One of the challenges is to ensure sufficient delivery of functional protein to the biomimetic matrix.

Fusion of protein containing lipid vesicles (proteoliposomes) with planar membranes has been used for many years and is a powerful technique to incorporate membrane proteins into planar lipid bilayers[12, 13]. In particular, this method has been valuable for studies where incorporation of only a few proteins (or even single protein) is sufficient. However, large scale systems based on lipid bilayers will often require substantial amounts of incorporated proteins. It is therefore of interest to evaluate the potential of up-scaling vesicle based protein delivery, an issue that will be addressed in this thesis.

A very important step in building a biomimetic membrane-based device is the demonstration of its final application. An artificially made lipid membrane may be a useful tool for biochemical studies of proteins and for the development of future sensor and separation technologies. This is the main subject of the last part of this thesis where a perspective application as a stochastic sensor of a protein of interest incorporated into a lipid bilayer will be investigated.

To summarize, biomimetic membranes have a great potential. Artificially made membranes are powerful tools for the fundamental biophysical studies of membrane proteins and may be used in sensor and separation technologies. However, there are many challenges that must be overcome in order to build biomimetic membrane devices for industrial applications and this work presents some ways of solving them.

2. Aim and structure of the thesis

This PhD project was linked to the project "Industrial biomimetic water membranes" funded by the Danish National Advanced Technology Foundation and was performed in close collaboration with Aquaporin A/S. The company's objective is to develop a new membrane technology for water purification. The technology copies nature's own filtration system, namely aquaporin proteins. Aquaporin proteins have very high and selective water permeability and are transmembrane proteins, which embedded in a lipid bilayer can act as highly specific biological water filters as only water can penetrate through the protein[1, 2]. The motivation for this work comes from the great potential of biomimetic membranes. They mimic the biological membranes that very often exceed the commercially available membranes in performance. Artificially made membranes are powerful tools for fundamental biophysical studies of membrane proteins and may be used in sensor and separation technologies, yet they have not been widely used due to their fragility and bad reproducibility. The aim of my PhD project was to investigate a new microfluidic way to form stable biomimetic membranes and a novel strategy for quantification of the protein delivered to the lipid bilayer that may be a useful tool in developing biomimetic membrane applications.

The thesis starts by giving the necessary background, including biomimetic membrane and microfluidic technologies (Chapter 3). The next chapter (Chapter 4) describes the main techniques used to fabricate microfluidic devices and characterise biomimetic membranes. Chapter 5 outlines the PhD project roadmap related to the four devices used in this thesis. Chapter 6 describes microfluidic device that has been designed and fabricated for investigating polymer based biomimetic membranes using AFM, where the microfluidic system was implemented mainly for the need of the microscope. The next chapter, Chapter 7 shows two ways of increasing biomimetic membrane arrays stability. The first way (section 7.1) studies the partition modification by plasma polymerisation, the second involves microfluidics, where a device was designed in a way that the microfluidic system facilitated formation of highly stable biomimetic membrane arrays (section 7.2). Chapter 8 presents the protein delivery and developing biomimetic membrane applications. Section 8.1 shows a direct protein incorporation using the microfluidic device, section 8.2 describes the proteoliposome fusion efficacy assay and section 8.3 the incorporation of a protein of interest in a biomimetic membrane, its functionality modulation and application perspectives as a stochastic sensor. The last part of the thesis (Chapter 9) summarizes the work that has been achieved and shows the future perspectives for it. The scientific papers that have been produced during the PhD project are enclosed as appendices.

3. Background

3.1. Biomimetic membranes

The term biomimetic membrane denotes a membrane that mimics a real cell membrane. The latter acts as a selective barrier defining the cell and organelles and is a very complex structure (Figure 3.1)[4]. Almost everything we perceive comes to us via the cell membrane. The reason for this is that it mainly consists of a lipid bilayer, which has specialized proteins incorporated in it that act as receptors, ion channels or transporters. Therefore, the cell membrane and its constituents are responsible for our main senses like sight, smell, taste, touch, and hearing. The cell membrane contains, depending on the cell, a variety of glycolipids, carbohydrates, cholesterols and other components in different combinations and quantities, all of which are held together by noncovalent interactions[6]. The fundamental structure of the artificially made membrane is a lipid- or recently also a polymer[14-17] bilayer with proteins embedded in it. This simple membrane-protein configuration is a simpler structure than an entire cell, but can be sufficient to study the functions of membrane spanning proteins.

In the following sections, the main components used to create biomimetic membranes; lipids and polymer bilayers and membrane proteins, will be described. Then, the strategies that are used to deliver proteins to the bilayer matrix will be discussed, and finally some biomimetic membrane applications will be shown.
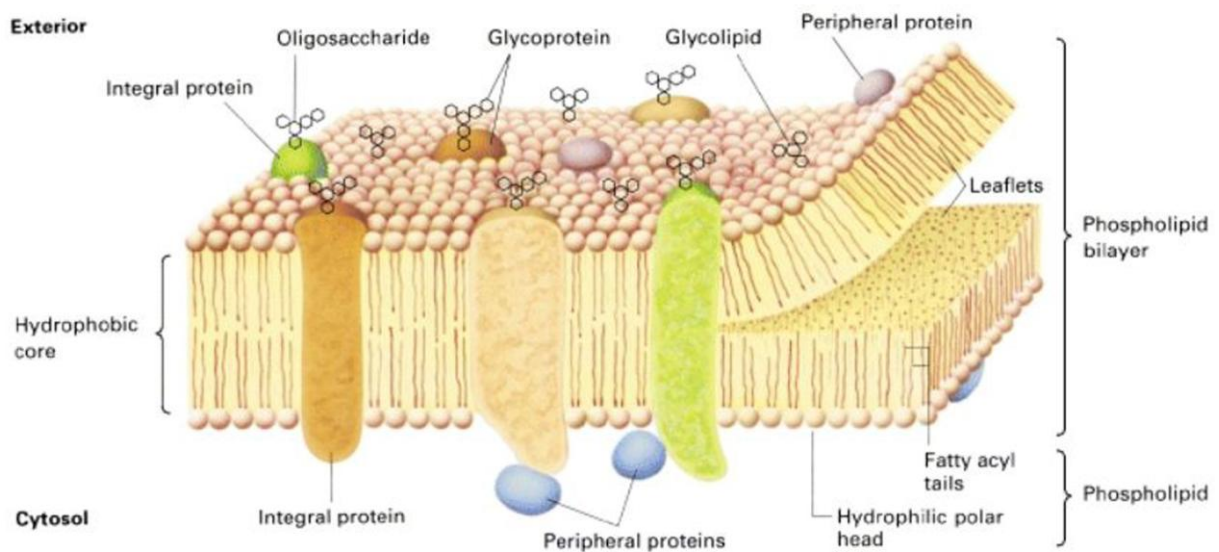
Figure 3.1. Schematic diagram of a cell membrane showing its two main components: lipid bilayer with embedded proteins and glycolipids and oligosaccharides. The phospholipid bilayer consists of two leaflets of phospholipid molecules whose fatty acyl tails form the hydrophobic interior of the bilayer; their polar, hydrophilic head groups line both surfaces. Most integral proteins span the bilayer as shown; a few are tethered to one leaflet by a covalently attached lipid anchor group. Peripheral proteins are primarily associated with the membrane by specific protein-protein interactions. Oligosaccharides bind mainly to membrane proteins; however, some bind to lipids, forming glycolipids. The full complexity of the cell membrane is not shown. (Picture taken from[18]).

3.1.1. Lipid and polymer bilayers

Lipid bilayer, as the name implies, consists of two lipid molecules. In particular, phospholipids, being amphiphilic compounds with a hydrophobic hydrocarbon chain at one end and a hydrophilic moiety at the other end of the molecule. The various phospholipids have a variable region in the polar group. Phospholipids have two fatty acid chains esterified to a glycerol molecule and on the third glycerol hydroxyl there is a phosphate group associated to a hydrophilic moiety, such as choline (phosphatidylcholine, PC), ethanoloamine (phosphatidylethanolamine, PE), serine (phosphatidylserine, PS) or inositol (phosphatidylinositol, PI). The acyl chains of fatty acids can vary both in chain length (usually 18, 19 or 20) and saturation (saturated – without double bonds, unsaturated – one or more double bonds). The major driving force for the formation of lipid bilayers is the hydrophobic interaction between the fatty acyl chains of the phospholipids. It is energetically favourable for the hydrocarbon to associate with hydrocarbon and to minimize the surface area of contact with water because of the so-called hydrophobic effect, i.e. the inability of hydrocarbons to form hydrogen bonds with water, which would cause a decrease in entropy. The close packing of the hydrophobic moieties in lipid bilayers are due to van der Waals interactions between the hydrocarbon chains, while the bilayer stabilization is achieved by hydrogen bonding and electrostatic interactions between the polar head groups and water molecules[6]. Common phospholipids that are used to build lipid bilayers are 1,2-diphytanoyl-sn-glycero-3- phosphocholine (DPhPC) and 1,2-dioleoyl-sn-glycero-3-phosphocholine (DOPC). Their structures are presented in Figure 3.2A and Figure 3.2B, respectively.
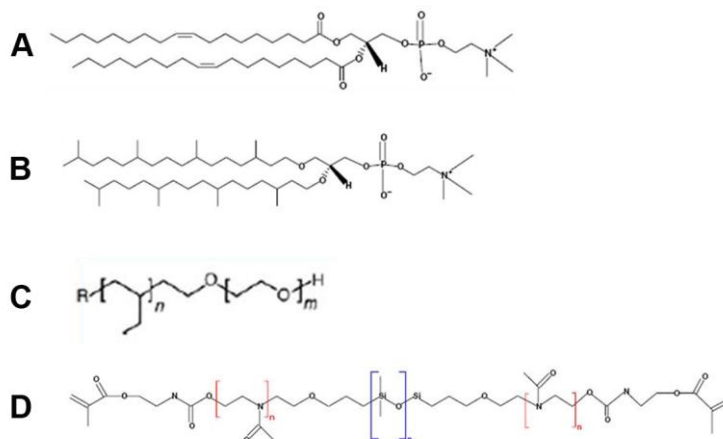
Figure 3.2. Common lipids and polymers used to build biomimetic membranes. (A) Phospholipid, 1,2-diphytanoyl-sn-glycero-3-phosphocholine (DPhPC). (B) Phospholipid, 1,2-dioleoyl-sn-glycero-3-phosphocholine (DOPC). (C) Diblock copolymer (polyethyleneoxide-polyethylethylene (PEO-PEE)). (D) Triblock copolymer (poly(2-methyloxazoline)-block-poly(dimethylsiloxane)-block-poly(2-methyloxazoline) (PMOXA-PDMS-PMOXA). Figure adapted from[3].

Diblock copolymer (polyethyleneoxide-polyethylethylene (PEO-PEE))[16] or triblock copolymer (poly(2-methyloxazoline)-block-poly(dimethylsiloxane)-block-poly(2-methyloxazoline) (PMOXA-PDMS-PMOXA)[15] are used as a lipid replacement to build biomimetic membranes. Their structures are presented in Figure 3.2C and D, respectively. Triblock copolymers have a hydrophilic-hydrophobic-hydrophilic composition while diblock copolymers consist of hydrophilic and hydrophobic blocks covalently linked together, thus resembling the amphiphilic nature of lipids. Polymer membranes show an increased overall mechanical stability[16, 19] and

are thicker [20, 21] than lipid based systems; nevertheless they have been shown to successfully incorporate transmembrane proteins[20, 22].

Biological membranes spontaneously typically arrange themselves in closed bilayer forms, achieving in this conformation the lowest total energy, while artificially made membranes can have several configurations: vesicular (Figure 3.3A), free standing (Figure 3.3B) and supported (Figure 3.3C).
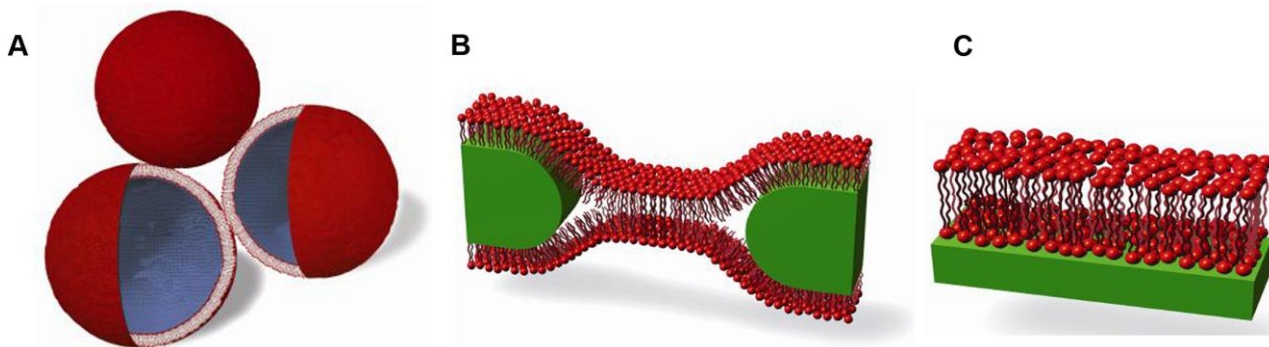

Figure 3.3. Lipid or polymer bilayer types. (A) Vesicular bilayers separating two aqueous compartments; lipid or polymer bilayers (red), the intravesicular aqueous compartment (blue). (B) Free-standing bilayers; black lipid or polymer bilayers (red) over an aperture in a hydrophobic scaffold (green). The membrane separates two aqueous compartments. The white triangular sections between the membrane monolayers and the scaffold contain an organic solvent. (C) Planar supported bilayers. Lipid or polymer bilayers (red) supported on a solid support (green).

Vesicles made from lipids are called liposomes whereas vesicles composed of polymers are called polymersomes. If vesicular structures of artificially made lipid or polymer bilayers contain proteins they are referred to as proteoliposomes or proteopolymersomes, respectively. Vesicle size and lamellarity (number of bilayers that formed the vesicle) depends on the method that is used for its formation, and based on that, vesicles may be divided into multilamellar vesicles (MLV), small unilamellar vesicles (SUV), large unilamellar vesicles (LUV) and giant unilamellar vesicles (GUV).

Dry lipid film hydration is a commonly used method to produce liposomes[23] and is based on the fact that natural or synthetic phospholipids dispersed in aqueous solution form large MLV[24]. Sonication is an easy method to form unilamellar vesicles (UVs) from MLVs. However, this method produces vesicles with a broad size distribution and extrusion into a narrower size distribution is needed. This is important for reliable and reproducible protein reconstitution and may also be valuable in many analytical techniques. Mechanical extrusion of MLVs through a filter membrane with a defined pore size results in UVs with a narrow size distribution (often monodisperse). Vesicle extrusion may be carried out by hand-held or with nitrogen pressurized barrel extruders. Dry film hydration, sonication and extrusion methods can also be used to obtain polymersomes from diblock and triblock copolymers[19, 21, 25].

Artificially made free-standing bilayers can be made from lipids or polymers and are called black lipid or black polymer membranes (BLMs or BPMs), respectively. They are named "black" because, due to their thickness of only a few nanometers, they appear black in reflected light. Conventionally, free-standing lipid or polymer bilayers are formed across apertures in a hydrophobic material separating two aqueous

compartments. In principle they can be established by two different methods; the Mueller-Rudin painting method[26] and the Montal-Mueller folding method[7]. In the painting method, lipid[26] or polymer[27, 28] bilayers are formed by self-assembly of an initially thick lipid or polymer solvent film spread over one side of an aperture submerged in aqueous solution. The lipid or polymer layer gradually thins down to form a bilayer due to the presence of the amphiphilic moiety on the lipids or polymers. The bilayer is formed in the middle of the aperture while the thick lipid or polymer solvent solution is left around the edges of the aperture forming the so-called Plateau-Gibbs border (Figure 3.4). In the folding method, a vertical setup is used. In one embodiment, a lipid[7] or polymer[15] monolayer is spread at the air-water interface in one compartment. By first lowering the lipid containing aqueous solution on one side of the aperture and then raising it results in bilayer formation across the aperture (Figure 3.5).
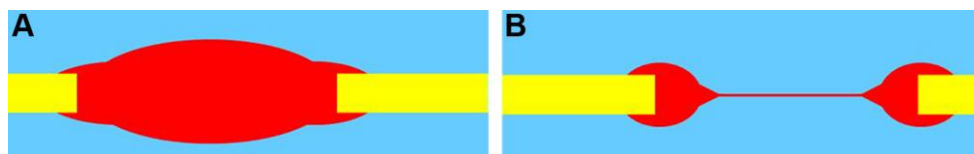

Figure 3.4. Schematic of the BLM and BPM formation by the painting method. (A) Lipid or polymer forming solution (in red) is applied to the aperture (in yellow) separated between two aqueous compartments (in blue). (B) The presence of amphiphilic components promotes the lipid of polymer layer thinning process. Bilayer is formed in the middle of the aperture while the thick forming solution is left around the edges of the aperture forming the so-called Plateau-Gibbs border.
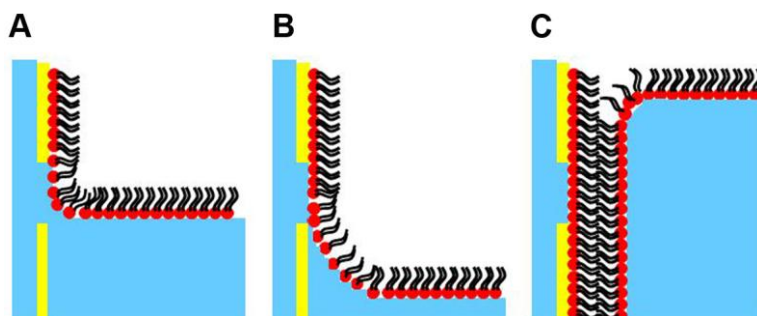
Figure 3.5. Schematic of the BLM and BPM formation by the folding method. (A) The lipid or polymer monolayer (in red and black) is lowered (B) and raised (C) so that a bilayer is formed along the wall and over the aperture in a hydrophobic partition (in yellow) separating the two aqueous compartments (in blue).

Supported planar membranes (Figure 3.3C) are another type of biomimetic membranes and show the potential in applications where membrane durability plays an important role. They can be made up from lipids or polymers and are both formed by the Langmuir-Blodgett (LB) and Langmuir-Schaefer (LS) techniques[29-31] or by vesicle deposition[32-34]. The LB and LS technology is based on the particular properties of amphiphilic molecules to orient themselves at an air/water interface between a gaseous and liquid phase to minimise their free energy, forming an insoluble monolayer called Langmuir film. It is formed by vertical (LB) or horizontal (LS) movement of a solid substrate through the monolayer/air interface. For vesicle deposition, the solid support must be hydrophilic, why silica, mica and borosilicate glass are the most commonly used support materials.

3.1.2. Membrane proteins and transport

Membrane proteins are the second component of a biomimetic membrane. Biological membranes contain peripheral and integral membrane proteins. Peripheral membrane proteins interact with integral membrane

proteins or with the polar head groups of membrane phospholipids. They do not enter the hydrophobic core of the membrane. Integral membrane proteins include transmembrane- and lipid-anchored proteins. In transmembrane proteins two types of membrane-spanning domains are found: one or more α-helices and multiple β-strands (porins) (Figure 3.6). A major class of proteins contain seven membrane-spanning α-helices (e.g. bacteriorhodopsin and many cell-surface receptors). When the polypeptide chain of a transmembrane protein spans the membrane multiple times, the core of the protein generally is hydrophilic, permitting passage of water-soluble molecules, and the surface is hydrophobic, permitting interaction with the interior of the lipid bilayer. Lipid-anchored proteins are covalently attached to one membrane leaflet by amino acid residues modified with long-chain hydrocarbons[18].
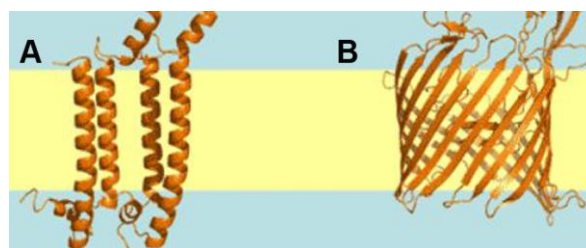

Figure 3.6. Types of membrane-spanning domains found in transmembrane proteins. (A) α-helices and (B) multiple β-strands. Both proteins span a lipid membrane (in yellow) which is suspended in an aqua solution (blue). Figure taken from[35].

The cell membrane regulates the movements of molecules into and out of the cell. Gases and small hydrophobic molecules diffuse directly across the phospholipid bilayer while ions, sugars, amino acids, and sometimes water (at sufficient rates) cannot diffuse across the phospholipid bilayer and must be transported. This is accomplished by three groups of integral transmembrane proteins: channels, transporters and pumps. Channel proteins transport water or specific types of ions down their concentration or electric potential gradients at a very rapid rate - up to 10^9 molecules per second. The transmembrane channels that permit facilitated diffusion can be open or closed. They are said to be "gated". Based on gating properties there are ligand-, mechanically-, voltage-, and light-gated channels. Transporters move a wide variety of ions and molecules across cell membranes against gradients (active transport). In contrast to channel proteins, transporters bind only one or a few substrate molecules at a time, and for movement a conformational change in the transporter is required. Therefore, transporters move only about $10^2 - 10^4$ molecules per second, thus having a lower rate than that associated with channel proteins. Pumps (ATP-powered pumps) use the energy of adenosine triphosphate (ATP) hydrolysis to move ions or small molecules across a membrane against a chemical concentration gradient or electric potential[18].

Channel proteins and transporters are interesting groups of proteins that may be used in biomimetic sensor and separation devices. Channels are attractive due to their high transport rate and transporters, although having a lower turnover, are capable of transport against gradients. However, their functional incorporation into artificially made lipid or polymer bilayers is not easy and will be discussed in more details in the next section.

9

3.1.3. Strategies for protein delivery

Integration of membrane proteins with lipid or polymer bilayers to form a functional biomimetic membrane is not a trivial process, mainly due to protein softness and membrane fragility. This is of significant importance in the design of novel sensor and separation technologies. In this section, the strategies that are used to deliver proteins to three different types of lipid or polymer bilayers, i.e., vesicular, free standing and supported (Figure 3.7) will be described.
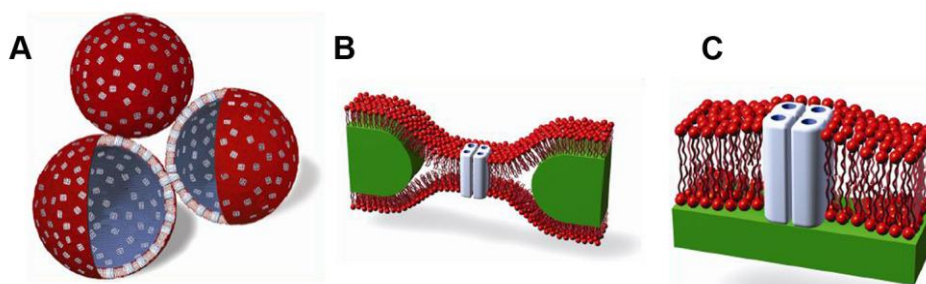

Figure 3.7. Integration of proteins with different types of lipid or polymer bilayers. (A) Vesicular membranes separating two aqueous compartments; lipid or polymer membranes (red), the intravesicular aqueous compartment (blue), incorporated transmembrane proteins (white squares). (B) Free-standing membrane; black lipid or polymer membranes (red) over an aperture in a hydrophobic scaffold (green) with an incorporated transmembrane protein (white rods). The membrane separates two aqueous compartments. The white triangular sections between the membrane monolayers and the scaffold contain an organic solvent. (C) Planar supported membranes. Lipid or polymer membranes (red) supported on a solid support (green) with an incorporated transmembrane protein (white rods).

A protein and lipid bilayer integration will mainly be affected by the hydrophobic interactions of the hydrophobic protein segment(s) with the acyl chains of the lipids. The hydrophobic thickness of the membrane and the length of the hydrophobic segments of the protein are expected to be matched. If there is a difference between them (known as hydrophobic mismatch), the protein may be hampered or even misfolded exposed to an unfavourable hydrophilic environment.

There are several methods available for reconstituting membrane proteins into vesicles. They depend on the protein purification conditions and the majority of these involve the use of detergents, which play a dual role for membrane proteins in solution: they solubilise the native membrane, releasing the contained membrane spanning protein into solution, and maintain the proteins folded and soluble in an aqueous state[36]. To produce protein reconstituted liposomes (proteoliposomes), removal of the detergent is necessary in order to transfer the proteins from an aqueous detergent solubilised state into the lipid bilayer. Conventional techniques for removing the detergent include dialysis, gel exclusion chromatography and adsorption onto polymeric materials.

An important parameter to consider before carrying out the protein reconstitution process is the LPR. There is an upper limit of how much protein that physically can be incorporated into a defined amount of lipid. This limit depends on the surface area of the protein and the area of the lipid bimolecular structure. Based on the protein and lipid area values a minimum mol/mol ratio between these two biomimetic membrane components may be estimated. The area per lipid of phosphatidylcholines has for example been characterized by NMR spectroscopy[37] and the various membrane proteins surfaces have been determined based on their crystal structures. The spinach aquaporin SoPIP2;1 is just one example[38]. Protein reconstitution into liposomes has

been the dominant method, however, there are a few examples of successful reconstitution of proteins into polymersomes[14, 39-41, 42]. This can be done by using drop-wise addition of polymer-protein-organic solvent solutions to the aqueous phase. However, the use of solvents (e.g. ethanol) is often detrimental to protein stability and this has severely limited the use of polymer-based biomimetic matrices[43].

There are many strategies to incorporate membrane proteins with free-standing and supported lipid or polymer bilayers. Supported membranes can be functionalized with membrane proteins by spreading vesicles that contain reconstituted transmembrane proteins and by preparing supported membranes incorporating 'anchor' molecules and then coupling engineered proteins to those anchors[44]. Small hydrophobic molecules and peptides such as gA or alamethicin spontaneously self-insert into pre-established free-standing lipid[45] or polymer[15] membranes. In contrast, medium to large membrane proteins (35-500 kDa) do generally not reliable self-insert into pre-established free-standing membranes[46]. An exception is the α-HL[47]. In addition, several *E. coli* OMPs such as outer membrane protein A (OmpA), outer membrane protein F (OmpF) and FomA may be reconstituted into planar membranes directly from a detergent solubilised state[48, 49, 50]. Although the detergent solubilised proteins can be added in a few microliter aliquots to the lipid bilayer chamber, the presence of detergent tends to make the established membrane(s) unstable. Therefore, fusion of proteoliposomes with a planar membrane is typically used to incorporate large membrane proteins into planar bilayers.

The fusion technique has been known for many years[13, 51] and is inspired by the biological phenomena of endo/exocytosis[52]. Optimization of the fusion of proteoliposomes with biomimetic membranes depends on increasing proteoliposome fusogenicity. Theoretical studies indicate that the early stages of fusion involve formation of a fusion pore or an intermediate, a neck-like connection between two bilayers, with an initial size of about 10 nm[53, 54]. The fusion time scale has not been measured experimentally, but patch-clamp electrophysiology[55] and ultrafast optical microscopy of GUVs[56] indicate that the fusion pore can be formed in less than 100 µs. Fusogenicity may be increased by lowering the energetic barriers for formation of fusion intermediates, which may be induced by lipids having opposite charges in vesicle and receiving planar membrane[57, 58]. Another strategy involves the use of fusogenic peptides in the two fusing membranes, as demonstrated by the use of soluble N-ethylmaleimide-sensitive factor attachment protein (SNAP) and associated receptor (SNARE), leading to the formation of SNAP–SNARE complexes and vesicle fusion[59, 60]. Fusion can also be driven solely by osmotic gradients across the planar receiving membrane provided that the vesicles are permeable to solutes[61]. The latter has been demonstrated using vesicles with the antibiotic nystatin and ergosterol[13, 51, 62].

In the nystatin-ergosterol method protein delivery to the biomimetic membrane can be monitored. Vesicles containing a protein of interest, nystatin and ergosterol may be fused to the ergosterol free planar membrane. A nystatin channel remains open in the presence of ergosterol but after fusion, it dissociate due to the ergosterol diffusion into the excess amount of lipids. However, in voltage clamp measurements while the fusion occurs a characteristic "current spike" can be seen, which then follows by a slow decrease in current while the ergosterol diffuses and the nystatin channels fall apart. The number of "current spikes" may be used to monitor the fusion activity. However, it is difficult to directly determine the amount of proteins

loaded into the planar membranes. By using ion channels that remain open after incorporation into the planar membrane one may asses the amount of inserted protein by detecting the increase in bilayer macroscopic conductance G after transfer of ion channels from the vesicle membrane to the bilayer. When the single-channel conductance g is known one may use the ratio G/g to estimate the total number of (ion channel) proteins that has been incorporated by fusion during this process (the fusion efficacy). This method has been demonstrated by using the voltage dependent anion channel (VDAC)[52, 63]. Another way of assessing the fusion efficacy is fluorescent tracer fusion assay. Fluorescence may be used to label the receiving planar lipid membrane with fluorescence label while having a different fluorescence label of the lipid vesicles or a labelled protein reconstituted into the fusiogenic vesicles. In this case vesicle fusion will result in incorporation of the fluorescent dye of the vesicles or of the labelled proteins reconstituted in the vesicles, respectively, into the planar fluorescently labelled membrane[64].

A novel strategy for reconstituting membrane proteins into planar membranes is by direct incorporation, which refers to reconstitution of membrane proteins simultaneously with establishing the planar membrane. Even though there are still very limited reports on this subject; it has been described for bacteriorhodopsin[65] and the nicotinic acetylcholine receptor[66]. A clear advantage of the direct incorporation approach is that the amount of protein reconstituted into the model membrane may be precisely controlled. The ability to incorporate large quantities of protein into model membranes may especially be important for using planar protein-based biomimetic membranes for separation techniques, where a high protein content is desired[3]. More information about biomimetic membrane applications will be presented in the next section of this thesis. However, my intention is not to review the extensive research performed in this field, but rather to highlight some of the applications.

3.1.4. Biomimetic membrane applications

Biomimetic membranes have a potential in a diverse range of applications; from biomedicine to separation technologies. Some examples of their biomedical applications are biosensing and platforms for high-throughput screening in the drug discovery process. The importance of biomimetic membranes as drug-screening platforms is rapidly growing as more and more human diseases are found to be caused by defects in ion channel functions. Such diseases include well-known examples like cystic fibrosis, cardiac arrhythmias and epilepsy. Nowadays, more than 60% of the pharmaceutical drug targets are proteins, in particular membrane proteins[5].

The biomimetic membrane application is determined by the format of the membrane (vesicular, free-standing or supported) and the effective membrane area. One example of vesicle based sensors is vesicles immobilized on the sensor surface[67-69]. Free standing membranes have been used extensively as model membranes[6] and for analytical applications[70], but have insufficient long term mechanical stability to be viable as portable biosensing devices. Integration of the bilayer with a solid surface provides far greater stability than a free-standing membrane and thus the majority of biomimetic membrane based biosensors employ supported BLMs[71, 72]. In most biomimetic membrane biosensor applications, the membrane serves as a passive matrix for the embedded proteins in which the protein (typically a receptor) can sense a signal and somehow transduce the information. This type of biosensor does not require massive flux of matter across

12

the membrane in order to function. Therefore, the membrane matrix can be supported on solid supports[3] and a low protein incorporation rate is sufficient. If biomimetic membranes are scaled to a sufficiently large effective area with a high protein incorporation rate, they can be used for separation applications. Here, the demand for massive flux across the biomimetic membrane precludes the use of non-porous cushion support. The extreme alternative - a free-standing lipid bilayer with incorporated proteins (e.g. ion channels) formed across an aperture - is not sufficiently stable to be used in a technological separation device.

Biomimetic membranes with protein pores have recently found an application in stochastic sensing. This technique is based on single molecule detection and measures the presence and transit of molecules in a small pore. The time for the molecules to diffuse to the pore and the time of their transit are random in nature. The name "stochastic sensor" refers to the discreteness of the output signal and to the unpredictability of the occurrence and duration of the molecule/pore interaction[73]. Stochastic sensor is capable of identifying the variety of analaytes sensing from their current signatures thus providing their identity and concentration. The sensor element has two states providing different output associated with each: occupied (by analyte) and unoccupied. A protein pore that has a binding site for an analyte is placed in a planar lipid membrane. Each time the analyte binds to the pore the current is modulated. This technique detects individual binding events. The frequency of occurrence of the events reveals the concentration of the analyte, whereas the current signature (the mean duration and amplitude of the events) reveals its identity. Stochastic sensing provides therefore useful kinetic data that are difficult to obtain by other techniques. In the case of a simple equilibrium, the relation between is the mean dwell time of the analyte τ_{off} and the dissociation rate constant k_{off} is described by Eq. 3.1, and the relation between the mean time between binding events τ_{on} and the association rate constant k_{on} by Eq. 3.2, where [A] is the analyte concentration[74].

$$\tau_{off} = \frac{1}{k_{off}} \tag{3.1}$$

$$\tau_{on} = \frac{1}{k_{on}}[A] \tag{3.2}$$

Among the protein pores, the heptameric α-HL is the most commonly used as a stochastic sensor. Engineered versions of α-HL have been used for sensing of ions[75, 76], proteins[77] and DNA[78, 79], while α-HL with a CD adapter was used for detection of small organic molecules[80]. To illustrate how the stochastic sensor works typical bilayer recordings showing the interaction of a single pore (α-HL) with a molecular adapter (β-CD) and the model analytes are presented in Figure 3.8.

Although biomimetic membranes show many application areas, there are significant concerns about improving their long-term stability. In addition, there is the question of how well the artificially made membrane can reproduce the native one. Therefore looking for new ways in building biomimetic membranes

have recently attracted much attention. In the next chapter, the microfluidic approach in biomimetic membrane formation will be introduced.
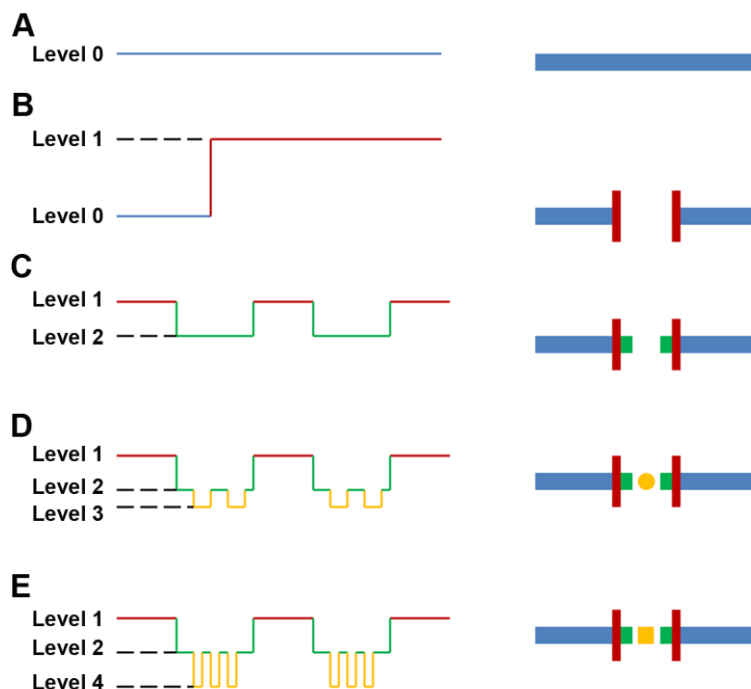

Figure 3.8. Schematic illustrations (on the right) and associated with them bilayer electrical recordings (on the left) showing principles of stochastic sensing. Electrical traces showing: (A) Signal across a lipid bilayer (blue), Level 0. (B) Incorporation into the lipid bilayer single protein pore, α-HL (red), Level 1. (C) Interaction of the single pore (red) with a molecular adapter, β-CD (green), Level 2. (D-E) Interaction of the single pore, α-HL (red) with β-CD (green) and the two model analytes (yellow), Levels 3 and 4.

3.2. Microfluidic approach in biomimetic membrane formation

The previous sections described the main components that build biomimetic membranes, their integration and applications. However, in order to form the membrane and further investigate its properties and applications some kinds of tools are needed. Many techniques used for membrane formation require manual intervention of the operator [81]. They are laborious processes and require experience and skill. Using these techniques only for making one or a few biomimetic membranes for biophysical studies of membrane proteins may satisfy the operator. However, when the membranes are meant for biomedical or separation technologies and many of them must be formed and investigated at ones, an alternative needs to be found. Here, microfluidic approach proved to be helpful. Recently, several groups have developed lab-on-a-chip systems for that matter[8, 10, 82].

In the following sections, the advantages of using microfluidic techniques in building biomimetic membranes will be discussed. Firstly, the microfluidic world with the theoretical background and fabrication techniques used for biomimetic microfluidic devices will be introduced. At the end the strategies involving microfluidics for biomimetic membranes formation will be presented.

3.2.1. Theoretical background in microfluidics

Chip-based bilayer technologies present a number of challenges compared with conventional bilayer systems. In microworld laminar behaviour of flows and diffusion become the dominant processes and the

reduced dimensions lead to an increase in the surface-to-volume ratio. This has consequences and must be kept in mind when attempting to design microsystems. In this section some basic insight into flow behaviour and processes and phenomena that rule at micro scales will be given. More detailed information can be found in[83, 84].

The Navier-Stokes equations are used to analyze the fluid flow. These equations combine the fundamental laws of conservation (mass, momentum and energy) with constitutive equations for fluids (governing viscosity and thermal conductivity) and are expressed by Eq. 3.3, where v is the flow velocity, ρ is the fluid density, p is the pressure, T is the (deviatoric) stress tensor, and f represents body forces (per unit volume) acting on the fluid, and ∇ is the del operator.

$$\rho(\frac{\partial v}{\partial t} + v \cdot \nabla v) = -\nabla p + \nabla \cdot T + f \qquad (3.3)$$

If we consider an incompressible, Newtonian fluid such as water, the Navier-Stokes equations can be simplified and different terms in the equation can be regarded as a connection between inertial forces and viscous forces (Eq. 3.4)

$$\rho(\frac{\partial v}{\partial t} + v \cdot \nabla v) = -\nabla p + \mu \nabla^2 v + f \qquad (3.4)$$

Here f represents "other" body forces (forces per unit volume), such as gravity or centrifugal force. The shear stress term ∇T becomes the useful quantity $\mu \nabla^2 v$ (∇^2 is the vector Laplacian) when the fluid is assumed incompressible, homogeneous and Newtonian, where μ is the dynamic viscosity. The left hand site of the equation represents inertia (per volume) $\rho(\frac{\partial v}{\partial t} + v \cdot \nabla v)$, where the right hand side divergence of stress $-\nabla p + \mu \nabla^2 v$ plus other body forces (f). The following parts of the equation, $\frac{\partial v}{\partial t}$, $v \cdot \nabla v$, $-\nabla p$, and $\mu \nabla^2 v$ represent unsteady acceleration, convective acceleration, pressure gradient and viscosity, respectively.

However, the Navier-Stokes equations contain more unknown parameters than equations, making complete analytical solution impossible. To solve them several boundary conditions are needed, for example the so-called no-slip condition, which states that the velocities at phase boundaries must be equal. A well known solution to the Navier-Stokes equation is the Hagen-Poiseuille-equation, which gives a relation between a fluidic resistance and the viscosity of a substance. Assuming circular cross-section of the microchannel, the fluidic resistance R can be described by Eq. 3.5, where L is the length, r the diameter of the channel, η is the kinematic viscosity. As seen from that equation, the fluidic resistance increases drastically when the channel dimensions are reduced. As consequences, to move liquids through smaller channels higher pressure is necessary.

15

$$R = \frac{8\eta L}{\pi r^4} \qquad (3.5)$$

To get an impression what kind of flow is common to microsystems, in channels that have microdimensions, relations between the magnitudes of the inertial and viscous forces needs to be found. This is well described by the dimensionless Reynolds number, Re, which is defined by the Eq. 3.6, where η is the viscosity, ρ the density, v the velocity and d describes a characteristic length scale of a microchannel.

$$\mathrm{Re} = \frac{\rho d v}{\eta} \qquad (3.6)$$

From empirical observation, $Re > 2300$ correspond to turbulent flow, which is the typical behavior of flow in a macroworld. Under this regime inertial forces are dominant. The region $2000 < Re < 3000$ is called the regime of transitional flow. The region where the $Re < 2000$ is referred as the laminar flow, region which is the dominant one in microsystems.

The useful equations that help during the design of microfluidic system are the *continuity equation* and the *Bernoulli equation*. The first one describes the behavior of flow in channels with changing cross sections; the product of the cross-sectional area A and the flow velocity v is constant,

$$A_1 v_1 = A_2 v_2 = const. \qquad (3.7)$$

The latter one describes flows when pressure and high differences play a role and is a direct application of the law of energy conservation, relating pressure p, kinetic $\frac{1}{2}\rho v^2$ and potential $\rho g h$ energies in the following way:

$$p + \frac{1}{2}\rho v^2 + \rho g h = const. \qquad (3.8)$$

Depending on the driving agent, there are two different types of transport in microfluidic system, statistical and direct transport. The first one is entropy driven transport and its good example is a diffusion process. Directed transport is transport that is generated by external work, for example mechanically by a pump or by a voltage. The common situation in the microworld is that the mixed of direct and diffusion transports occur, where one or the other dominates or both are of equal importance. To evaluate the ratio between them a dimensionless Peclét number is used, P_e. The number is given by the Eq. 3.9, where v is the velocity, d is a characteristic length of the microfluidic system and D is diffusion constant.

$$P_e = \frac{v \cdot d}{D} \qquad (3.9)$$

3.2.2. Fabrication of microfluidic devices for biomimetic membranes

As described earlier lipid or polymer membranes can be formed across apertures in a hydrophobic material separating two aqueous compartments. By microfluidic propulsion lipid or polymer forming solution is brought in close proximity of the aperture(s). The two main components of the microfluidic device, apertures and microfluidic channels, can be fabricated by using the full spectrum of known microtechnologies in combination with polymers or silicon. It will be the focus of this section of the thesis.

The apertures used for biomimetic membranes formation have been produced in silicon[10, 85], silicon nitride[86], glass[87, 88, 89] and plastics by using different techniques. For example, by using a simple hot needle in plastic cups[90], glass pipette pushed onto the plastic sheet[91], micromilling in poly(methyl methacrylate) (PMMA)[92], eximer laser microfabrication in PMMA, polytetrafluoroethylene (PTFE), poly(ethylene terephthalate) (PET) and fluorinated ethylene propylene (FEP) films[11] and carbon dioxide (CO_2) laser ablation in ETFE partition[93]. The microfluidic channels for biomimetic membrane formation have been fabricated in silicon with poly(p-xylylene) (parylene) coating[10] and plastics: in PMMA using hot embossing[11, 94] and micromilling[95, 92], and in PDMS by casting liquid PDMS in a precision-casting mould[89].

There are several disadvantages of using silicon-based devices for biomimetic membrane formation. They include the low resistivity of silicon, the time consuming and expensive fabrication process of silicon based devices, fragility of the silicon based microfluidics and the complexity in their integration. Polymeric devices have the potential to overcome all of the mentioned disadvantages: they are electrically insulating, robust, and can be fabricated using rapid, low cost methods that are amenable to the simple production of large scale microfluidic systems[94]. Therefore the following section will cover state-of-the-art strategies for biomimetic membrane formation by microfluidics in polymeric devices.

3.2.3. Strategies for biomimetic membrane formation by microfluidics

As mentioned before, biomimetic membranes can be established by the Mueller-Rudin painting method[26] and the Montal-Mueller folding method[7]. In the conventional painting method, membranes are formed by self-assembly of an initially thick lipid-solvent film spread over one side of an aperture submerged in aqueous solution. The lipid layer gradually thins down to form a bilayer. However, this spontaneous process is rather slow and several ways to induce the thinning process have been presented, e.g. manual thinning[81], solvent extraction[96], pressure induced thinning[47, 91, 92], agitation by removing and re-injection of the buffer solution in one of the compartment[88], removing excess lipid solution[91], air-exposure technique and a device architecture that promotes spontaneous thinning[11] and finally thinning aided by microfluidics[11].

The motivation to form biomimetic membranes in a microfluidic system is that it enables rapid exchange of electrolytes, use of small quantities of materials, rapid transport of material to and from the lipid membranes and finally the possibility for automation[11, 89]. Automated formation of lipid bilayers in a microfluidic system was proposed by Malmstadt et al.[96], presenting a method using solvent extraction through the walls of a microfluidic channel, and by Funakoshi et al.[95] by contacting two lipid monolayers in a microfluidic device. In both cases the bilayers were formed inside the microfluidic channels perpendicular to the channel wall and therefore electrolyte exchange was not possible. Several studies on membrane formation in a microfluidic

system, enabling liquid exchange on both sides of the membrane, have been presented with a microfluidic channel on one side of the membrane, leaving the top compartment of the device open[8, 46]. Open systems like this may however lead to problems with solvent evaporation and limited membrane stability. Mach et al.[89] designed a microfluidic device for automated formation of a single lipid bilayer by GUV adsorption across a micron-sized aperture in a glass slide, sandwiched between two PDMS channels, allowing fast perfusion on each side of the membrane. Suzuki et al.[10] and Kawano et al.[97] presented an automated and closed double-layered channel device for one micro-sized and one very stable nano-sized lipid bilayer formation, respectively. Sandison et al.[11] proposed a closed system fully accessible via microfluidic channels on both sides of the membrane and also showed that they were able to form a single lipid bilayer membrane by spontaneous thinning of the lipid solution, promoted by buffer agitation in both channels.

Whereas creation of a single biomimetic membrane across an aperture is a well-established technique, creation of biomimetic membrane arrays is not straightforward. Microfluidic aid for this purpose was suggested by Suzuki et al.[10, 82] and Sandison et al.[11]. These authors mentioned the possibility for up-scaling the effective membrane area by producing many apertures along the channel and arrays of apertures in polymer partitions, respectively. However, these approaches did not establish BLM arrays in a fully closed microfluidic device. This will be one of the subjects of this thesis.

In summary, the advantages and challenges of using microfluidic techniques in building biomimetic membranes have been discussed. In the following chapter the techniques used for microfluidic devices fabrication and for biomimetic membranes characterization and investigation will be described.

4. Techniques used in this thesis

This chapter describes techniques that were used during my PhD study to achieve the results presented in this thesis. It addresses the physical principles behind the techniques that were used for microfluidic device fabrication and biomimetic membrane formation and investigation.

4.1. Carbon dioxide laser ablation

The first laser was constructed by T. H. Maiman in 1960. A laser is a device that produces a monochromatic, coherent, and highly collimated beam of electromagnetic radiation with wavelengths ranging from ultra-violet to infrared. A laser can deliver very low (~mW) to extremely high (1 – 100 kW) focused power with a precise spot size/dimension and interaction/pulse time (10^{-3} to 10^{-15} s) on any kind of substrate through any medium. Up to this date, there are practically hundreds of different types of lasers and the applications of lasers are increasing every day. The term "LASER" is an acronym for (L)ight (A)mplification by (S)timulated (E)mission of (R)adiation. To understand the laser, one needs to understand the meaning of these terms. The term "light" is generally accepted to be electromagnetic radiation ranging from 1 nm to 1000 µm in wavelength. Stimulated emission is a quantum mechanical phenomenon discovered (on theoretical grounds) by Albert Einstein and is the process by which an atomic electron, interacting with an electromagnetic wave of a certain frequency, may drop to a lower energy level transferring its energy to that field. A photon created in this manner has the same phase, frequency, polarization, and direction of travel as the photons of the incident wave. This stimulated emission is the heart of a laser. The basic setup for a laser consists of a gain medium with a suitable set of energy levels to support laser action, a source of pumping energy in order to establish a population inversion (having more atoms in the upper energy level than in the lower level) and an optical cavity or resonator to introduce optical feedback and so maintain the gain of the system overcoming all losses. The basic laser setup is presented in Figure 4.1.
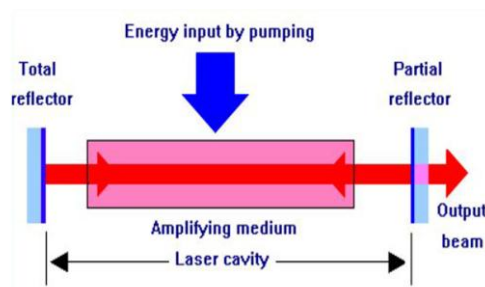

Figure 4.1. A schematic illustration of the basic laser setup. It consists of an amplifying medium with a suitable set of energy levels to support laser action, a source of pumping energy in order to establish a population inversion and an optical cavity or resonator to introduce optical feedback and so maintain the gain of the system overcoming all losses. Figure taken from[98].

Many lasers emit beams that approximate a Gaussian profile, in which case the laser is said to be operating on the fundamental transverse mode (TEM$_{00}$ mode) of the laser's optical resonator. The irradiance distribution of the Gaussian TEM$_{00}$ beam is expressed by Eq. 4.1, where I represents the intensity of field, r is a radial coordinate, ω is a beam radius, measured as a distance where the intensity falls in e² times as compare as the value on the axis $I = I_0 \cdot e^{-2}$ (Figure 4.2).
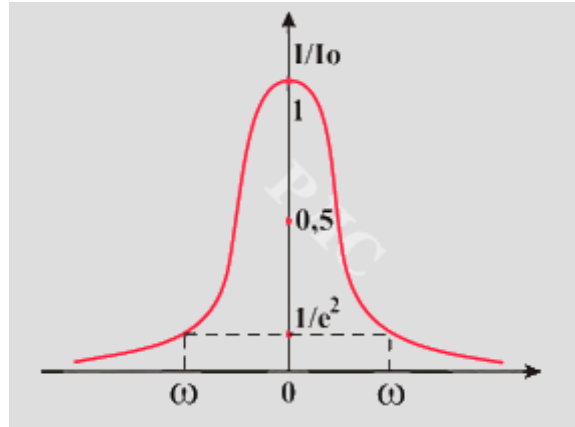
$$I(r) = I_0 \cdot e^{-2r^2/\omega^2} \tag{4.1}$$

Figure 4.2. Gaussian intensity distribution. The radius of the beam ω is equal to the distance between the optical axis and the spot where the irradiance is divided by $1/e^2$ in relation to the maximum irradiance of the wave. Figure taken from[99].

The CO_2 laser is one of the earliest developed and most popular lasers for material processing because it is electrically more efficient (15 – 20 %) and produces higher power (0.1 – 50 kW) than other lasers in the continuous mode. CO_2 laser ablation is the process of removing material from a solid surface by irradiating it with a CO_2 laser beam and can be used for realizing microstructures in polymer material. A CO_2 laser emits infrared radiation continuously with the principal wavelength bands centring around 9.4 and 10.6 micrometers. The ablation mechanism is purely thermal. Wherever the focused laser beam meets the polymer surface, the temperature of the irradiated spot will rise so rapidly, that the material will first melt and then decompose, leaving a void in the polymer. The dimensions of any laser ablated structure depend on the optical and mechanical setup of the laser system and on the material properties of the specific polymer. The depth of a channel D produced by a single pass of the laser beam with the width W and power Φ_{in} at a speed v across a polymer surface with the density ρ and absorbance α is given by the Eq. 4.2. Q_{th} is a threshold heat that has to be exceeded before the removal of material starts and k is a proportionality constant.

$$D = \frac{k}{\rho}(\frac{\alpha \cdot \Phi_{in}}{W \cdot v} - \frac{Q_{th}}{W^2}) \tag{4.2}$$

The cross section of the channels depends on the thermal diffusivity of the material (on the speed of the heat dispersion in the material) and on the intensity distribution within the laser beam. As for polymeric materials the thermal diffusivity is very low, the channel cross section is mostly determined by the laser beam intensity distribution. An example of such is a Gaussian-like profile, which has an intensity peak in the centre.

In this thesis a CO_2 laser ablation was the main technique used for polymeric microdevices fabrication. Specifically, the ablation in PMMA, ETFE and Viton® polymers was performed. The laser micromachining was carried out using a Synrad Inc. (Mukilteo, WA, USA) 48-5S Duo Lase carbon dioxide laser. A computer

aided design program WinMark Pro® version 4 from Synrad Inc. (Mukilteo, WA, USA) was used to set the movements of the laser beam, number of laser beam passes over a given design, laser beam speed and laser output power. The laser had a maximum output power of 65 W, which could be varied linearly. The laser system was equipped with a marking head containing a field lens and two swivel-mounted mirrors. The lens was able to focus the laser beam to a 290 μm diameter spot at a focal distance of 190 mm. The mirrors allowed the placement of the focused laser beam anywhere on a 110 by 110 mm large working area. The maximum speed of the beam was 1000 mm s^{-1}.

4.2. Voltage clamp

Voltage clamp is one of the main electrophysiological techniques used for investigating artificially made lipid or polymer membranes. It is used to study the electric behaviour of the membrane, providing information about the membrane area and thickness, thus determining the membrane quality. Monitoring the ionic current flowing through the protein channel under voltage-clamp conditions is used to inspect insertion and function of transmembrane proteins. It is used to characterize the stimulus that open or close the protein channel (open probability of the channel versus voltage, ligand concentration or membrane tension), the conductance of the protein channel under specific ionic conditions and the specificity of the protein channel (which ions can pass). Moreover, it can be extended to a pharmacological study by looking for ions or molecules that can block or open the protein channel.

The voltage clamp setup that was used for measurement of the biomimetic membrane electrical properties is schematically illustrated in Figure 4.3, as described in[100].
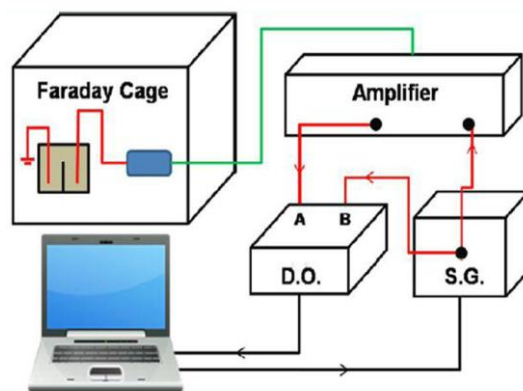

Figure 4.3. Schematic representation of the instrumental setup for voltage clamp measurements. Illustrated is the electrical instrumental voltage clamp setup consisting of an amplifier, signal generator (S.G.), combined analogue-digital converter and an oscilloscope (D.O.) and a personal computer. Indicated is the BNC coaxial connectors (red lines), amplifier head stage (blue box), biomimetic membrane system (brown box), USB cable (black lines), the amplifier head stage probe (green line) and the head stage probe (blue filled rectangle). All electrical components as well as the Faraday cage are electrically grounded. Figure taken form[100].

Ag/AgCl electrodes were placed in the aqueous solutions on each side of the membrane. An alternating voltage was applied across the membrane using a signal generator and the resulting transmembrane currents were recorded with a combined analogue-digital converter and an oscilloscope. A low pass filter was used to filter the response signals to reduce current-noise of low conductance (high sensitivity) measurements such as current measurements across single transmembrane ion channels.

By using the voltage clamp technique membrane resistance and capacitance can be determined. Furthermore, low conductance activities of inserted transmembrane proteins can be measured. This can be done due to the electrical behaviour of biomimetic membranes, which can be represented by an equivalent circuit consisting of a resistor in parallel with a capacitor[101].
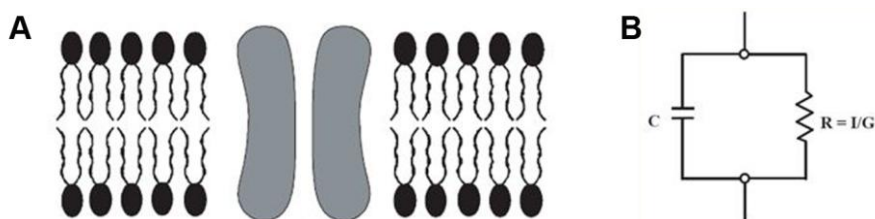

Figure 4.4. The biomimetic membrane behaviour compared with an electrical circuit. (A) Biomimetic membrane; lipid bilayer representing capacitance (black structures) with incorporated ion channel representing conductance (in gray). (B) An electrical circuit consisting of a resistor (R) in parallel with a capacitor (C).

The resistance of a biomimetic membrane is an indication of the membrane seal across the aperture(s). This value is especially important for high sensitivity measurements such as measurements of current across single ion channels (in the range of pA) where an electrical seal in the range of GΩ is required. To determine the membrane resistance, a square voltage signal (U) is applied across the membrane and the measured steady-state transmembrane current amplitude (I) is converted into a membrane resistance (R) using Ohm´s Law:

$$U = R \cdot I \tag{4.3}$$

The membrane capacitance (C_m) is used to determine the thickness and the effective membrane area[102, 103]. For lipid membranes, the bilayer area usually does not cover the entire aperture on which it is formed[104]. Therefore, the estimation of the bilayer area is an important measure of the effective membrane area that is suitable for functional reconstitution of membrane proteins. Capacitance (C) is a measure of the amount of charge that can be stored in a capacitor at a given voltage. A simple capacitor consists of two parallel conducting plates separated by an insulator. The amount of charge that can be stored in such a capacitor is directly proportional to the area of its surfaces (A), the dielectric constant (κ), the permittivity of free space (ε_0), and the distance between the plates (d).

$$C = \frac{(\varepsilon_0 \cdot \kappa \cdot A)}{d} \tag{4.4}$$

In the case of biomimetic membranes, the two plates are formed by the head groups, separated by an insulator, the hydrophobic membrane core. These membranes thus behave electrically as capacitors. Furthermore, since all biological membranes have a similar bilayer composition, Eq. 4.4 can be simplified to:

$$C = C_s \cdot A \tag{4.5}$$

The capacitance is thus directly proportional to membrane area (A), depending otherwise only on a constant, the specific capacitance C_s, which is determined for similar membranes and available in the literature[102]. C_s values for solvent-containing lipid membranes have been determined to lie in the range $0.3 - 1$ µF cm^{-2}, depending on the amount and type of solvent present. Membranes containing solvents made up of short alkanes like decane, exhibit C_s of 0.3 - 0.4 µF cm^{-2}, whereas larger molecules such as squalene produce "solvent-free" lipid membranes with a C_s of 0.78 µF cm$^{-2, \, 103, \, 105}$. To determine the membrane capacitance, a triangular voltage signal (U) is applied across the membrane. The accumulated charge (Q) across the membrane is given by:

$$Q = C \cdot U \tag{4.6}$$

The membrane cycles between charging (when the applied voltage increases) and discharging (when the applied voltage decreases). The transmembrane current (I) is given by the change in accumulated charge over time:

$$I = \frac{dQ}{dt} = C \cdot \frac{dU}{dt} \tag{4.7}$$

When dU/dt becomes negative, the capacitive current changes direction. By applying a triangular voltage signal, a constant dU/dt is obtained in between the direction changes. Therefore, the capacitive charging and discharging transmembrane currents are constant, ideally giving rise to a square-shaped membrane response signal (Figure 4.5). Since dU/dt and I are constant, the capacitance can easily be calculated.
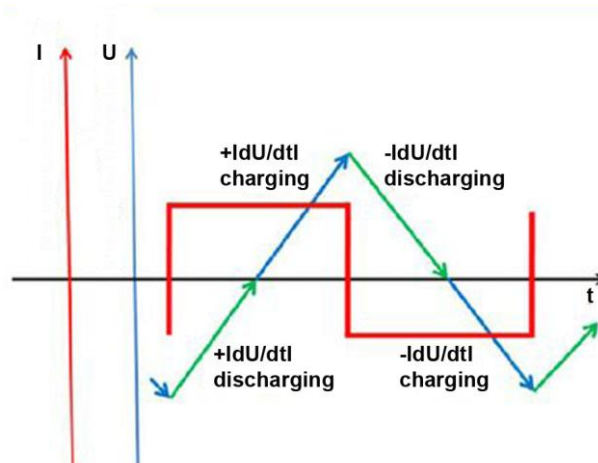
Figure 4.5. A membrane capacitance measurement, showing theoretical relationships between applied triangular input signal, U and the resulting membrane response, I (red). The membranes can be regarded as parallel plate capacitors that continuously cycle between charging and discharging. Whenever dU/dt changes sign the capacitive current changes direction. In between the direction changes the charging and discharging currents are constant since dU/dt is constant. This gives rise to the square shaped membrane response signals. Figure taken from[100].

A membrane with a good electrical characteristic (with a capacitance value indicating sufficient effective membrane area and with a resistance in the range of GΩ indicating membrane tightness) may be selected to

ion channel incorporation. Voltage clamp measurements may be used as well for this kind of experiments. By applying a dc voltage across the membrane, ion channel incorporation can be observed by an increase in conductance due to ionic current through the channel. In this thesis, additionally to C_m and resistance measurements, incorporation of two ion channels, α-HL and FomA, into lipid bilayers using the described technique, is presented.

4.3. Fluorescence microscopy

Fluorescence microscopy is a technique that can be used to optically study biomimetic membranes. This technique can monitor the membrane formation process as well as protein incorporation. Moreover, it can detect the distribution of lipids and proteins in the membrane. The main requirement of fluorescence microscopy is that the object of interest fluoresces. Fluorescence is the emission of light that occurs within nanoseconds after the absorption of light that is typically of shorter wavelength. The critical property that makes this technique so powerful is the Stokes shift – the difference between the exciting and emitted wavelengths. By completely filtering out the exciting light without blocking the emitted fluorescence, it is possible to see only the objects that are fluorescent. In contrast to absorption techniques in which objects are stained with agents that absorb light and the amount of light absorbed becomes only infinitesimally different from the background for small objects, in fluorescence, even single fluorescent molecules are visible if the background has no autofluorescence.

Molecules that are used by virtue of their fluorescent properties are called fluorophores. Many lipids and proteins are labelled with them and are commercially available. The fluorophores are covalently linked to the biomolecule of interest. Common fluorophores used for labelling lipids include fluorescein, rhodamine and 4-nitrobenzo-2-oxa-1,3-diazole (NBD). In this thesis, the fluorescent lipid analogue 1-Oleoyl-2-[6-[(7-nitro-2–1,3-benzoxadiazol-4-yl)amino]hexanoyl]-sn-glycero-3-phosphocholine (NBD-PC) in the membrane bilayer forming solution (BFS) and Texas Red® labelled FomA protein were used for bilayers formation and protein incorporation observation, respectively.

In fluorescence microscopy, the specimen is illuminated with light of a specific wavelength (or wavelengths), which is absorbed by the fluorophores, causing them to emit light of longer wavelengths. The illumination light is separated from the much weaker emitted fluorescence through the use of a spectral emission filter. Typical components of a fluorescence microscope are a light source (xenon arc lamp or mercury-vapour lamp), the excitation filter, the dichroic mirror (or dichroic beamsplitter), and the emission filter (see Figure 4.6). The filters and the dichroic mirror are chosen to match the spectral excitation and emission characteristics of the fluorophore used to label the specimen. In this manner, the distribution of a single fluorophore (colour) is imaged at a time. For multicolour images several single colour images must be obtained and combined.
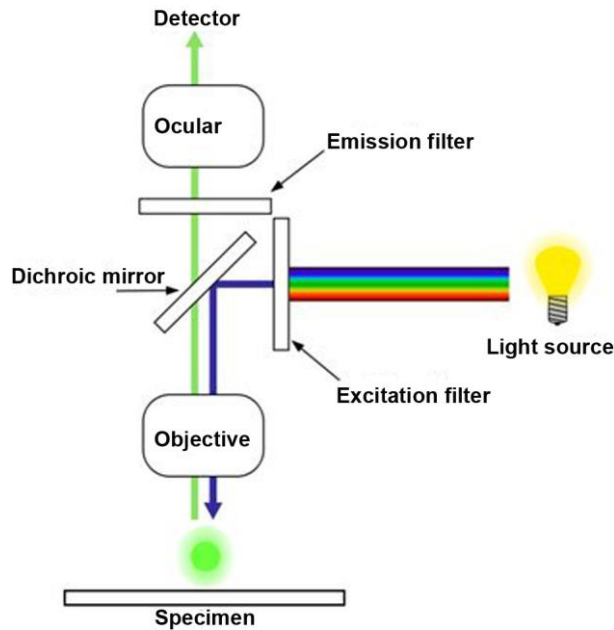
24

Figure 4.6. A schematic of a fluorescence microscope. Typical setup consists of a light source, the excitation filter, the dichroic mirror and the emission filter. The specimen is illuminated with light of a specific wavelength (or wavelengths), which is absorbed by the fluorophores, causing them to emit light of longer wavelengths. The illumination light is separated from the much weaker emitted fluorescence through the use of a spectral emission filter. Figure taken from[106].

4.4. NanoSight technology

NanoSight technology provides an instrument and analysis method to determine the size of nanoparticles in liquid down to 10 nm. NanoSight visualises, measures and characterizes virtually all nanoparticles. The used analysis method "Nanoparticle Tracking Analysis" (NTA) relates the rate of Brownian motion to particle size. The rate of particle movement is related only to the viscosity of the liquid, the temperature and size of the particle and is not influenced by particle density or refractive index (for particles with size between 10 nm and 1 μm).
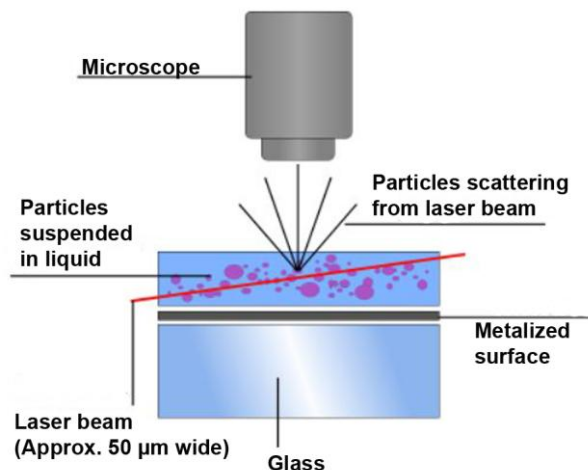

Figure 4.7. A schematic of NanoSight technology principles. The particles are illuminated by the laser light and then visualised by virtue of the light they scatter. Figure taken from[107].

In NanoSight's instrument, the sample with nanoparticles of approximately 0.3 ml in volume is injected into a viewing chamber. The particles are illuminated by the laser light and then visualised by virtue of the light they scatter. Sample concentration is adjusted to between 10^7 and 10^9 particles/ml to ensure accuracy and statistics of analysis. Typical analysis time is approximately 30 s. A charge-coupled device (CCD) camera captured the light scattered by the particles, then the motion of each particle is traced from frame to frame. The NTA software is then able to identify and track individual nanoparticles moving under Brownian motion and relates the movement to a particle size according to the following formula derived from the Stokes-Einstein equation:

$$\overline{(x, y)^2} = \frac{2 \cdot k_B \cdot T}{3 \cdot r_h \cdot \pi \cdot \eta} \tag{4.8}$$

where k_B is the Boltzmann constant and $\overline{(x, y)^2}$ is the mean squared displacement of a particle at a temperature T, in a medium of viscosity η, with a hydrodynamic radius of r_h. The Eq. 4.8 takes into account the fact that the particles are tracked in only two dimensions.

In this thesis, liposomes and proteoliposomes were characterized using the above described technology. Size distribution analyses of nanoparticles were performed with NanoSight LM10 and NTA 2.0 Analytical software (NanoSight Ltd., Amesbury, UK). Around 1 ml of 0.001 mg/ml sample was needed to perform each measurement three times. The samples were measured for 90 s with manual shutter and gain adjustments. Mean and standard deviation values were obtained from mono-modal model fittings using the nanoparticle tracking analysis (NTA) 2.0 software and are presented in Chapter 8 of this thesis.

4.5. Atomic Force Microscopy

The microfluidic device presented in Chapter 6 was designed and fabricated for AFM measurements of fluidic biomimetic membranes and therefore the basic principles of this technique are described in this section.

AFM is a technique used for imaging, measuring, and manipulating matter at the nanometer scale. The main components of the AFM are a cantilever ended with a sharp tip (probe) that is used to scan the specimen surface, the feedback system and the XYZ scanners. Commonly, silicon or silicon nitride cantilevers are used with a tip radius curvature on the order of nanometers (typically less than 50 nm). The sample area scanned in AFM is generally less than 100 μm x 100 μm and the heights of surface features scanned are less than 20 μm. The tip of the cantilever is brought into close proximity of a sample surface, and then the cantilever is deflected, according to Hooke's law, due to the forces between the tip and the sample. To measure the deflection, typically, a laser spot reflected from the top surface of the cantilever into an array of photodiodes is used. Other methods include optical interferometry, capacitive sensing or piezoresistive AFM cantilevers. To adjust the tip to sample distance, to maintain a constant force between the tip and the sample and avoid a risk that the tip collides with the surface, a feedback mechanism is implemented. This is a piezoelectric tube (which expands and contracts proportionally to an applied voltage) that can move the sample in *x, y* and *z* directions for scanning the sample and maintaining a constant force, respectively. The

resulting map of the area *z = f(x,y)* represents the topography of the sample. A schematic illustration of the AFM setup is presented in Figure 4.8. Depending on the application, the AFM can operate in many modes. Generally, possible imaging modes can be divided into static (contact) modes and dynamic (non-contact) modes where the cantilever is vibrated. In static mode, the cantilever is moved across the surface and its topography is measured directly using the deflection of the cantilever. In the dynamic mode, the cantilever is externally oscillated at or close to its fundamental resonance frequency or a harmonic. The oscillation amplitude, phase and resonance frequency are modified by tip-sample interaction forces. These changes in oscillation with respect to the external reference oscillation provide information about the sample's topography.
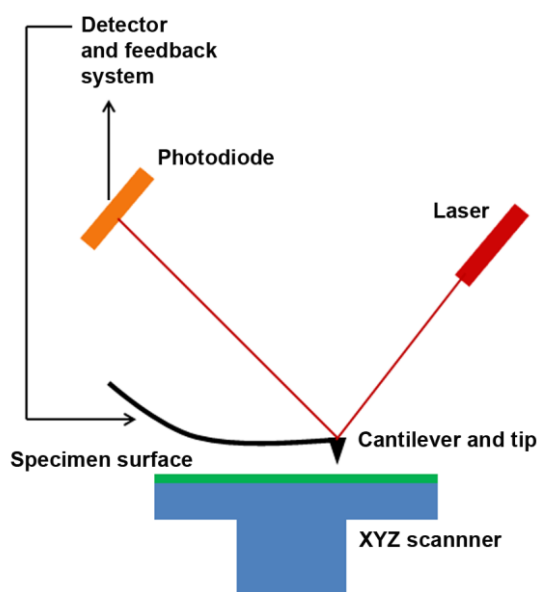

Figure 4.8. A schematic illustration of the AFM setup. The main components: a cantilever ended with a sharp tip (probe) that is used to scan the specimen surface, the feedback system and the XYZ scanners.

In this thesis, the designed and fabricated microfluidic AFM device was specifically used for AFM investigation of fluid polymeric membranes suspended over 300 µm in diameter apertures separating two aqueous compartments. Previously, it had been recognized that using the most prevalent tapered AFM probes to study fluidic systems is problematic due to a non-constant wetting. On the other hand, the usefulness of the nanoneedle probe in this kind of studies was shown[108]. Therefore the fluid biomimetic membranes were scanned with both types of tips, a nanoneedle probe (Nauganeedles, Louisville, KY, US) that was modified with a Ag_2Ga crystal grown out from the end of a tetrahedral tip and a AC240TS probe (Olympus, Ballerup,Denmark), which has a tetrahedrally shaped tip, was used as a reference. With both probes, force volume maps consisting of force-distance (deflection of probe vs. the Z-distance) data were collected in 2D grids and analysed. The measurements were done in contact mode and both probes were fully submerged in the water at all times. The use of the nanoneedle probe significantly reduced the amount of measurement artefacts and increased the precision of the probing comparing to the tetrahedrally shaped tip[28].

5. Devices used in this thesis

In this PhD project biomimetic membranes were formed and investigated by different methods. This required the use of different devices to satisfy the experimental conditions for the different performed experiments. I was involved in either design, fabrication or testing of four different devices as described below. A device roadmap (Figure 5.1) is provided to show the order in which the devices appeared in the thesis (see arrows), their names, illustrations and possibilities, chapters they are used in and the description of my role related to each device. Characteristics of these devices and formed in them biomimetic membranes are presented in Table 1.
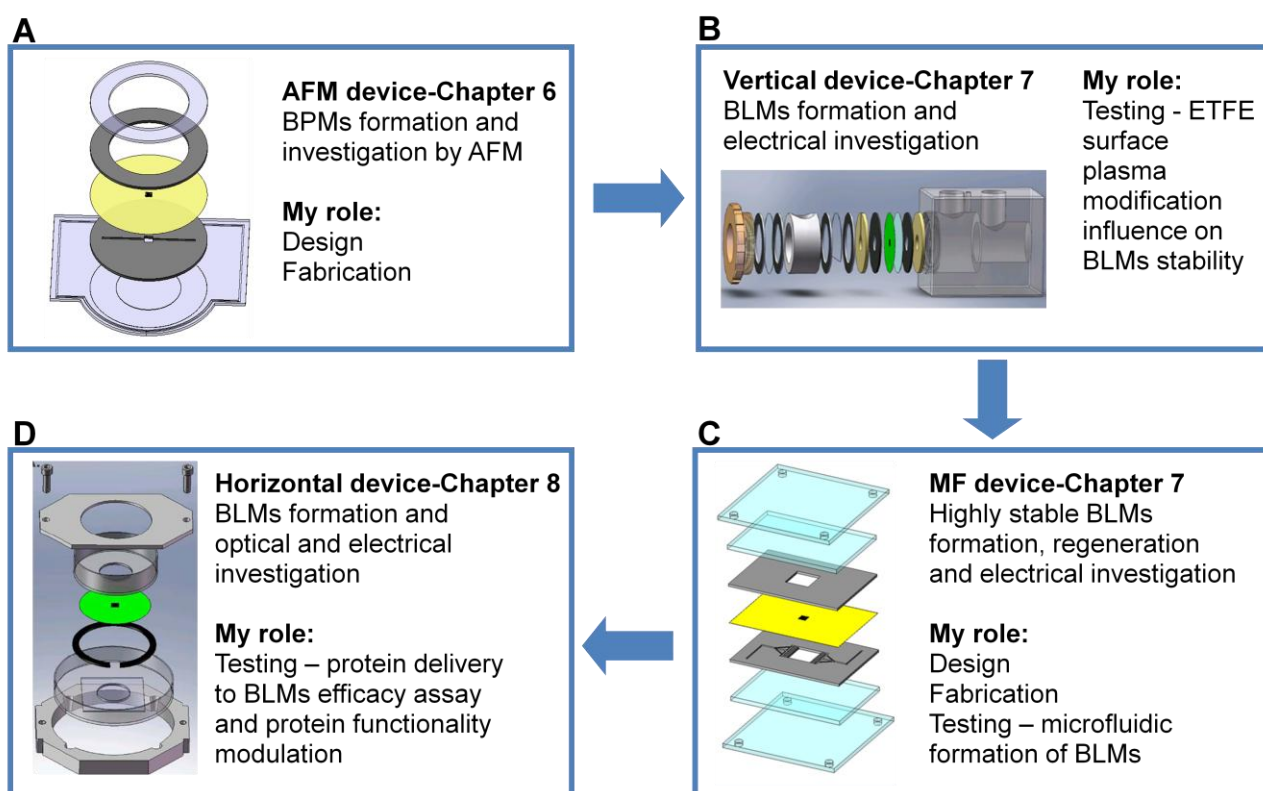

Figure 5.1. The PhD project roadmap related to the four devices used in this thesis. Arrows show the order in which the devices appear in the thesis.
(A) Atomic force microscopy device (AFM device); the component order of assembly is from bottom to top: a PMMA plate (grey), a Viton® with microchannels and a small chamber (black), an ETFE partition with an array of apertures in the middle (yellow), a Viton® ring (black), a PMMA ring (grey).
(B) Vertical device; the component order of assembly into the main Teflon chamber (grey) is from right to left: a Teflon spacer (yellow), a Viton® ring (black), a circular cellulose sheet (blue), an ETFE partition (green), a Viton® ring (black), a Teflon spacer with a slit (yellow), a Viton® ring (black), a cut glass cover slip (transparent) and another Viton® ring (black). Following this, a cylindrical Teflon tube (grey) is placed onto to the inserted components, and a glass cover slip (transparent) is clamped between two Viton® rings (black) to create a window for visual inspections into the assembled chamber. Finally, an annular brass screw is used to clamp all of the components to ensure a tight chamber, figure taken from[9].
(C) Microfluidic device (MF device); the component order of assembly is from bottom to top: a PMMA clamping holder (blue), a PMMA plate (blue), a Viton® with microchannels (black), an ETFE partition with an array of apertures in the middle (yellow), a Viton® with microchannels (black, note that the microchannels contact the ETFE partition and are invisible in the view shown here), a PMMA plate (blue), and a PMMA clamping holder (blue).
(D) Horizontal device; the chamber order of assembly is from bottom to top: an aluminium holder (grey), a MatTek 50-mm-glass-bottom culture dish (transparent), cut Viton® ring (black), a MatTek 35-mm-diameter with a micro-structured ETFE partition (green) glued onto the bottom across the centre hole, an aluminium holder (gray), figure taken from[81].

Table 1. Characteristics of devices used in this thesis and membranes formed in each device.

	Device characteristic				Membrane array characteristic			
	Partition orientation	**System type**	**Process type**	**Operation mode**	**Lifetime /h**	**Capacitance /pF**	**Coverage of the aperture array area with the bilayer area/% [a]**	**Conductance /nS**
AFM device	Horizontal	Open	Flow	Manual	-	-	-	-
Vertical device	Vertical	Open	Batch	Manual	~140 [b, d]	~8600 [b, d]	~50 [b, d]	~40 [b, d]
MF device	Horizontal	Closed	Flow	Automatic	~42 [b, e]	~4300 [b, e]	~24 [b, e]	~250 [b, e]
Horizontal device	Horizontal	Open	Batch	Manual	~1 [b, f] ~16 [c, f]	~9750 [b, f] ~50000 [c, f]	~54 [b, f] ~31 [c, f]	~61 [b, f] 2000-5000 [c, f]

[a] calculations were made taking the C_s value of a decane containing lipid bilayer equal to 0.4 µF cm^{-2}, [103]

[b] membranes were made across 8×8 array of apertures in ETFE[93]

[c] membranes were made across 24×24 array of apertures in ETFE[81]

[d] membranes characteristic was taken from Paper II

[e] membranes characteristic was taken from Paper III

[f] membranes characteristic was taken from[81]

6. Microfluidic device for biomimetic polymer membrane imaging with atomic force microscopy

In developing biomimetic-membrane based devices, lipid or polymer bilayers must first be formed, and further investigated in order to incorporate functionally active proteins. The advantages of using microfluidics for this purpose were presented in Chapter 3 (section 3.2). Here, the design, fabrication and utility of a microfluidic device for biomimetic membranes formation and investigation by AFM are presented. The content of this chapter is based on results described in Paper I and some unpublished material. The complete publication is enclosed at the end of the thesis.

Free-standing BLMs or BPMs serve as model biomimetic membranes and characterizing their mechanical, optical and electrical properties has been investigated for many years[6]. Recently, AFM has been increasingly attracting interest to give topographic information of free-standing membranes where free-standing lipid membranes with diameters up to 250 nm have been investigated[109, 110, 111]. However, characterization of micrometer-scale biomimetic membranes is challenging due to difficulties with probing large membranes with commonly used AFM probes[112]. To investigate the probes that may be useful to study biomimetic membranes a microfluidic device was designed and fabricated (Figure 5.1A). The device facilitates AFM measurements of BPMs.

In order to design a device for investigating biomimetic membranes by AFM, several requirements must be fulfilled. As mentioned in Chapter 3 (section 3.1.1), BPMs are usually formed across a perforated hydrophobic partition separating two aqueous compartments. In our research group an array of apertures was recently designed, fabricated and optimized in a hydrophobic ETFE partition with its optical image presented in Figure 6.1A[93]. Moreover, both lipid and polymer membranes were successfully formed on it[9, 15, 81], which is why it was also used to build the AFM device. The polymer forming solution must be brought in close proximity to the apertures where a slow thinning process may be induced. Manual delivery of polymer forming solution by pipetting and thinning into bilayers with an air bubble or an inoculation loop is feasible and sufficient for simple electrical and optical measurements of biomimetic membranes, however, it is not a suitable method for biomimetic membranes characterization with AFM. Here, several limitations is imposed by the AFM instrument and must be considered. The device should be small enough to fit onto a microscope stage and should have an open access from the top in order to probe the membrane with the AFM tip. Therefore, the only access to apply the polymer forming solution is from the bottom. A microfluidic channel placed underneath the partition seemed to be the best choice; since it may deliver the polymer forming solution to the apertures and induce the membrane thinning process. Moreover, the dimensions of the top compartment should fit to the tetrahedral tip of the AFM cantilever and the device should be transparent in order to monitor the membrane formation process optically. The major challenge was to seal the device against leakage, which was a serious problem when combining the microfluidic channel with the highly hydrophobic ETFE partition. Figure 6.1B shows a schematic cross-sectional view of the conceptual device that fulfil the above mentioned requirements (Paper I)[28].
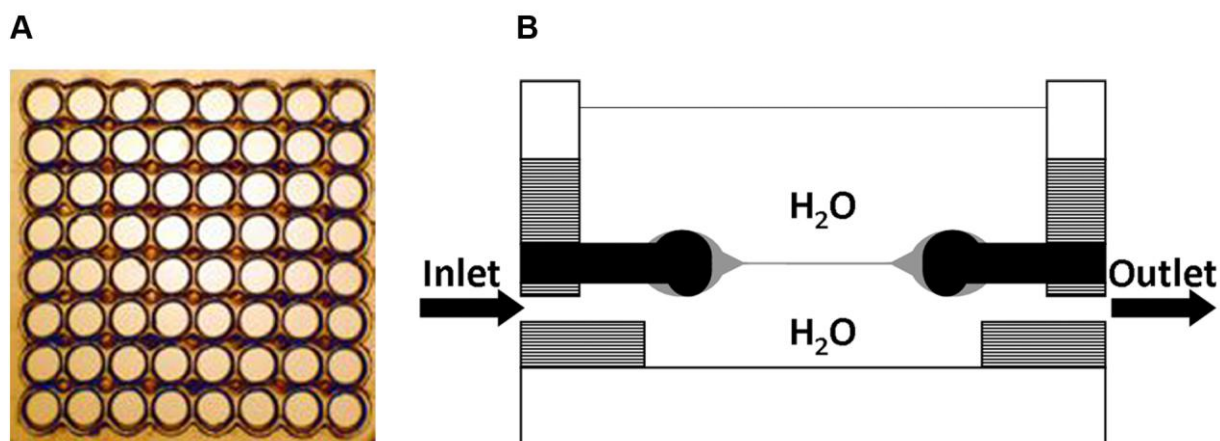
Figure 6.1. (A) An optical image of an array (8x8) of apertures (300 μm in diameter, 400 μm neighbouring apertures centre to centre distance) made in ETFE partition used for biomimetic membrane formation in a device constructed for AFM imaging[93]. (B) A schematic cross-sectional view of the conceptual device for BPMs investigation with AFM. The fluid polymer membrane (gray) is formed across a circular aperture (300 μm diameter) in an ETFE scaffold (black) by injecting the polymer solution through inlet and outlet microchannels made in a spacer ring (dashed grey boxes) of the bottom chamber. The top chamber is open for AFM. The device is clamped via two supportive transparent structures (white boxes)[28].

The final AFM device design is presented in Figure 5.1A and a photo of the assembled device is shown in Figure 6.2B. The device was entirely fabricated by CO_2 laser ablation, in PMMA, ETFE and Viton® materials. Laser settings (number of laser beam passes, laser power and velocity) were adjusted individually to each device part. Two microchannels (21×0.4 mm) and a small chamber (4×4 mm) between them were fabricated in 1 mm thick fluoroelastomeric (Viton®) material (Φ=52 mm). This part was then mounted with double adhesive tapes to a supportive and transparent PMMA plate (7.7×8.8 mm) and ETFE partition (Φ = 52 mm) in a way that microchannels were placed underneath the ETFE partition. A supportive PMMA plate worked as a device holder that had a shape and dimensions fitting well onto the microscope stage. A second fluoroelastomeric part, a ring (Φ_{inner} = 32 mm, Φ_{outer} = 52 mm) was glued with a double adhesive tape on the other side of the ETFE partition. On top of that a second PMMA part, a ring (Φ_{inner} = 32 mm, Φ_{outer} = 52 mm) was mounted again with a double adhesive tape. The two rings, PMMA and Viton® formed an open access chamber for the AFM probing of membranes formed across an array of 8×8 apertures (300 μm in diameter, 400 μm - centre-centre distance between neighbouring apertures) made in the central 50 μm thick ETFE partition by laser micromachining as previously described[93]. The ETFE surface was covalently modified by plasma treatment with the mixture of hexene isomers, resulting in a hydrophobic surface coating (Paper II).

Prior to alignment and assembly the different parts were cleaned by flushing or sonication with ethanol and water. To enable connection of the Viton® microchannels to the outer world, prior to sealing, 0.5 mm in diameter needles were put on two sides of the Viton® material. The needles' plastic parts were glued to the PMMA plates providing stable interconnection between the Viton® microchannels and PTFE tubing with an inner diameter of 0.8 mm and an outer diameter of 1.6 mm (Bohlender GmbH, Germany), see Figure 6.2A.
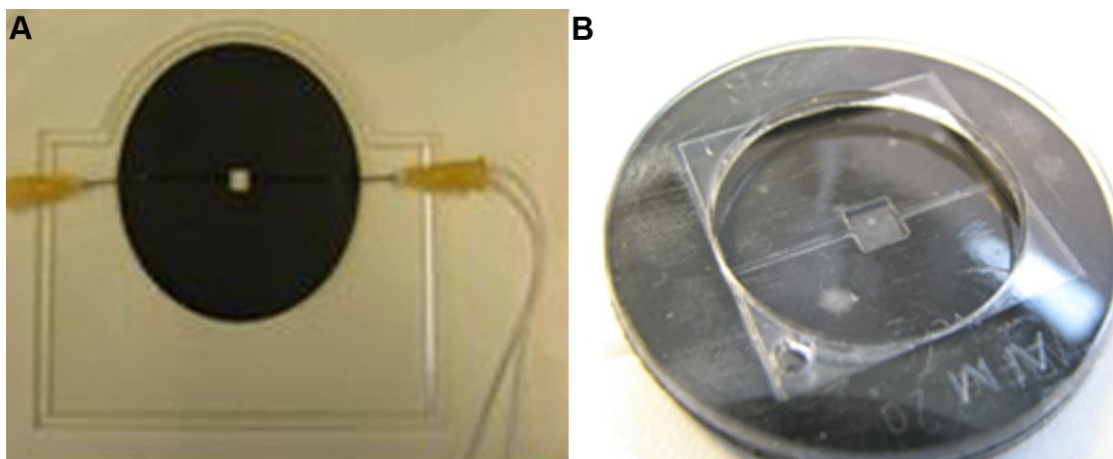
Figure 6.2. Photos of the AFM device; (A) the device assembly process, on top of a transparent PMMA plate, a black Viton® with microchannels and a small chamber is placed, then needles with PTFE tubing are inserted (B) A fully assembled device.

The designed, fabricated and assembled microfluidic device was suitable for AFM measurements of biomimetic membranes. The device fitted perfectly on the AFM microscope stage, specifically on the MFP-3D AFM instrument (Figure 6.3A). It enabled a micrometer-scale membranes formation and investigation. Microfluidic channels were implemented from one side of the device, leaving its top compartment accessible for membranes probing with the AFM tip. A fluoroelastomeric material, Viton®, provided an excellent chemical resistance to solvents used for biomimetic membranes formation and together with double adhesive tapes greatly sealed the device. On the other hand, a stiffness and transparency of the PMMA material provided a compact device and enabled to observe membranes formation process optically. In this design, the membrane thinning process was induced by manual controlling the velocity of the injected into the microchannel fluid.

The final testing of this device is presented in Paper I[28]. While monitoring the scaffold with the AFM instrument's internal camera, BPMs were created by injecting polymer solution, followed by Mili-Q water into into the bottom chamber of the AFM device. Membrane thinning was promoted by controlling the velocity of the injected water and optical observation (inserts in Figure 6.3B and C). By the aid of the AFM device, topographic maps of the BPMs were constructed with an AC240TS probe (Figure 6.3B) and a nanoneedle probe (Figure 6.3C). The topographic maps demonstrated that the nanoneedle probe was suitable to study fluidic polymer membranes, and that it significantly reduced measurement artefacts and increased the precision of the probing comparing to the conventional tetrahedrally shaped tip.
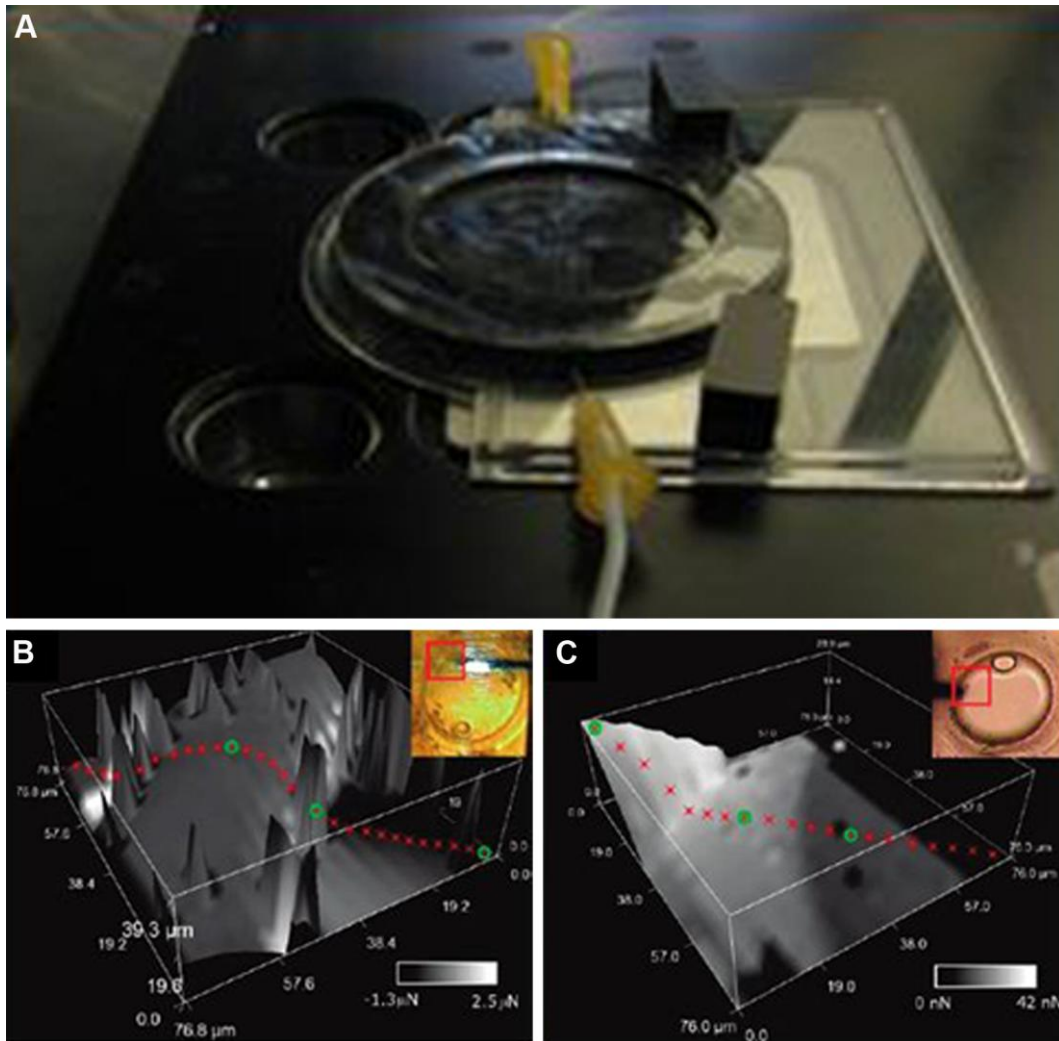
Figure 6.3. (A) AFM device mounted on the AFM microscope stage; (B) and topographic maps of the BPM probed with the AC240TS probe and (C) with the nanoneedle probe. Inserts show optical images of the probed membrane systems where the red squares delimit the areas measured by AFM. (B) and (C) taken from Paper I[28].

7. Formation of highly stable biomimetic membrane arrays

Among the difficulties that must be overcome to build a biomimetic membrane-based device are the inherent fragility of lipid membranes and the challenge of up-scaling the effective membrane area. Various methods for the formation of membrane arrays with long lifetimes (>days) have recently been investigated. Some of them addressed coupling/adhesion at the interface between the biomimetic membrane and its surrounding scaffold[81], others involved microfluidics[8]. The two approaches are presented in this chapter and are based on results described in Paper II and Paper III as well as some unpublished material. Here, the papers are shortly summarized and only the results that I was involved in achieving are presented. Information that is more detailed can be found in the complete publication and manuscript that are enclosed at the end of the thesis.

7.1. Surface modification of partition for stabilizing biomimetic membrane arrays

A partition pre-treatment step is commonly used before stable lipid bilayers can be created. This process typically consists of applying a hydrocarbon solvent to the partition, which then is allowed to dry prior to filling the chamber compartments with the electrolyte solution[113]. This provides a proper interaction of the lipid molecules around the aperture edge and ensures stabilization of the lipid bilayer. The traditional pre-treatment process can be mimicked by changing of the chemical composition of the partition surface. In case of an inert ETFE partition, surface plasma polymerization may be used[114-117]. The investigation how the ETFE partition modification by plasma polymerisation influences the biomimetic membrane array' lifetime and quality is presented in Paper II.

The average lifetime for membranes formed across partitions modified on both sides with three different modifications (*n*-hexene, 1-decene and HMDSO) were tested and the membranes' quality was assessed by characterizing their electrical properties, specifically membrane conductance, G_m and capacitance, C_m. Lipid bilayers were established in the vertical device, see Figure 5.1B. *n*-Hexene applied on both sides of the ETFE greatly improved the average membrane array lifetime (a maximum lifetime of 6 days) compared to the other two modifications and an unmodified partition. Membranes formed across *n*-hexene treated ETFE partition evolved from G_m = 210 nS and C_m = 1800 pF immediately after membrane formation to G_m = 40 nS and C_m = 8640 pF after 140 h. Taking the C_s value of a decane containing lipid bilayer to be 0.4 µF cm^{-2}, [103], the final capacitance of the membrane in double-sided n-hexene coated partition corresponded to a bilayer membrane area which is roughly 50% of the available aperture area (Table 1).
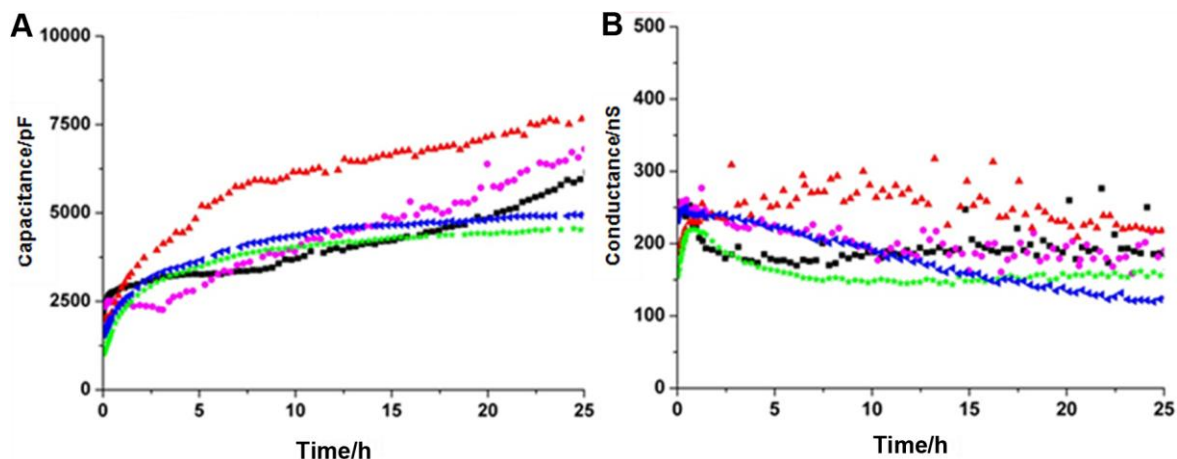
Figure 7.1. BLMs thinning kinetics. (A) Capacitance and (B) Conductance versus time. Values for five different BLMs formed across double-sided n-hexene modified 8×8 ETFE partition arrays. BFS: DPhPC in decane, 50 mg/ml. Note that the total lifetime of BLMs was up to 6 days. Figure adapted from Paper II.

The reproducibility of double-sided *n*-hexene coatings can be quantified by examining the change in C_m and G_m over time. Solvent containing membranes generally undergo a "thinning" process evidenced by an increase in C_m over time while G_m remains constant. The double-sided modification with *n*-hexene resulted in reproducible thinning kinetics (Figure 7.1). Thus *n*-hexene wetting of both front and back surfaces was important for BLM array stability – consistent with BLM stabilization originating from the stability of the Plateau-Gibbs border[113].

7.2. Microfluidic device for formation and regeneration of highly stable biomimetic membrane arrays

A microfluidic approach was pursued to see if the process of generation stable and long-lived biomimetic membranes was achievable in an automated and horizontal setup, with a perfusion system on both sides of the membranes. So far the most stable BLMs (see Table 1) were accomplished in our group using the vertical device presented in Figure 5.1B, in which the process of multiple bilayer formation was established by manual raising the aqueous electrolyte solution leading to raising of the BFS across an array of apertures (Figure 7.2)[9].

Moreover, it was shown that scaling up the membrane area was a means to increase the membrane array lifetime: 8×8 membrane arrays (an average lifetime 1 h) vs. 64×64 membranes array (an average lifetime 16 h)[81], see Table 1. Based on this, the hypothesis was that it should be possible to create stable bilayers by microfluidic pumping of a lipid solution across an array of apertures in a fully automated horizontal device. Subsequent pumping of electrolyte would then induce lipid film thinning. In the design and fabrication of the microfluidic device, experience from the AFM device described in Chapter 6 was taken, the main difference being that not one but two microchannels were implemented on both sides of the perforated ETFE partition. Otherwise, the same materials and fabrication technique were used.
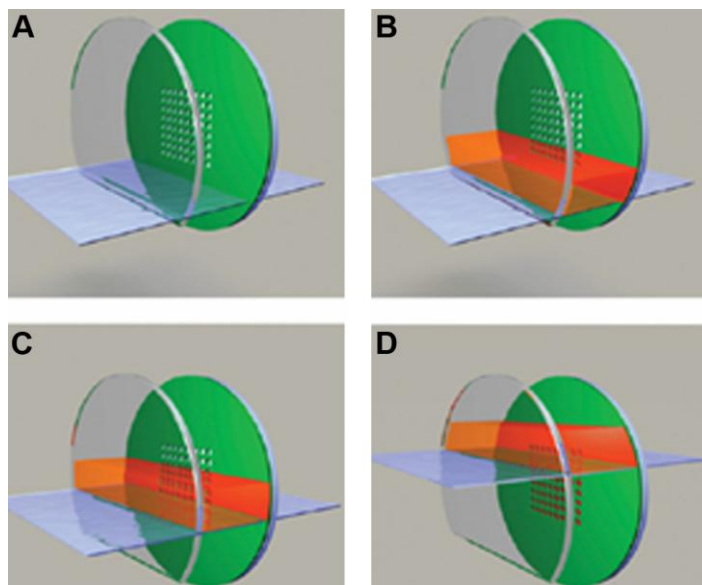
Figure 7.2. Principle of the technique for the establishment of multiple bilayers in the array in a vertical device (Figure 5.1B). The aqueous electrolyte solution (blue) is filled up to the cut glass cover slip (transparent) (A) and the BFS (red) is applied from the top through the slit in the front Teflon spacer (B). The aqueous electrolyte solution is then slowly applied to the front chamber thereby raising the BFS across the multiple aperture partition (green) to form an array of lipid bilayers (C)–(D). Figure taken from[9].

The MF device design, fabrication and assembly process are described in Paper III. Its design is depicted in Figure 1 in that paper. A picture of the fully assembled MF device is shown in Figure 7.3.
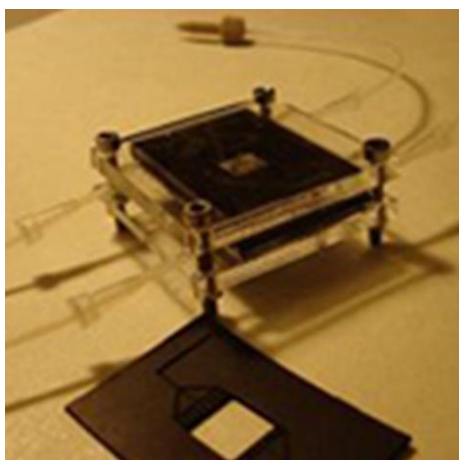
Figure 7.3. Picture presenting the fully assembled MF device.

The microfluidic system set-up, with pumps, injector, syringe barrels and electrodes is illustrated in Figure 2 in Paper III. The whole system was placed in an in-house manufactured Faraday cage in which voltage clamp measurements were performed (Figure 4.3).

Planar lipid membranes were established across the laser microfabricated ETFE partition array by a modification of the lipid bilayer painting method (Figure 3.4)[26]. The main difference was that the lipid bilayer was automatically formed and thinned aided by microfluidics.

Figure 7.4. The procedure for bilayer membranes formation in the MF device; (A) the electrolyte is pumped at a flow rate of 50 µl/min, through the Viotn® microchannels (white boxes) and both compartments of the MF device, (B) 40 µl of the BFS (black) is then injected into the bottom compartment, (C) the excess BFS (black) is removed and the membrane thinning process induced by the continuous flow of electrolyte on both sides of the ETFE partition (grey), (D) finally, electrical measurements on the formed bilayer lipid membranes (black) can be performed. Figure taken from Paper III.

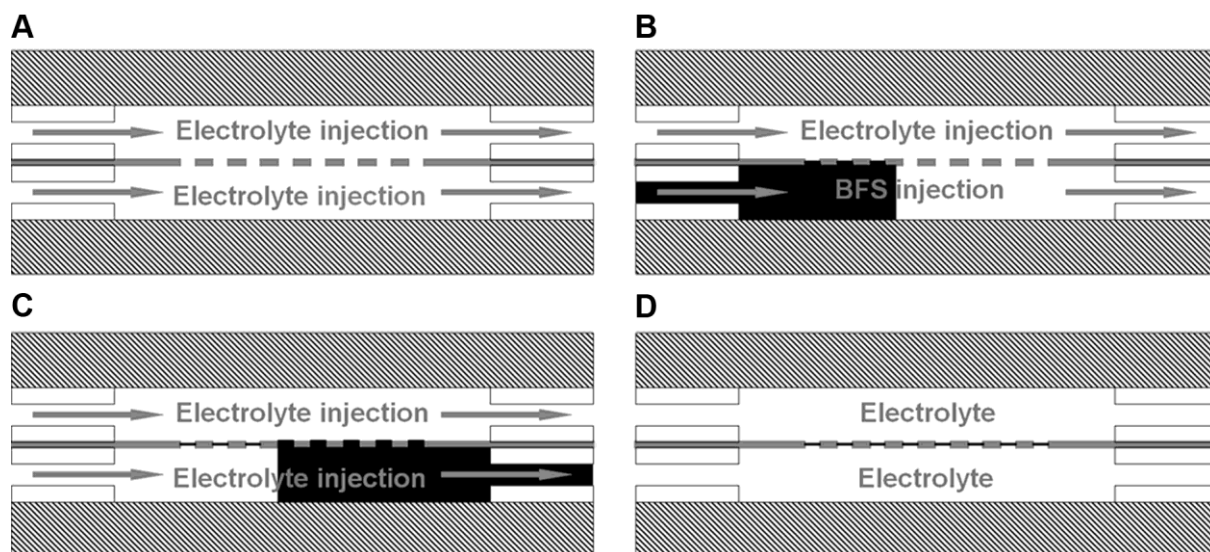The procedure for bilayer membrane formation in the MF device is shown in Figure 7.4. A pre-defined volume of the BFS was injected into the lower compartment of the device, covering the entire membrane support; a process that could be repeated many times (1st, 2nd 3rd generation membrane). Continuous monitoring of C_m and G_m over time indicated whether the BFS thinned into lipid bilayers in the ETFE partition using microfluidic pumping. By continuously pumping electrolyte into the two compartments of the device, excess BFS was removed and the thinning process was electrically studied. For the most stable lipid bilayer arrays; after a first portion of BFS was injected, an increase in C_m was observed after approximately 25 min (increase in effective bilayer area) while the G_m remained at the same level (indicating a tight membrane) (Figure 7.5A, 1st generation membrane). Further pumping resulted in membrane leakage, which finally resulted in breakage of the membrane (an increase in C_m was concomitant with an increase in G_m indicating an increase in ionic leak across the membrane). A 2nd generation membrane was created by injecting a new portion of BFS. As seen in Figure 7.5A, the same behaviour of capacitance and conductance over time was observed as for the 1st generation membrane. When injecting a 3rd BFS portion (Figure 7.5B), it can be seen that the membrane life time (3rd generation membrane) was significantly increased, however, the effective membrane area did not change (the same capacitance value as for the 1st and 2nd generation membranes). Successful formation of the 3rd generation membrane was thus likely enabled by the pre-painting (1st and 2nd generation membranes) of the ETFE partition by the BFS, similarly as previously described[9]. The most stable lipid bilayer arrays established under these conditions had a lifetime of ~42 h and exhibited C_m and G_m values of ~4300 pF and ~250 nS, respectively. The capacitance for lipid bilayers, on a 8×8 array with 300 µm average diameter apertures and a C_s of 0.4 µF cm^{-2} for solvent containing lipid bilayers[113], was expected to be ~18100 pF. This indicated that the lipid bilayers were established and the area of the most stable membranes constituted around ~24 % of the total area of the array.

The lifetime of the 1st, 2nd and 3rd generation membranes created in the MF device was around 5 to 45 min (n = 5), 10 to 180 min (n = 6) and 25 to 42 hours (n = 2), respectively, while their capacitance value was around 1000 to 3300 pF (n = 5), 1700 to 4800 pF (n = 6) and 4300 to 4500 pF (n = 2), respectively.

The results shown here indicate that microfluidics aid and induce the thinning process of the thick lipid-solvent to form highly stable lipid bilayers in an array. Kawano et al.[97] reported that a BLM formed in a micropore was unstable in a device with upper and lower flow channels and that they could improve the stability by forming a lipid membrane across a nanopore instead. The here presented results demonstrate another approach of increasing BLM stability in a closed microfluidic device; by using an array of micropores and microfluidic assisted thinning. This may be attributed to a self-repairing process of the membranes by the surrounding reservoirs.
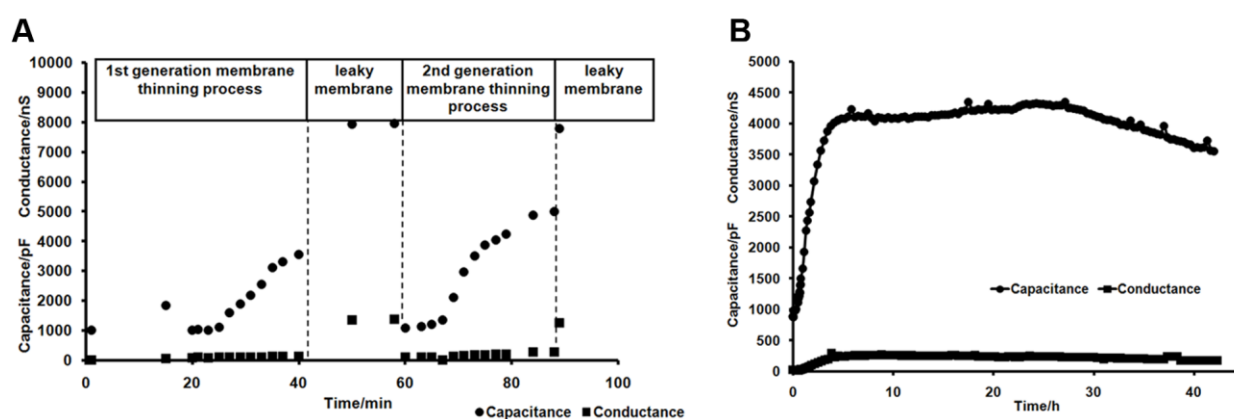

Figure 7.5. Capacitance and conductance versus time created in the MF device. (A) 1st, 2nd and (B) 3rd generation membranes. Membrane thinning process was induced by microfluidic pumping. Figure adapted from Paper III.

7.3. Manual-vertical vs. Microfluidic-horizontal devices for biomimetic membranes formation

The results presented in sections 7.1 and 7.2 showed that membranes formed in two different devices, i.e. manual-vertical (Paper II, Figure 5.1B) and microfluidic-horizontal, MF device (Paper III, Figure 5.1C) went through the "thinning process", an increase in C_m over time while G_m remains constant (Figure 7.1 and Figure 7.5). This is a typical behaviour of solvent containing membranes and indicated that both procedures, i.e. manual-vertical and microfluidic-horizontal enabled the membranes formation. In both devices, the BFS was moved across apertures resulting in the establishment of multiple bilayers in the array (Figure 7.2 and Figure 7.4). However, the advantage of using the MF device is that it enabled the automatic exchange of fluids on both sides of the membranes, what would be beneficial for example in high-throughput screening technologies. Moreover, its horizontal configuration can facilitate membranes characterization by microscopy techniques.

Comparing the lifetimes and areas of membranes formed across double-sided n-hexene modified ETFE partition, created in two different devices, i.e. manual-vertical (Paper II, Figure 5.1B, Table 1) and microfluidic-horizontal, MF device (Paper III, Figure 5.1C, Table 1), both values are smaller for the second device, approximately 3 and 2 times, respectively. This may be attributed to the fact that in a vertical device sometimes more than "three generations" of membranes were formed. Some of them were formed by

lowering and raising the aqueous electrolyte solution with the remaining first portion of the BFS only, other required a new portion of BFS. However, in both cases the membrane stability was improved. Therefore, a future optimisation of the microfluidic system could prove important in order to obtain a uniform lipid/electrolyte solution flow through the device, to have a better control of the pressure applied to the system and to form more than three generation membranes; in this way possibly increasing the effective lipid bilayer area and the membrane array lifetime.

8. Protein delivery and developing biomimetic membrane applications

One of the challenges in building membrane-based devices is sufficient delivery of functional protein to the bilayers. As described in Chapter 3 (section 3.1.3) there are several strategies available for reconstituing proteins into membranes. α-HL membrane protein self-insert into pre-established membranes[47], several *E. coli* OMPs may be reconstituted into planar membranes directly from a detergent solubilised state[48, 49, 50] and in general to incorporate large membrane proteins into planar lipid bilayers vesicle fusion is used[12, 13]. Depending on final application, different amounts of protein must be delivered. Large scale systems, like aquaporin based separation device will require substantial amounts of incorporated proteins, while for sensor applications a smaller amount of protein will be sufficient. It is therefore of interest to evaluate the up-scaling potential of protein delivery system. The direct delivery of the α-HL membrane protein, the vesicle based FomA protein delivery and the FomA delivery from a detergent solubilised state to a bilipid membrane/membrane array are presented in this chapter. Furthermore, the FomA protein functionality is modulated in order to investigate its potential application as a sensor. The content presented in this chapter is based on results described in Paper III and Paper IV as well as some unpublished material.

8.1. Direct protein delivery

To evaluate if functional lipid bilayers were established in the MF device (Figure 5.1C), additionally to C_m and G_m measurements (Figure 7.5), the pore-forming α-HL membrane protein was reconstituted into the lipid bilayer membrane array. The membrane pore of α-HL can be created in a lipid bilayer upon assembly of seven 33 kDa monomeric polypeptides to form an ion conducting pore[118, 119]. The α-HL membrane protein was injected into the bottom compartment of the microfluidic system incorporating in the pre-formed bilayer lipid membrane arrays, and the obtained current trace was recorded (Figure 8.1). Stepwise current increases could be observed and compared with previously presented results[120]. Knowing that α-HL forms pore in lipid bilayers with approximately ohmic conductance we scaled the literature single channel incorporation current value [~35 pA] to our experimental conditions [~70 pA] according to electrolyte conductivity, and our results demonstrate that several α-HL pores were inserted into a lipid bilayer at the time. This electrical recording together with C_m and G_m measurements (Figure 7.5) confirmed that functional lipid bilayers were established in the MF device (Paper III).

The results presented here showed that the MF device enabled the direct α-HL protein delivery to biomimetic membranes. In general, the system provides an environment for reconstituting proteins that is similar to their native one, having the bilayer surrounded on both sides by water, thus providing the possibility of fast and precise measurement of exchange of analytes and ligands through transmembrane protein pores and channels. The developed system shows the potential for formation of biomimetic membrane arrays that could be useful for biochemical studies of proteins and for the development of future sensor arrays and separation technologies.
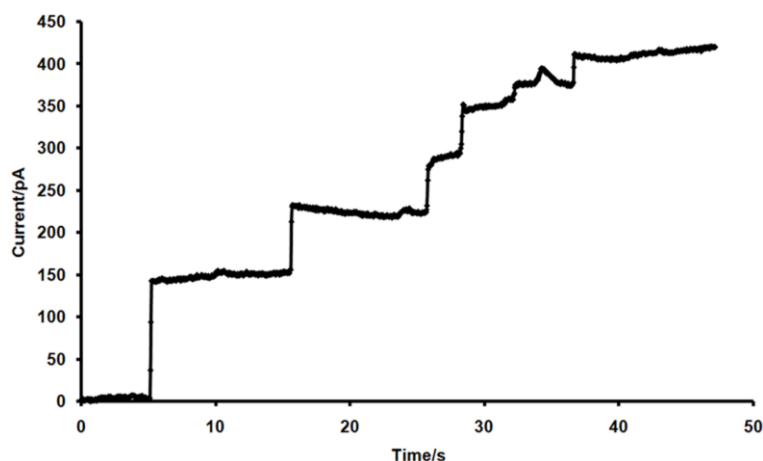
Figure 8.1. Current trace of the reconstitution of the pore-forming heptameric α-HL membrane protein in established in the MF device 8×8 bilayer arrays. Figure taken from Paper III.

8.2. Proteoliposome fusion efficacy assay

As described in Chapter 3 (section 3.1), by using ion channels that remain open after incorporation, the fusion efficacy may be calculated. It has been demonstrated by using the VDAC[52, 63]. With this method about ~100 fusion events corresponding to the insertion of about 500 VDACs in 10 min per mm² membrane area could be obtained. Still VDAC incorporation has to be driven by applying an osmotic gradient across the planar membrane and by addition of divalent cations. In Paper IV, the hypothesis was that one could use FomA as a reporter for vesicle fusion with planar membranes, even in the absence of a transmembrane osmotic gradient. FomA forms trimeric β-barrels where each barrel is predicted to consist of 14 β-strands[121] with the single-channel conductance known[122]. Thus, it should be possible to quantify proteoliposome fusion with planar membranes via the increase in bilayer macroscopic conductance G after incorporation of ion channels, i.e. the G/g ratio can be calculated where g represents the single-channel conductance. Since porins can be tailored to specific functions[123] vesicles with fusigenic engineered FomA porins could also constitute building blocks for functional planar biomimetic membranes per se. FomA vesicle fusogenicity was thus assessed and dependence on proteoliposome LPR and incubation time on FomA membrane incorporation were investigated. The strategy used for FomA protein delivery to the lipid bilayers is presented in Figure 8.2.
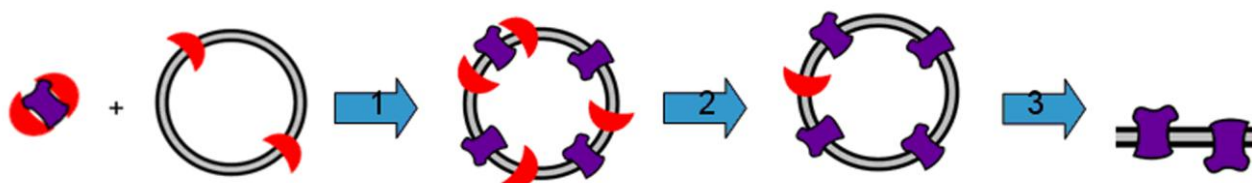
Figure 8.2. Strategy for protein delivery to the biomimetic membrane. Protein (violet) in detergent octyl-β-D-glucopyranoside (OG) (red), mixed with liposome (grey circles) with detergent (arrow 1). The detergent is then removed by dialysis (arrow 2) and the resulting proteoliposome can then be fused with the membrane (grey), (arrow 3). Figure adapted from[3].

The fusion of FomA proteoliposomes with an array of planar membranes was characterized and protein functional activity was assessed by voltage-clamp recordings of lipid bilayers formed using the device

42

presented in Figure 5.1D. A stepwise increase of the current across the bilayer was observed when FomA proteoliposomes were applied in close proximity of the membrane (Figure 1A in Paper IV, upper current trace). The conductance amplitude histogram (Figure 1B in Paper IV) revealed a broad distribution with a mean value of 0.07 nS for a total of 139 fusion events, what is in good agreement with the literature value[122]. These results demonstrated that functionally active FomA was successfully reconstituted into an array of planar membranes at physiologically relevant electrolyte concentrations. Fusion occurred spontaneously when FomA proteoliposomes were placed close to the membrane array, in the absence of osmotic gradients across the membrane needed in other fusion methods, e.g.[13].

In order to evaluate the influence of the protein content of the proteoliposomes on fusion, experiments with proteoliposomes prepared with different LPRs were performed (Figure 2A in Paper IV). The highest fusion efficacy (measured as *G/g*) was achieved with LPR 50 (see Table 2). Fusion efficacy increases when the LPR value decreases from 200 to 50. However, with LPR equal to 25 functional protein incorporation is close to that observed for LPR equal to 200. A reason for the low efficacy at low LPR may be due to the fact that an LPR equal to 25 corresponds to a protein area coverage of 64%. This may be the upper limit for FomA protein reconstitution in proteoliposomes before protein precipitation occurs. It may thus be that only small amounts of protein were reconstituted into proteoliposomes at the nominal LPR equal to 25, leading to concomitant low protein incorporation with the planar membranes. There were no significant size differences between protein-free liposomes and proteoliposomes with nominal LPR equal to 200, 100 and 50, as evidenced by nanoparticle tracking analysis (Figure 2B in Paper IV). Proteoliposomes with nominal LPR equal to 25 has a mean diameter of 200 nm, which is significantly different from the observed liposome diameter of 150 nm. Although we do not know the reason for the apparent size difference, it may be related to the very high protein concentration (and potential precipitation) during the mixing and dialysis steps in proteoliposome production.

Table 2. Proteoliposomes fusion efficacy.

LPR[a]	Proteoliposome FomA coverage %[b]	Number of FomA proteins per proteoliposome[c]	Maximal fusion efficacy G/g [d]
25	64	5,146 ± 933	11,429 ± 4,343
50	47	2,682 ± 971	147,619 ± 31,527
100	31	1,754 ± 635	40,417 ± 16,020
200	18	934 ± 618	524 ± 179

[a] LPR at the step of proteoliposomes preparation. [b] Assuming 0.72 nm^2 lipid polar head surface and 16 nm^2 FomA monomer area. [c] Calculation based on the nominal LPR and the size of proteoliposomes determined by NTA measurements. [d] Assuming single FomA conductance equal to 0.07 nS.

In order to assess how proteoliposome LPR is related to fusion kinetics and membrane stability, membrane currents I (I ~ G/g) over time were analyzed with the two LPR values giving the highest efficacy (LPR equal to 50 and 100) (Figure 8.3A). After addition of 2 μl proteoliposomes (0.16 mg/ml) with LPR equal to 50, the fusion efficacy showed an initial lag phase followed by a second order rise phase (I ~ t^2) within the first 6 s. This is followed by a longer first order (I ~ t) rise phase and finally the current is levelling off, approaching a saturation level. For LPR equal to 100, the initial lag phase is shorter and is followed by a longer first order

rise phase until 6 min (the jumps just after 0.53 min reflect insertion of multiple FomA proteins, cf. Figure 8.3A). After 6 min, an inoculation loop was swept across the entire membrane array. The induced stirring caused the incorporation to follow an exponential time course until a saturating level was reached after 90 min. In cases where some membranes in the array broke during the first order rise phase, they could be recreated by careful local application of an inoculation loop with the efficacy level resulting in current levels returning to the level just prior to membrane breakage. Although LPR equal to 100 results in free-standing membranes reaching saturating incorporation levels, fusion with proteoliposomes having LPR equal to 50 reach several fold higher levels within 10 min. Thus, one may use either slow first-order kinetics, corresponding to passive diffusion of the proteoliposomes up to the membrane, or use stirring for rapid delivery of vesicles to the receiving membrane. The two different kinetic schemes may be considered as part of a microfluidic design where flow conduits and rates may be adjusted for various types of flow, e.g. turbulent flows for creating efficient stirring of the membrane interfacial regions. Subsequently membranes may be stabilized, e.g. via hydrogel encapsulation[124]. Table 2 shows the maximal fusion efficacy (G/g) corresponding to the effective number of trimeric FomA channels incorporated. For LPR equal to 100 the total G corresponds to about 40,000 FomA trimers whereas for LPR equal to 50 a total of 150,000 FomA trimers appears to have been inserted. With the theoretical numbers for single proteoliposome conductances based on their LPRs, this corresponds to insertion of about 54 and 22 proteoliposomes, respectively. However, this is under the assumption that all proteoliposomes have functional protein content corresponding to their LPR and that all proteins retain their functionality after insertion. This may not be the case, and there may be non-functional protein material inserted the membrane together with the functional FomA channels. However, we noted that the G levels off with time for both LPR equal to 50 and 100, approaching a steady state. If the membrane stability was generally compromised due to the presence of non-functional (mis-folded) protein, this would be manifest in large conductance fluctuations and membrane rupture. We did not see evidence of this and conclude that the receiving membrane may contain non-functional protein but that this does not compromise membrane overall integrity.

In order to further characterize proteoliposome fusion into planar membranes, we simultaneously monitored the membrane array optically and electrically. Using the fluorescent lipid analog NBD-PC (1 mol%) in the membrane BFS and Texas Red® labelled FomA, we could observe bilayer formation and protein incorporation (Figure 8.3B and C). For both LPR equal to 50 and 100 we observed high-intensity dots in some membranes in the array moving within the membrane area delimited by the Plateau–Gibbs border. This heterogeneity may reflect that the incorporated protein aggregate in the membrane or that proteoliposomes (or proteins) aggregate on the membrane surface. The heterogeneity is most pronounced for LPR equal to 50 which may reflect the high protein concentration (and possible precipitation) for LPR equal to 50 proteoliposomes.

In summary, an OMP fusion efficacy assay was established and used to quantify proteoliposomes fusion with an array of planar membranes. The influence of LPR on FomA proteoliposomes reconstitution yield was shown. Maximal fusion obtained was almost 150,000 porin insertions during 20 min with proteoliposomes prepared with LPR equal to 50. Incorporation could be established as a process with either first order or

exponential kinetics. This may be of interest to microfluidic designs involving protein delivery to biomimetic membranes developed for sensor and separation applications.
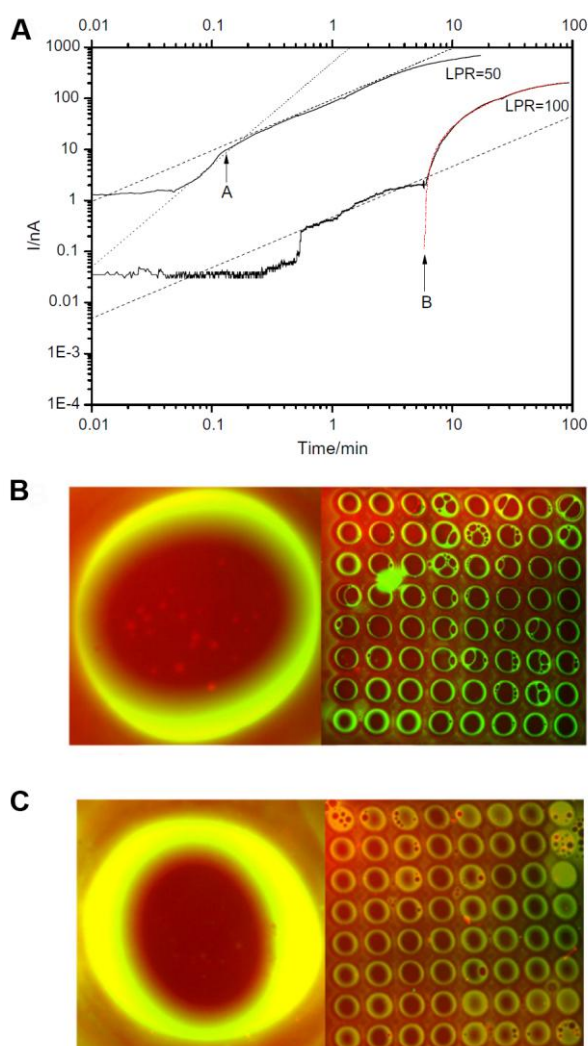

Figure 8.3. Characterization of proteoliposome fusion into planar membranes. (A) Total membrane current I versus time t for proteoliposome LPR = 50 and 100. Straight (guiding) lines indicate first order (I ~ t) (dashed lines) and second order (I ~ t^2) (dotted lines) proportionality, respectively. Arrow A indicates transition from second to first-order kinetics and arrow B indicates onset of exponential kinetics: I ~ A · (1 – exp(-t/τ)). Dashed-dot line (red) represents a fit to the exponential kinetics equation with τ = 30.1 min. (B) Combined fluorescent images of FomA (red) proteoliposomes with LPR = 50 fused into planar membranes (left: single aperture; right: the 8 × 8 bilayer array). (C) As in (B) with LPR = 100. Images were acquired with a 20× (B and C, left) and 2.5× (B and C, right) air-corrected objective. Average ± SD outer aperture diameter for the 8 × 8 array is 300 ± 5 μm. Figure taken from Paper IV.

8.3. Modulation of protein functionality

In the previous section the FomA protein was presented as a reporter that can be used to quantify the protein delivery to biomimetic membranes. In order to achieve this protocol for the functionally active FomA protein delivery was established and the amount of FomA pores that were fused into the biomimetic matrix was calculated. Here, this experience was used for the FomA protein functionality modulation in order to investigate its potential application as a stochastic sensor. The stochastic sensing principles are described in Chapter 3 (section 3.1.4).

FomA belongs to bacterial pore proteins that are typically used as sensor elements due to their robust channel scaffold and ease in production[73]. The use of these proteins in stochastic sensing has recently become popular, where a single channel is used as the stochastic sensing element. Very often proteins are engineered or equipped with molecular adapters to detect the needed substances. Among β-barrel proteins the heptameric α-HL is the most commonly used. Engineered versions of α-HL have been used for sensing of ions[75, 76], proteins[77] and DNA[78, 79], while α-HL with a CD adapter was used for detection of small organic molecules[80]. It was shown that CDs can bind to a variety of other pores, e.g. outer membrane protein G (OmpG)[125, 126], outer membrane protein of *Klebsiella oxytoca* (CymA)[127], and connexins[128]. When placed in α-HL and OmpG pores, the CDs reduce the ionic conductance and small organic molecules reduce it further, which makes it useful in stochastic sensing. In contrast, CDs fully blocked the ionic conductance of CymA pores[127]. The main subject of this part of the thesis is to investigate if FomA can be a candidate pore for stochastic sensing. β-CD was selected as a molecular adapter and its interaction (blocking) with the FomA pore was studied by electrical measurements.

In this part of the thesis, if not mentioned, the same materials, methods and experimental conditions as in the Paper IV were used. Blocking of FomA with β-CD was achieved by adding increasing amount of 10 mM β-CD solution to the top compartment of the horizontal device (Figure 5.1D) or by performing FomA fusion experiments in β-CDs presence. Blocking was observed as changes in current traces.

For the fusion experiments described in Paper IV, proteoliposomes prepared with four different LPRs (200, 100, 50 and 25) were used. In section 8.2 membrane currents I (I ~ G/g) over time were analyzed with the two LPR values giving the highest efficacy (LPR equal to 50 and 100) (Figure 8.3A) in order to assess how proteoliposome LPR is related to fusion kinetics and membrane stability. Here the performance over time for four different proteoliposomes is presented (Figure 8.4) in order to decide on the system that could be used for blocking experiments based on fusion efficacy. The proteoliposomes prepared with LPR equal to 200 (Figure 8.4B) and LPR equal to 50 (Figure 8.4A, in red) were selected for FomA delivery to the lipid bilayers and further blocking with β-CD. The reason for this was that with these two types of proteoliposomes the lowest and the highest fusion rates were achieved, respectively. A small fusion (LPR equal to 200) would be sufficient to monitor a single FomA channel interaction with β-CD, whereas a high fusion would be appropriate to show FomA blocking in bulk.
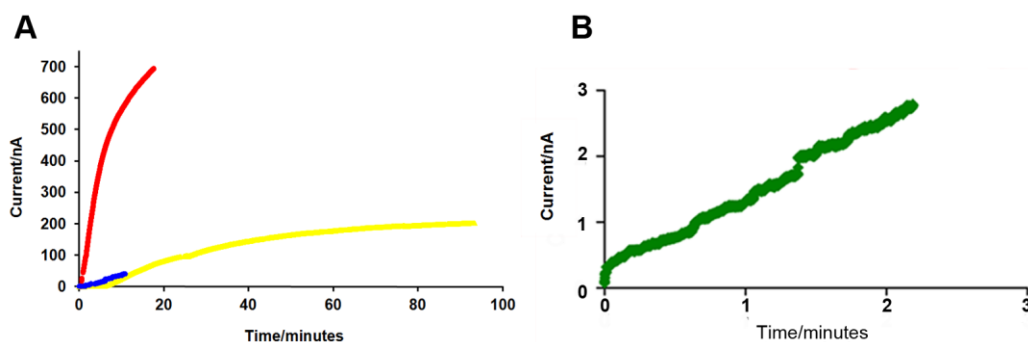

Figure 8.4. Current traces of FomA incorporation into an 8x8 DPhPC/decane membrane array over time for proteoliposomes prepared with different LPRs. (A) LPR=25 (blue), LPR=50 (red), LPR=100 (yellow) (B) LPR=200 (green).

In the case where the protein was delivered using proteoliposomes prepared with LPR equal to 200, a stepwise decrease of the current across the bilayer was observed when increasing amount of β-CD was added, see Figure 8.5A. Red arrows indicate addition of a new portion of blocking agent (β-CD). It can however be seen that an increase of the current with addition of β-CD was sometimes also observed (see blue arrows in Figure 8.5A). This may be attributed to that: (i) not all proteoliposomes used in the fusion experiment were fused and thus still present in the chamber when the blocking experiment was performed; therefore shortly after β-CD addition fusion was as well observed. (ii) the formation of the FomA- β-CD complex is a reversible process.
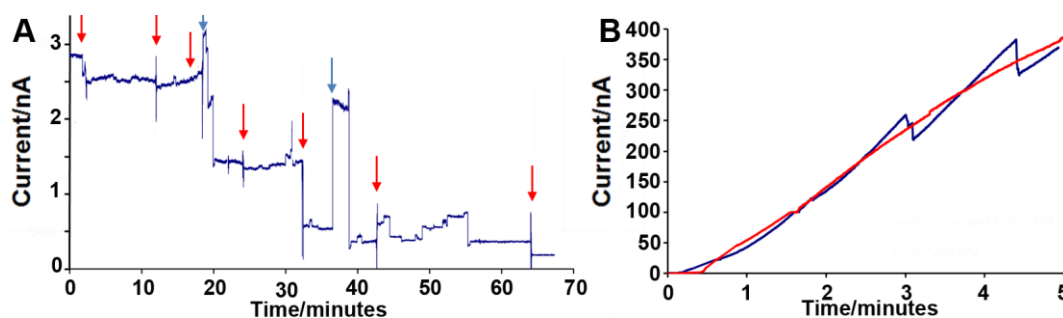

Figure 8.5. Electrical recordings showing: (A) the blocking of FomA (delivered to biomimetic membrane using proteoliposomes prepared with LPR = 200) after addition of increasing amounts of β-CD (red arrows). The β-CD concentraton in the chamber was step-wise increased from 0.14, 0.29, 0.68, 1.28, 2.27, 3.41, to 4.55 mM. (B) FomA (delivered to biomimetic membrane using proteoliposomes prepared with LPR = 50) fusion (red) and blocking in 0.2 mM β-CD in PBS (blue).

When FomA was delivered using proteoliposomes prepared with LPR equal to 50, the large fusion induced current increases and shadowed any FomA blocking upon increasing the amount of β-CD. Therefore the fusion was performed while the blocking agent (β-CD) was already in the solution, see Figure 8.5B (in blue) and compared with the fusion that occurred without the blocking agent (Figure 8.5B in red). The competition between FomA fusion and FomA blocking with β-CD in this system was observed as stepwise decreases on an increasing trend.

The two experimental conditions both comprised of an array of lipid membranes where FomA proteins were incorporated by FomA proteoliposomes fusion. Blocking of several FomA channels at the same time was observed and therefore the information if FomA blocking with β-CD was partial or complete could not be revealed. Moreover, the competition between fusion and blocking in this system shadowed the information about any reversibility of the blocking. To find out if the nature of the blocking mechanism we attempted experiments where a single FomA channel interacting with β-CD could be observed.

To monitor the blocking of a single FomA channel with β-CD, FomA was incorporated from a detergent solubilised state into a membrane formed in the horizontal device shown in Figure 5.1D. FomA dissolved in 10 mM borate buffer (3.4 mg/ml, pH 10 with 2 mM EDTA) was refolded in N-lauryl-N,N-dimethylammonium-N-oxide (LDAO) micelles (LDAO/FomA mol:mol ratio = 1000). The FomA incorporation and functional activity was characterized by voltage clamp recordings of bilayer formed from DPhPC/decane solution separating two aqueous compartments containing 1 M KCl. Stepwise increases of the current across the bilayer were observed when 0.2 µl of FomA solution was applied in close proximity of the membrane (Figure 8.6A, upper current trace). No transmembrane currents were observed for the DPhPC bilayer alone (Figure 8.6A, middle

47

current trace) or when a detergent (LDAO) in buffer was applied in close proximity of the DPhPC membrane (Figure 8.6A, lower current trace). The conductance amplitude histogram reveals a broad distribution with a mean value of 0.8 nS for 141 incorporation events (Figure 8.6B). This value is in good agreement with the 1.17 nS measured previously for FomA trimeric channel conductance in 1 M KCl[122]. The incorporation of a few (even one) protein trimers was observed and revealed the channel gating properties. FomA channels opened and closed spontaneously (Figure 8.6A, upper current trace).
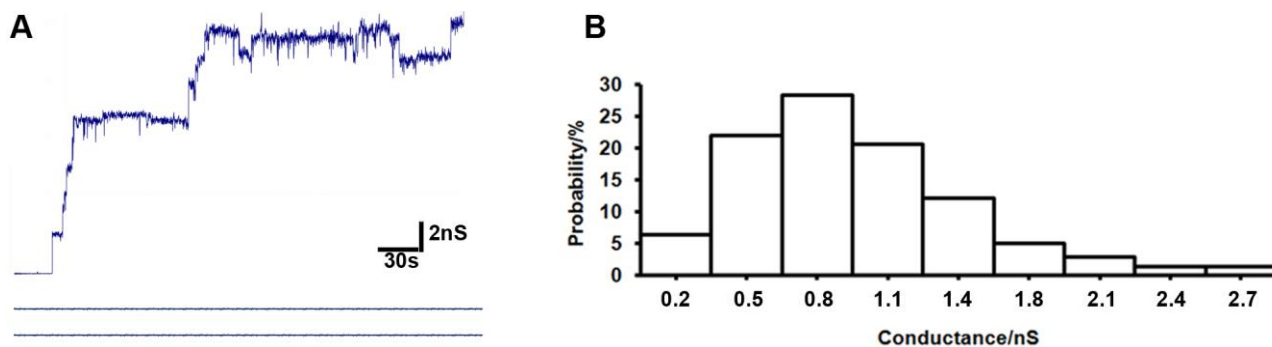

Figure 8.6. FomA reconstitution from a detergent solubilized state into a membrane made across 0.7 mm hole in Teflon partition. (A) Conductance across: a DPhPC membrane in 1 M KCl after addition of FomA refolded in LDAO micelles (upper trace), a DPhPC membrane alone in 1 M KCl (middle trace), and after addition of LDAO micelles (lower trace). (B) Histogram of the probability of the occurrence of a given conductivity unit (141 fusion events were recorded) during FomA reconstitution into a DPhPC planar membrane. The applied potential across the membrane was +60 mV. The conductance of single FomA channel in 1M KCl was in the range 0.2–2.7 nS with a maximum probability for a conductance of 0.8 nS.

Single FomA channel blocking experiments were performed by adding 10 µl of β-CD solution (10 mM prepared in 1M KCl) to the top compartment of the horizontal device (Figure 5.1D). No transmembrane currents were observed when β-CD solution (Figure 8.7A, upper current trace) or when a detergent (LDAO) in buffer followed by β-CD solution were applied to the DPhPC membrane (Figure 8.7A, lower current trace), level 0. The current incorporation value (level 1 - 72 pA) and its fluctuation (~one third of the total current) indicated that a single FomA trimer was delivered to the lipid bilayer (Figure 8.7B) and further subjected to blocking (Figure 8.7C). The blocking trace presented in Figure 8.7C suggested that FomA trimers were reversibly blocked by β-CD stepwise up to ~85 %. A closer look into the blocking mechanism indicated three blocking steps (from level 1 to levels 2a, 2b, and 2c) as seen on the trace in Figure 8.7D. An increased fluctuation in the current (level 2a on the trace) compared with currents corresponding to the empty (level 1 on the same trace) and blocked (level 2c on the same trace) channel may represent the moment that a β-CD molecule leaves the FomA porin.

The β-CDs interacted with the FomA trimer for about 0.5 of second (Figure 8.7D). These current blocking events have much longer life times than those reported for wild-type α-HL, which is commonly used as a stochastic sensor, i.e. β-CD in the wild-type α-HL pore resided for several hundred microseconds and its residence time could be extended to several milliseconds by the manipulation of pH and transmembrane potential[80]. Our results were however comparable to those reported for mutant homoheptameric α-HL pores (tens of seconds)[129].

Due to the fact that the blocking of the FomA trimer by β-CDs was partial (~85 %) and because β-CDs act as hosts for a variety of guest molecules, investigation of whether guests could further reduce single-channel

currents would be an important test. If they could, then the FomA system would work as a stochastic sensor for organic molecules, in a similar way as α-HL and OmpG proteins do. However, since FomA exhibits spontaneous gating activities, this could interfere with a signal arising from an analyte binding and thus the application of this pore as a stochastic sensor would not be suitable. Therefore, eliminating or even reducing the protein gating activities would be an important step towards the development of a biosensor based on FomA. Additionally, the investigation of the interaction between the FomA pore and the β-CD molecular adapter either from the extracellular or periplasmic entrances would be of importance, as previously shown for another bacterial protein, OmpG[125, 126].
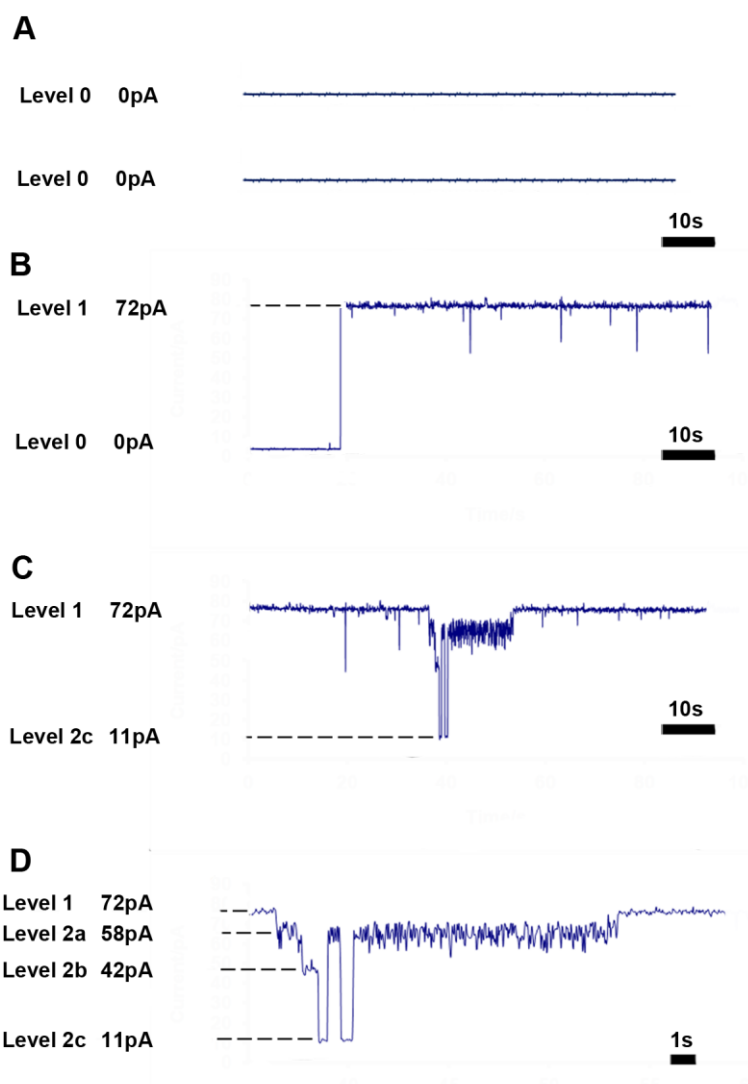
Figure 8.7. Electrical recordings showing: (A) No transmembrane currents (Level 0) observed when β-CD (upper current trace) or when a detergent (LDAO) in buffer followed by β-CD addition (lower current trace) were applied to the DPhPC/decane membrane made across a 0.7 mm hole in Teflon in 1 M KCl using a horizontal device. (B) FomA trimer incorporation into a lipid bilayer, Level 1. (C-D) FomA current blockage after addition of 10 µl of 10 mM β-CD, Levels 2a, 2b and 2c. The applied potential across the membrane was +60 mV.

Additionally to the development of a biosensor, the FomA-β-CD complex could be used in periodontal disease treatment. It is well known that the attachment of *Fusobacterium nucleatum* to the surfaces of teeth

and oral mucosa plays a major role in plaque formation and the development of periodontitis[130]. FomA has been proposed to be directly involved in binding to *Streptococcus sanguinis*[131] and *P. gingivalis*[132, 133], which is envisioned as a mechanism for the growth of human dental plaque. Therefore, the described FomA- β-CD complex would be of importance to investigate FomA associated diseases.

In summary, the FomA- β-CD complex may be used as a stochastic sensor for single-molecule detection or in periodontal diseases treatment if the strength of the complex could be increased. Due to the difficulties in reproducibility of the results presented here, additional observation of the single FomA channel interaction with β-CD is suggested. Here, a microfluidic device designed especially for this purpose would be valuable. This could be a system comprised of two microfluidic channels separated by a nanopore across which a FomA proteliposome could form a lipid membrane with a single FomA trimer.

9. Summary, conclusions and perspectives

Biomimetic membrane-based devices have a high potential use in a diverse range of technical applications. This is why scientists and engineers put a lot of attention into their development, however, the device' complexity remains a challenge. To develop the biomimetic membrane-based device, first lipid or polymer membranes have to be formed, and then proteins of interest incorporated. Finally, biomimetic membranes have to be encapsulated in order to protect them and make them sufficiently stable in a final application. The stability of the created membranes, the up-scaling of the effective membrane area, delivery and quantification of functional proteins are still difficult tasks. This thesis shows some possible ways to overcome some of these difficulties, as well as showing some application perspectives of FomA protein incorporated into biomimetic membranes.

Polymer or lipid membrane formation is a first step in developing biomimetic membrane-based devices. The device design needs to be carefully developed depending on the membrane formation methods, which may differ from its form in a final application. In this study, two microfluidic devices for membrane formation and investigation were designed and fabricated. The use of CO_2 laser ablation in ETFE, PMMA and Viton® materials resulted in successful production of various microfluidic devices. This process is quick and inexpensive compared to existing technologies such as micromilling, casting or silicon technology for microarray based device production.

The first device was developed for BPMs imaging with AFM. The device enabled probing and characterisation of free-standing fluidic biomimetic membranes with thickness in the nanometer scale suspended over 300 μm wide apertures using both normal tetrahedrally shaped tips and needle shaped Ag_2Ga rods (Paper I). For AFM microscopy, microfluidic channels were implemented from one side of the device, leaving its top compartment accessible for membranes probing with the AFM tip. In this simple design, the membrane thinning process was promoted by manual controlling the velocity of the injected water.

The work then continued with utilization of microfluidic channels on both sides of the perforated ETFE partition for inducing the membrane thinning process. A fully automated and closed microfluidic device for the formation, regeneration and investigation of an array of planar lipid membranes by electrical measurements was developed. Highly stable membranes (lifetime of ~42 h) with a bilayer membrane area of ~24 % of the available aperture area were created in the developed MF device. Further, reconstitution of α-HL membrane proteins in the BLMs was performed (Paper III). The benefits of this automated and closed MF device include controlled deposition of lipid solution into the apertures, thick lipid film thinning facilitated by microfluidic pumping, improvement of the membrane stability and lifetime, and solution exchange on both sides of the membrane.

In parallel, membrane array stability was increased by surface modification of support partitions by employing plasma polymerisation. BLMs were established in a vertical device. The ETFE surface was covalently modified by plasma, resulting in a hydrophobic (n-hexene) coating that greatly improved the

51

average membrane array lifetime (a maximal lifetime of 6 days) with a bilayer membrane area of ~50% of the available aperture area, (Paper II).

Reconstitution of functionally active membrane proteins into artificially made membranes is the next step in creating membrane-based biomimetic devices. A novel assay for quantifying protein incorporation into lipid membranes was developed and presented in this thesis. The efficacy of FomA proteoliposome fusion with planar membrane array was characterized by electrical conductance measurements and fluorescence microscopy. It was shown that FomA vesicles are inherently fusigenic. Optimal FomA incorporation was obtained with a proteoliposome LPR equal to 50, meaning that more than 10^5 FomA proteins was incorporated in a bilayer array with a total membrane area of 2 mm^2 within 20 min (Paper IV).

Exploring strategies for functional FomA protein delivery to the biomimetic membrane resulted in selecting a new protein for stochastic sensing. A few (even one) FomA trimers were spontaneously incorporated into biomimetic membrane and revealed the channel gating properties. FomA channels opened and closed spontaneously. Furthermore, the FomA complex formation with a β-CD molecular adapter (blocking agent) was investigated. The single FomA trimer interaction with β-CD shown in this thesis suggested that FomA trimers were reversibly blocked by β-CD stepwise up to 85 %.

The data presented in this thesis show that membrane proteins could be reconstituted in a controlled manner into highly stable biomimetic membranes. This may be utilized in new technologies for, e.g. stochastic sensing based on the FomA protein, water purification based on aquaporin proteins etc.

Biomimetic membrane arrays are attractive as alternatives to cell-based arrays to be used for screening of potential drug candidates that interact with membrane proteins. The biomimetic membrane-based high throughput technologies have the advantage of recording the specific interactions between the protein of interest and a drug, eliminating the drug acting on unwanted proteins. Other exciting applications of biomimetic membrane arrays are separation technologies that involve membrane proteins as a driving force for separation processes. Recently progress in biomimetic membrane stability, scalability and functional protein incorporation has been achieved. However, further developments are required in order to obtain commercially available biomimetic membrane-based high throughput screening or separation devices.

In this study the MF device for biomimetic membrane formation and investigation was developed. The system provides an environment for reconstituting proteins that is similar to their native one, having the bilayer surrounded on both sides by water, thus providing the possibility of fast and precise measurement of exchange of analytes and ligands through transmembrane protein pores and channels. Further development of the MF device could address the membranes stability after protein incorporation. This could be achieved by optimizing microfluidic channels or employing one of several membrane stabilization strategies in the MF device. For instance, membrane stabilization could be accomplished by encapsulation in a hydrogel or replacing lipid membranes with black triblock copolymer membranes (which show improved stability over lipid membranes) and encapsulate them in hydrogel. The device could be used for water purification, having stable membrane arrays with aquaporin proteins incorporated, enabling liquid exchange on both sides of the membrane. Novel aquaporin based biomimetic membranes would potentially be superior to current reverse

and forward osmosis membranes in performance. Another approach for developing MF devices could be the redesign to read multiple results. Such design could implement microfluidic channels above and underneath each row of apertures and employ microelectrode arrays positioned beneath the membrane scaffold, providing new means for high throughput screening system in drug discovery.

A novel assay for quantifying protein delivery into lipid bilayers presented in this thesis can be a useful tool in developing biomimetic membrane applications. The number of functionally active proteins can specify if the biomimetic membrane-based device is used in sensor or/and separation application. Proteoliposomes fusion with planar membrane, as presented here, can be applied for the creation of novel protein biosensor and drug–screening applications, whereas the efficiency is likely insufficient to support fabrication of large scale separation systems based on membrane protein function. Here alternative protein reconstitution strategies need to be explored.

The presented results open up a new application area for the non-specific porin FomA. Due to its partial blocking by β-CD it could be used as a stochastic sensor for single-molecule detection. Future work should eliminate or significantly reduce the presented gating activity of FomA as it may interfere with a signal arising from analyte binding. Moreover, engineering of the FomA channel to improve the strength of FomA-β-CD complex formation would be beneficial in periodontal diseases treatment. In the future β-CD could for example be added to the toothpaste preventing the growth of dental plaque.

References

1. Agre P, Bonhivers M, Borgnia MJ. The aquaporins, blueprints for cellular plumbing systems. J Biol Chem 1998;273(24):14659-62.

2. Borgnia MJ, Kozono D, Calamita G, Maloney PC, Agre P. Functional reconstitution and characterization of AqpZ, the E. coli water channel protein1. J Mol Biol 1999;291(5):1169-79.

3. Nielsen CH. Biomimetic membranes for sensor and separation applications. Analytical and Bioanalytical Chemistry 2009;395(3):697-718.

4. Alberts B, Johnson A, Lewis J. Molecular biology of the cell. New York,NY: Garland; 2002. .

5. Bally M, Bailey K, Sugihara K, Grieshaber D, Vörös J, Städler B. Liposome and lipid bilayer arrays towards biosensing applications. Small 2010;6(22):2481-97.

6. Tien HT, Ottova-Leitmannova A. Planar lipid bilayers (BLMs) and their applications /. Amsterdam : Elsevier; 2003. Series: Membrane science and technology series, 0927-5193 ; 7.

7. Montal M, Mueller P. Formation of bimolecular membranes from lipid monolayers and a study of their electrical properties. Proc Natl Acad Sci U S A 1972;69(12):3561-6.

8. Zagnoni M, Sandison ME, Morgan H. Microfluidic array platform for simultaneous lipid bilayer membrane formation. Biosensors and Bioelectronics 2009;24(5):1235-40.

9. Hansen JS, Perry M, Vogel J, Vissing T, Hansen CR, Geschke O, Emnéus J, Nielsen CH. Development of an automation technique for the establishment of functional lipid bilayer arrays. J Micromech Microengineering 2009;19(2):025014.

10. Suzuki H, Tabata K, Kato-Yamada Y, Noji H, Takeuchi S. Planar lipid bilayer reconstitution with a micro-fluidic system. Lab on a Chip 2004;4(5):502-5.

11. Sandison ME, Morgan H. Rapid fabrication of polymer microfluidic systems for the production of artificial lipid bilayers. J Micromech Microengineering 2005;15(7):S139-44.

12. Woodbury DJ, Hall JE. Vesicle-membrane fusion observation of simultaneous membrane incorporation and content release. Biophys J 1988;54(2):345-50.

13. Woodbury DJ. Section II. purification and reconstitution - 17 - Nystatin/Ergosterol method for reconstituting ion channels into planar lipid bilayers. Meth Enzymol 1998;1999(294):319.

14. Nardin C, Thoeni S, Widmer J, Winterhalter M, Meier W. Nanoreactors based on (polymerized) ABA-triblock copolymer vesicles. Chem Commun 2000(15):1433-4.

15. González-Pérez A, Stibius KB, Vissing T, Nielsen CH, Mouritsen OG. Biomimetic triblock copolymer membrane arrays: A stable template for functional membrane proteins. Langmuir 2009;25(18):10447-50.

16. Discher BM, Won YY, Ege DS, Lee JC, Bates FS, Discher DE, Hammer DA. Polymersomes: Tough vesicles made from diblock copolymers. Science Science 1999;284(5417):1143-6.

17. Ho, Chu, Schmidt, Brooks, Montemagno. Hybrid protein-polymer biomimetic membranes. IEEE Trans Nanotechnology 2004;3(2):256-63.

18. Lodish H, Berk A, Zipursky SL. Molecular cell biology. New York,NY: Freeman; 2001. .

19. Lee JC-, Bermudez H, Discher BM, Sheehan MA, Won Y, Bates FS, Discher DE. Preparation, stability, and in vitro performance of vesicles made with diblock copolymers. Biotechnol Bioeng 2001;73(2):135-45.

20. Kumar M, Grzelakowski M, Zilles J, Clark M, Meier W. Highly permeable polymeric membranes based on the incorporation of the functional water channel protein aquaporin Z. Proc Natl Acad Sci U S A 2007;104(52):20719-24.

21. Ruysschaert T, Sonnent AFP, Haefele T, Meier W, Winterhaltert M, Fournier D. Hybrid nanocapsules: Interactions of ABA block copolymers with liposomes. J Am Chem Soc 2005;127(17):6242-7.

22. Meier W, Nardin C, Winterhalter M. Reconstitution of channel proteins in (polymerized) ABA triblock copolymer membranes. Angewandte Chemie International Edition 2000;39(24):4599-602.

23. Woodle MC, Papahadjopoulos D. Liposome preparation and size characterization. Methods Enzymol 1989;171:193-217.

24. Gabrile NE, Roberts MF. Spontaneous formation of stable unilamellar vesicles. Biochemistry (N Y) 1984;23(18):4011-5.

25. Liang X, Mao G, Ng KYS. Effect of chain lengths of PEO-PPO-PEO on small unilamellar liposome morphology and stability: An AFM investigation. J Colloid Interface Sci 2005;285(1):360-72.

26. Mueller P, Rudin DO. Bi molecular lipid membranes techniques of formation study of electrical properties and induction of ionic gating phenomena. Passow, h.and r.Stampfli (Edited by).Laboratory Techniques in Membrane Biophysics.an Introductory Course.Viii + 201p.Illus.Springer-Verlag: Berlin, Germany and New York n.y., u.s.a 1969:141-56.

27. Nardin C, Meier W, Winterhalter M. Giant free-standing ABA triblock copolymer membranes. Langmuir 2000;16(20):7708-12.

28. Rein C, Pszon-Bartosz K, Stibius KB, Bjørnholm T, Hélix-Nielsen C. Free-standing biomimetic polymer membrane imaged with atomic force microscopy. Langmuir 2011;27(2):499-503.

29. Belegrinou S, Kita-Tokarczyk K, Meier W, Dorn J, Kreiter M, Sinner. Biomimetic supported membranes from amphiphilic block copolymers. Soft Matter 2009;6(1):179-86.

30. Wang L, Cruz A, Flach CR, Pérez-Gil J, Mendelsohn R. Langmuir-blodgett films formed by continuously varying surface pressure. characterization by IR spectroscopy and epifluorescence microscopy. Langmuir 2007;23(9):4950-8.

31. Kita-Tokarczyk K, Itel F, Grzelakowski M, Egli S, Rossbach P, Meier W. Monolayer interactions between lipids and amphiphilic block copolymers. Langmuir 2009;25(17):9847-56.

32. Richter R, Mukhopadhyay A, Brisson A. Pathways of lipid vesicle deposition on solid surfaces: A combined QCM-D and AFM study. Biophys J 2003;85(5):3035-47.

33. Dorn J, Kreiter M, Belegrinou S, Meier W, Sinner E. Planar block copolymer membranes by vesicle spreading. Macromol Biosci 2011;11(4):514-25.

34. Rakhmatullina E, Meier W. Solid-supported block copolymer membranes through interfacial adsorption of charged block copolymer vesicles. Langmuir 2008;24(12):6254-61.

35. http://www2.warwick.ac.uk/alumni/services/eportfolios/msrfas/research/ [Internet].

36. le Maire M, Champeil P, Moller JV. Interaction of membrane proteins and lipids with solubilizing detergents. Biochimica Et Biophysica Acta - Biomembranes 2001;1508(1-2).

37. Petrache HI, Dodd SW, Brown MF. Area per lipid and acyl length distributions in fluid phosphatidylcholines determined by 2H NMR spectroscopy. Biophys J 2000;79(6):3172-92.

38. Törnroth-Horsefield S, Wang Y, Hedfalk K, Johanson U, Karlsson M, Tajkhorshid E, Neutze R, Kjellbom P. Structural mechanism of plant aquaporin gating. Nature 2006;439(7077):688-94.

39. Choi H, Montemagno CD. Artificial organelle: ATP synthesis from cellular mimetic polymersomes. Nano Lett 2005;5(12):2538-42.

40. Choi H, Brooks E, Montemagno CD. Synthesis and characterization of nanoscale biomimetic polymer vesicles and polymer membranes for bioelectronic applications. Nanotechnology 2005;16(5):S143-9.

41. Choi H, Germain J, Montemagno CD. Effects of different reconstitution procedures on membrane protein activities in proteopolymersomes. Nanotechnology 2006;17(8):1825-30.

42. Kumar M, Grzelakowski M, Zilles J, Clark M, Meier W. Highly permeable polymeric membranes based on the incorporation of the functional water channel protein aquaporin Z. Proc Natl Acad Sci U S A 2007;104(52):20719-24.

43. Nielsen CH. Biomimetic membranes for sensor and separation applications. Analytical and Bioanalytical Chemistry 2009;395(3):697-718.

44. Tanaka, Sackmann. Supported membranes as biofunctional interfaces and smart biosensor platforms. Phys Status Solidi A (Germany) Physica Status Solidi A, Applied Research 2006;203(14):3452-62.

45. Andrew Woolley G, Wallace BA. Model ion channels: Gramicidin and alamethicin. J Membarin Biol Journal of Membrane Biology 1992;129(2):109-36.

46. Zagnoni, Sandison, Marius, Lee, Morgan. Controlled delivery of proteins into bilayer lipid membranes on chip. Lab on a Chip 2007;7(9):1176-83.

47. Suzuki H, Tabata KV, Noji H, Takeuchi S. Electrophysiological recordings of single ion channels in planar lipid bilayers using a polymethyl methacrylate microfluidic chip. Biosensors and Bioelectronics 2007;22(6):1111-5.

48. Arora A, Rinehart D, Szabo G, Tamm LK. Refolded outer membrane protein A of escherichia coli forms ion channels with two conductance states in planar lipid bilayers. J Biol Chem 2000;275(3):1594-600.

49. Pocanschi CL, Apell HJ, Puntervoll P, Hogh B, Jensen HB, Welte W, Kleinschmidt JH. The major outer membrane protein of fusobacterium nucleatum (FomA) folds and inserts into lipid bilayers via parallel folding pathways. J Mol Biol 2006;355(3):548-61.

50. Schmitt EK, Vrouenraets M, Steinem C. Channel activity of OmpF monitored in nano-BLMs. Biophys J 2006;91(6):2163-71.

51. Woodbury DJ, Miller C. Nystatin-induced liposome fusion, a versatile approach to ion channel reconstitution into planar bilayers. Biophys J 1990;58(4):833-40.

52. Zimmerberg J, Cohen FS, Finkelstein A. Fusion of phospho lipid vesicles with planar phospho lipid bi layer membranes 1. discharge of vesicular contents across the planar membrane. J Gen Physiol 1980;75(3):241-50.

53. Grafmuller, Shillcock, Lipowsky. Pathway of membrane fusion with two tension-dependent energy barriers. Phys Rev Lett 2007;98(21):218101/1-4.

54. Shillcock JC, Lipowsky R. Tension-induced fusion of bilayer membranes and vesicles. Nature Materials 2005;4(3):225-8.

55. Lindau M, Alvarez de T. The fusion pore. Biochimica Et Biophysica Acta (BBA)/Molecular Cell Research 2003;1641(2-3):167-73.

56. Haluska CK, Riske KA, Marchi-Artzner V, Lehn J, Lipowsky R, Dimova R. Time scales of membrane fusion revealed by direct imaging of vesicle fusion with high temporal resolution. Proc Natl Acad Sci U S A 2006;103(43):15841-6.

57. Simberg D, Weisman S, Talmon Y, Barenholz Y. DOTAP (and other cationic lipids): Chemistry, biophysics, and transfection. Crit Rev Ther Drug Carrier Syst 2004;21(4):257-317.

58. Stamatatos L, Leventis R, Zuckermann MJ, Silvius JR. Interactions of cationic lipid vesicles with negatively charged phospholipid vesicles and biological membranes. Biochemistry (N Y) 1988;27(11):3917-25.

59. Nickel W, Weber T, McNew JA, Parlati F, Sollner ,T.H., Rothman JE. Content mixing and membrane integrity during membrane fusion driven by pairing of isolated v-SNAREs and t-SNAREs. Proc Natl Acad Sci U S A 1999;96(22):12571-6.

60. Parlati F, Weber T, McNew JA, Westermann B, Sollner ,T.H., Rothman JE. Rapid and efficient fusion of phospholipid vesicles by the alpha-helical core of a SNARE complex in the absence of an N-terminal regulatory domain. Proc Natl Acad Sci U S A 1999;96(22):12565-70.

61. Cohen FS, Akabas MH, Finkelstein A. Osmotic swelling of phospholipid-vesicles causes them to fuse with a planar phospholipid-bilayer membrane. Science 1982;217(4558):458-60.

62. de Planque ,M.R.R., Mendes GP, Zagnoni M, Sandison ME, Fisher KH, Berry RM, Watts A, Morgan H. Controlled delivery of membrane proteins to artificial lipid bilayers by nystatin-ergosterol modulated vesicle fusion. 2006.

63. Cohen FS, Zimmerberg J, Finkelstein A. Fusion of phospho lipid vesicles with planar phospho lipid bi layer membranes 2. incorporation of a vesicular membrane marker into the planar membrane. J Gen Physiol 1980;75(3):251-70.

64. Ganesan PV, Boxer SG. A membrane interferometer. Proc Natl Acad Sci U S A 2009;106(14):5627-32.

65. Bamberg E, Dencher NA, Fahr A, Heyn MP. Transmembranous incorporation of photoelectrically active bacteriorhodopsin in planar lipid bilayers. Proc Natl Acad Sci U S A 1981;78(12):7502-6.

66. Beddow JA, Peterson IR, Heptinstall J, Walton DJ, Peterson IR. Reconstitution of nicotinic acetylcholine receptors into gel-protected lipid membranes. Anal Chem 2004;76(8):2261-5.

67. Falconnet D, Koenig A, Assi F, Textor M. A combined photolithographic and molecular-assembly approach to produce functional micropatterns for applications in the biosciences. Advanced Functional Materials 2004;14(8):749-56.

68. Städler B, Falconnet D, Vörös J, Pfeiffer I, Höök F. Micropatterning of DNA-tagged vesicles. Langmuir 2004;20(26):11348-54.

69. Pfeiffer I, Höök F. Quantification of oligonucleotide modifications of small unilamellar lipid vesicles. Anal Chem 2006;78(21):7493-8.

70. Trojanowicz M, Mulchandani A. Analytical applications of planar bilayer lipid membranes. Anal Bioanal Chem 2004;379(3):347-50.

71. Ottova AL, Hianik T, Ziegler W, Tvarozek V, Sabo J, Passechnik VI, Ivanov SA, Tien HT. Self-assembled and supported BLMS as a smart system for biosensors. Proc SPIE Int Soc Opt Eng 1997;2976:342-9.

72. Martin DK. Nanobiotechnology of biomimetic membranes /. New York : Springer; 2007. Series: Fundamental biomedical technologies ; vol. 1.

73. Schmidt J. Stochastic sensors. J Mater Chem 2005;15(8):831-40.

74. Bayley H, Cremer PS. Stochastic sensors inspired by biology. Nature 2001;413(6852):226-30.

75. Braha O, Walker B, Cheley S, Kasianowicz JJ, Song L, Gouaux JE, Bayley H. Designed protein pores as components for biosensors. Chem Biol 1997;4(7):497-505.

76. Braha O, Gu LQ, Zhou L, Lu X, Cheley S, Bayley H. Simultaneous stochastic sensing of divalent metal ions. Nat Biotechnol 2000;18(9):1005-7.

77. Kasianowicz JJ, Henrickson SE, Weetall HH, Robertson B. Simultaneous multianalyte detection with a nanometer-scale pore. Anal Chem 2001;73(10):2268-72.

78. Kasianowicz JJ, Brandin E, Branton D, Deamer DW. The detection of individual nucleic acid polymers traversing a protein ion channel. Progress in Biophysics and Molecular Biology 1996;65:PB127-.

79. Henrickson SE, Robertson B, Kasianowicz JJ, Misakian M. Driven DNA transport into an asymmetric nanometer-scale pore. Phys Rev Lett 2000;85(14):3057-60.

80. Gu LQ, Braha O, Conlan S, Cheley S, Bayley H. Stochastic sensing of organic analytes by a pore-forming protein containing a molecular adapter. Nature 1999;398(6729):686-90.

81. Hansen JS, Perry M, Vogel J, Groth JS, Vissing T, Larsen MS, Geschke O, Emnéus J, Bohr H, Nielsen CH. Large scale biomimetic membrane arrays. Analytical and Bioanalytical Chemistry 2009;395(3):719-27.

82. Suzuki H, Pioufle BL, Takeuhci S. Ninety-six-well planar lipid bilayer chip for ion channel recording fabricated by hybrid stereolithography. Biomed Microdevices 2009;11(1):17-22.

83. Geschke O, Klank H, Telleman P. Microsystem engineering of lab-on-a-chip devices. Weinheim: Wiley; 2004. .

84. Bruus H. Theoretical microfluidics. Oxford: Oxford Univ. Pr; 2010. Series: Oxford master series in physics 18; Literaturverz. S. 333 - 338.

85. Simon A, Picollet D'Hahan N, Chatelain F, Fuchs A, Sauter F, Pudda C, Girard-Egrot A, Blum L. Formation and stability of a suspended biomimetic lipid bilayer on silicon submicrometer-sized pores. J Colloid Interface Sci 2007;308(2):337-43.

86. van Rijn CJM, Nijdam W, Kuiper S, Veldhuis GJ, van Wolferen H, Elwenspoek M. Microsieves made with laser interference lithography for micro-filtration applications. J Micromech Microengineering 1999;9(2):[d]170-172.

87. Fertig N, Meyer C, Blick RH, Trautmann C, Behrends JC. Microstructured glass chip for ion-channel electrophysiology.Physical Review E, Statistical, Nonlinear and Soft Matter Physics 2001;64(4).

88. Sandison ME, Zagnoni M, Abu-Hantash M, Morgan H. Micromachined glass apertures for artificial lipid bilayer formation in a microfluidic system. J Micromech Microengineering 2007;17(7):S189-96.

89. Mach T, Chimerel C, Fritz J, Fertig N, Winterhalter M, Fütterer C. Miniaturized planar lipid bilayer: Increased stability, low electric noise and fast fluid perfusion. Analytical and Bioanalytical Chemistry 2008;390(3):841-6.

90. Wonderlin WF, Finkel A, French RJ. Optimizing planar lipid bilayer single-channel recordings for high-resolution with rapid voltage steps. Biophys J 1990;58(2):289-97.

91. Ide T, Ichikawa T. A novel method for artificial lipid-bilayer formation. Biosensors and Bioelectronics 2006;21(4):672.

92. Suzuki H, Tabata KV, Noji H, Takeuchi S. Highly reproducible method of planar lipid bilayer reconstitution in polymethyl methacrylate microfluidic chip. Langmuir 2006;22(4):1937-42.

93. Vogel J, Perry M, Hansen JS, Bolinger P, Nielsen CH, Geschke O. A support structure for biomimetic applications. J Micromech Microengineering 2009;19(2):025026.

94. Sandison ME, Zagnoni M, Morgan H. Air-exposure technique for the formation of artificial lipid bilayers in microsystems. Langmuir 2007;23(15):8277-84.

95. Funakoshi K, Suzuki H, Takeuchi S. Lipid bilayer formation by contacting monolayers in a microfluidic device for membrane protein analysis. Anal Chem 2006;78(24):8169-74.

96. Malmstadt N, Nash MA, Purnell RF, Schmidt JJ. Automated formation of lipid-bilayer membranes in a microfluidic device. Nano Letters 2006;6(9):1961-5.

97. Kawano R, Osaki T, Sasaki H, Takeuchi S. A polymer-based nanopore-integrated microfluidic device for generating stable bilayer lipid membranes. Small 2010;6(19).

98. http://www.worldoflasers.com/laserprinciples.htm [Internet].

99. http://slab-laser.ru/eng-Glossary.html#Mode [Internet].

100. Perry M, Vissing T, Boesen TP, Hansen JS, Emnéus J, Nielsen CH. Automated sampling and data processing derived from biomimetic membranes. Bioinspiration 2009;4(4):044001.

101. Tien HT, Ottova AL. Supported planar lipid bilayers (s-BLMs) as electrochemical biosensors. Electrochim Acta 1998;43(23):3587-610.

102. White SH. A study of lipid bilayer membrane stability using precise measurements of specific capacitance. Biophys J 1970;10(12):1127-48.

103. Benz R, Froehlich O, Laeuger P, Montal M. Electrical capacity of black lipid films and of lipid bi layers made from monolayers. Biochim Biophys Acta 1975;394(3):323-34.

104. White SH, Thompson TE. Capacitance, area, and thickness variations in thin lipid films. Biochimica Et Biophysica Acta Biomembranes 1973;323(1):7-22.

105. White SH. Formation of "solvent-free" black lipid bilayer membranes from glyceryl monooleate dispersed in squalene. Biophys J 1978;23(3):337-47.

106. http://upload.wikimedia.org/wikipedia/commons/1/1c/FluorescenceFilters_2008-09-28.svg [Internet].

107. http://www.nanosight.com/technology/nanosights-technology [Internet].

108. Yazdanpanah MM, Hosseini M, Pabba S, Berry SM, Dobrokhotov VV, Safir A, Keynton RS, Cohn RW. Micro-wilhelmy and related liquid property measurements using constant-diameter nanoneedle-tipped atomic force microscope probes. Langmuir 2008;24(23):13753-64.

109. Hennesthal C, Steinem C. Pore-spanning lipid bilayers visualized by scanning force microscopy. J Am Chem Soc 2000;122(33):8085-6.

110. Steltenkamp S, Müller MM, Deserno M, Hennesthal C, Steinem C, Janshoff A. Mechanical properties of pore-spanning lipid bilayers probed by atomic force microscopy. Biophys J 2006;91(1):217-26.

111. Hennesthal C, Drexler J, Steinem C. Membrane-suspended nanocompartments based on ordered pores in alumina. ChemPhysChem 2002;3(10):885-9.

112. Quist AP, Ramachandran S, Lal R, Chand A, Daraio C, Jin S, Lal R. Atomic force microscopy imaging and electrical recording of lipid bilayers supported over microfabricated silicon chip nanopores: Lab-on-a-chip system for lipid membranes and ion channels. Langmuir 2007;23(3):1375-80.

113. White SH, Petersen DC, Simon S, Yafuso M. Formation of planar bilayer membranes from lipid monolayers. A critique. Biophys J 1976 5;16(5):481-9.

114. Inagaki N, Narushima K, Lim SK, Park YW, Ikeda Y. Surface modification of ethylene-co-tetrafluoroethylene films by remote plasmas. J Polym Sci Part B 2002;40(24):2871-82.

115. Park YW, Inagaki N. A new approach for selective surface modification of fluoropolymers by remote plasmas. J Appl Polym Sci 2004;93(3):1012-20.

116. Inagaki N, Narushima K, Kuwabara K, Tamura K. Introduction of amino functionalities on ethylene-co-tetrafluoroethylene film surfaces by NH_3 plasmas. J Adhes Sci Technol 2005;19(13-14):1189-205.

117. Inagaki N, Narushima K, Amano T. Introduction of carboxylic groups on ethylene-co-tetra fluoroethylene (ETFE) film surfaces by CO_2 plasma. J Adhes Sci Technol 2006;20(13):1443-62.

118. Dinges MM, Orwin PM, Schlievert PM. Exotoxins of staphylococcusaureus. Clin Microbiol Rev 2000;13(1):16-34.

119. Fink D, Contreras ML, Lelkes PI, Lazarovici P. Staphylococcus aureus α-toxin activates phospholipases and induces a $Ca2+$ influx in PC12 cells. Cell Signal 1989;1(4):387-93.

120. Hemmler, Bose, Wagner, Peters. Nanopore unitary permeability measured by electrochemical and optical single transporter recording. Biophys J 2005;88(6):4000-7.

121. Puntervoll P, Ruud M, Bruseth LJ, Kleivdal H, Hogh BT, Benz R, Jensen HB. Structural characterization of the fusobacterial non-specific porin FomA suggests a 14-stranded topology, unlike the classical porins. Microbiology (Reading) 2002;148(11):3395-403.

122. Kleivdal H, Benz R, Jensen HB. The fusobacterium nucleatum major outer-membrane protein (FomA) forms trimeric, water-filled channels in lipid bilayer membranes. European Journal of Biochemistry 1995;233(1):310.

123. Vrouenraets M, Wierenga J, Meijberg W, Miedema H. Chemical modification of the bacterial porin OmpF: Gain of selectivity by volume reduction. Biophys J 2006;90(4):1202-11.

124. Ibragimova S, Jensen KBS, Szewczykowski PP, Perry M, Bohr H, Helix Nielsen C. Hydrogels for in situ encapsulation of biomimetic membrane arrays. Polym Adv Technol 2010;21:1-8.

125. Chen M, Khalid S, Sansom MSP, Bayley H. Outer membrane protein G: Engineering a quiet pore for biosensing. Proc Natl Acad Sci U S A 2008;105(17):6272-7.

126. Chen M, Li Q, Bayley H. Orientation of the monomeric porin OmpG in planar lipid bilayers. ChemBioChem 2008;9(18):3029-36.

127. Orlik F, Andersen C, Danelon C, Winterhalter M, Pajatsch M, Böck A, Benz R. CymA of klebsiella oxytoca outer membrane: Binding of cyclodextrins and study of the current noise of the open channel. Biophys J 2003;85(2):876-85.

128. Locke D, Koreen IV, Liu JY, Harris AL, Locke D. Reversible pore block of connexin channels by cyclodextrins. J Biol Chem 2004;279(22):22883-92.

129. Li-Qun Gu, Cheley S, Bayley H. Prolonged residence time of a noncovalent molecular adapter, beta-cyclodextrin, within the lumen of mutant alpha-hemolysin pores. J Gen Physiol 2001;118(5):481.

130. Belibasakis GN, Meier A, Guggenheim B, Bostanci N. Oral biofilm challenge regulates the RANKL-OPG system in periodontal ligament and dental pulp cells. Microb Pathog 2011;50(1):6-11.

131. Kaufman J, Dirienzo JM. Isolation of a corncob coaggregation receptor polypeptide from Fusobacterium Nucleatum. Infect Immun 1989;57(2):331-7.

132. Kinder SA, Holt SC. Characterization of coaggregation between bacteroides-gingivalis T22 and Fusobacterium-Nucleatum T18. Infect Immun 1989;57(11):3425-33.

133. Kinder SA, Holt SC. Localization of the fusobacterium nucleatum T18 adhesin activity mediating coaggregation with porphyromonas gingivalis T22. J Bacteriol 1993;175(3):840-50.

Paper I

Free-Standing Biomimetic Polymer Membrane Imaged with Atomic Force Microscopy

Christian Rein,[†,‡] Kamila Pszon-Bartosz,[†,§] Karin B. Stibius,[†,||] Thomas Bjørnholm,[‡] and Claus Hélix-Nielsen*,[†,||]

[†]*Aquaporin A/S, Ole Maaløes Vej 3, DK-2200 Copenhagen N, Denmark,* [‡]*NanoScience Center, Copenhagen University, Universitetsparken 5, DK-2100 Copenhagen Ø, Denmark,* [§]*Department of Micro- and Nanotechnology, Technical University of Denmark, DK-2800 Kgs. Lyngby, Denmark, and* [||]*Department of Physics, Technical University of Denmark, DK-2800 Kgs. Lyngby, Denmark*

Fluid polymeric biomimetic membranes are probed with atomic force microscopy (AFM) using probes with both normal tetrahedrally shaped tips and nanoneedle-shaped Ag_2Ga rods. When using nanoneedle probes, the collected force volume data show three distinct membrane regions which match the expected membrane structure when spanning an aperture in a hydrophobic scaffold. The method used provides a general method for mapping attractive fluid surfaces. In particular, the nanoneedle probing allows for characterization of free-standing biomimetic membranes with thickness on the nanometer scale suspended over 300-μm-wide apertures, where the membranes are stable toward hundreds of nanoindentations without breakage.

Introduction

Research and development of biomimetic membranes is in rapid progress[1] and no longer a field where lipids are exclusively used.[2] Today, biomimetic membranes consisting of polymeric components such as amphiphilic block copolymers are increasingly attracting interest, as polymers provide desirable properties as building blocks for a stable matrix hosting transmembrane spanning proteins. Among the advantages polymers provide are high mechanical and chemical stability combined with low permeabilities for water, ions, and gases. In addition, amphiphilic block copolymers can be engineered to provide desired properties such as fluidity or morphology by the choice of blocks, block lengths,[3] and block length ratios.[4] Block copolymer membranes have been shown to incorporate transmembrane protein channels,[5−7] and despite the mismatch between the hydrophobic regions of membrane spanning proteins and the effective hydrophobic thickness of the membrane, proteins may still retain function even after cross-linking.[8]

Biomimetic polymeric membranes formed across circular apertures in a scaffold using a hydrocarbon cosolvent are surrounded by toroidal annuli of polymer and cosolvent[9] similar to what is observed for aperture spanning lipid membranes formed with a cosolvent.[10,11] The edge where the membrane terminates and the toroidal region begins is the so-called Plateau-Gibbs (PG) border. The presence of interface-active components (amphiphiles) promotes thinning of the film and results in a bifacial membrane region in equilibrium with the PG-border and the aqueous phases. Generally, the stability of the thin bifacial region depends on the wettability of the scaffold, charge density, molecular packing, and temperature.[12]

Since the emergence of free-standing lipid bilayers (or black lipid membranes) as model biomimetic membranes, analysis of these thin films has mainly focused on characterizing their electrical, mechanical, mechanoelectric, and optical properties.[13] Recently, atomic force microscopy (AFM) has been used to study membranes suspended over pores[14,15] in aqueous solutions, and recently, both topographic and force-spectroscopic information of free-standing lipid membranes up to 250 nm in diameter have been presented.[16] Unfortunately, most AFM probes have difficulties probing large lipid membranes,[17] and no micrometer-scale biomimetic membranes separating two aqueous compartments have to our knowledge been investigated by AFM.

Various groups have recognized that normal tapered AFM probes are difficult to apply in fluid systems (i.e., membranes) due to the nonconstant wetting while near-constant diameter probe tips (i.e., nanotubes) have been shown to be advantageous in such studies as long as the forces involved did not lead to deformation of the probe.[18−21] Recently, commercially available Ag_2Ga

---

*Corresponding author. Claus Hélix-Nielsen, Department of Physics, Fysikvej 309, Building 309, Office 138. Technical University of Denmark DK2800 Kgs. Lyngby Denmark. E-Mail: claus.helix.nielsen@fysik.dtu.dk.

(1) Martin, D. K. *Nanobiotechnology of Biomimetic Membranes*; Springer: Berlin, 2007.

(2) Nielsen, C. H. *Anal. Bioanal. Chem.* **2009**, *395*, 697.

(3) Discher, D. E.; Eisenberg, A. *Science* **2002**, *297*, 967.

(4) Zhang, L.; Eisenberg, A. *Science* **1995**, *268*, 1728.

(5) Meier, W.; Nardin, C.; Winterhalter, M. *Angew. Chem., Int. Ed. Engl.* **2000**, *39*, 4599.

(6) Ho, D.; Chu, B.; Lee, H.; Montemagno, C. *Nanotechnology* **2004**, *15*, 1089.

(7) Kumar, M.; Grzelakowski, M.; Zilles, J.; Clarck, M; Meier, W. *Proc. Natl. Acad. Sci. U.S.A.* **2007**, *104*, 20719.

(8) Meier, W.; Nardin, C.; Winterhalter, M. *Angew. Chem., Int. Ed.* **2000**, *39*, 4599.

(9) González-Pérez, A.; Stibius, K. B.; Vissing, T.; Nielsen, C. H.; Mouritsen, O. G. *Langmuir* **2009**, *25*, 10447.

(10) White, S. H. *Biophys. J.* **1972**, *12*, 432.

(11) Hansen, J. S.; Perry, M.; Vogel, J.; Groth, J. S.; Vissing, T.; Larsen, M. S.; Geschke, O.; Emneús, J.; Bohr, H.; Nielsen, C. H. *Anal. Bioanal. Chem.* **2009**, *395*, 719.

(12) Tien, H. T. *Bilayer Lipid Membranes (BLM) − Theory and Practice*; Marcel Dekker Inc.: New York, 1974.

(13) Tien, H. T.; Ottova-Leitmannova, A. *Membrane Science and Technology Series 7*; Elsevier: Amsterdam, 2003.

(14) Hennesthal, C.; Drexler, J.; Steinem, C. *Chem. Phys. Chem.* **2002**, *10*, 885.

(15) Hennesthal, C.; Steinem, C. *J. Am. Chem. Soc.* **2000**, *122*, 8085.

(16) Concalves, R. P.; Agnus, G.; Sens, P.; Houssin, C.; Bartenlian, B.; Scheuring, S. *Nat. Methods* **2006**, *3*, 1007.

(17) Quist, A. P.; Chand, A.; Ramachandran, S.; Daraio, C.; Jin, S.; Lal, R. *Langmuir* **2007**, *23*, 1375.

(18) Barber, A. H.; Cohen, S. R.; Wagner, H. D. *Phys. Rev. B* **2005**, *71*, 115443.

(19) Obataya, I.; Nakamura, C.; Han, S.; Nakamura, N.; Miyake, J. *Nano Lett.* **2005**, *5*, 27.

(20) Snow, E. S.; Campbell, P. M.; Novak, J. P. *Appl. Phys. Lett.* **2002**, *80*, 2002.
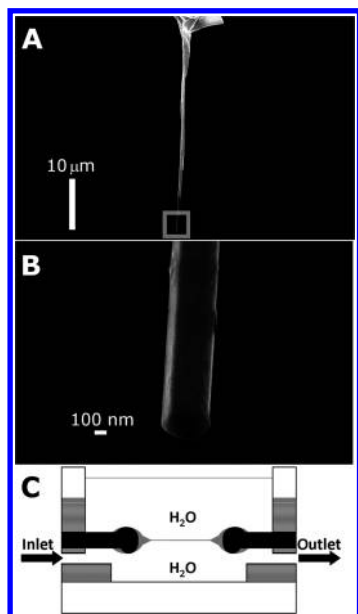

Figure 1. (A) SEM image of the nanoneedle AFM probe used. (B) SEM image of the nanoneedle tip (magnification corresponding to the gray square in A). (C) Schematic cross-sectional view of the custom-made AFM device. The fluid polymer membrane (gray) is formed across a circular aperture (300 μm diameter) in an ETFE scaffold (black) by injecting the polymer solution through inlet and outlet microchannels made in a spacer ring (dashed boxes) of the bottom chamber. The top chamber is open for AFM. The device is clamped via two supportive structures (white boxes).

nanoneedle probes[22] have been developed and present the experimentalist with, among many other possibilities, the option of doing nanoindentation (i.e., measuring the forces when an AFM probe is pressed on/into a sample) with a very precise and constant interaction profile between the probe and the fluid sample. By measuring the interaction between the nanoneedle probe and the fluid membrane, it should be possible to map out the various parts of the biomimetic membrane and map their positions both horizontally and vertically relative to the scaffold surface.

In this study, we demonstrate how nanoneedle probes can be used to study fluid polymeric membranes established in an ETFE scaffold by a horizontal autopainting technique[23] in a custom-made device. A 80 μm $\times$ 80 μm force volume (FV) map was made with an Ag_2Ga nanoneedle probe (see Figure 1A and B) on free-standing membranes near the aperture edge, and analyses of interaction (attraction force), surface tension, and topography data were combined to characterize the membrane and the PG-border. AC240TS probes with tetrahedrally shaped tips served as reference, and analysis of the force−distance curves using the Ag_2Ga and AC240TS probes shows the advantage (i.e., better resolution) of using the Ag_2Ga nanoneedle probe.

Experimental Section

Materials. Triblock copolymers consisting of a middle block of 60 units of poly(dimethylsiloxane) (PDMS) and two 7 unit side blocks of poly(2-methyloxazoline) (PMOXA) carrying methacrylate end groups with a total molecular weight (MW) of 5800 g/mol

($PMOXA_7$-$PDMS_{60}$-$PMOXA_7$) (in short ABA) were custom-synthesized. Tefzel ethylene tetrafluoroethylene (ETFE) LZ100 from DuPont Fluoropolymers (Detroit, MI, US) was used as a scaffold for the membrane.[24] All other chemicals (analytical grade) were purchased from commercial sources.

Methods. 300-μm-diameter apertures in ETFE scaffolds were fabricated by laser ablation as described by Vogel et al.[24] and the scaffold subsequently pretreated with a low-MW hydrocarbon. The partition was placed horizontally in the center of a circular interface between a top and bottom chamber in the AFM device. Two needles, each connected via tubings to a syringe, were inserted into the bottom chamber allowing a flow to be applied through the bottom chamber, while the top chamber was open for both optical and scanning force microscopy. The custom-made AFM device was specifically designed for the MFP-3D AFM instrument with the perforated ETFE partition sandwiched in the middle as shown in Figure 1C.

While monitoring the scaffold with the AFM instrument's internal camera, membranes were created by injecting polymer solution (4.6 mg polymer in 136 μL $CHCl_3$ + 232 μL toluene, 12.5 mg/mL) through one of the tubes connected to the bottom chamber and the other tube. Milli-Q water was injected in the same way afterward. Membrane thinning was promoted by controlling the velocity of the injected water, and care was taken to ensure that air bubbles did not appear in the bottom chamber when forming membranes.

Atomic Force Microscopy. Milli-Q water was used as imaging buffer for the two types of probes. The AC240TS probe (Olympus, Ballerup, Denmark), which has a tetrahedrally shaped tip, has a spring constant of 2 N/m. Tip radius and tip angle were estimated as < 10 nm and ∼35°, respectively.

The nanoneedle probe (Nauganeedles, Louisville, KY, US) was modified with a Ag_2Ga crystal grown out from the end of a tetrahedral tip. The quality was verified with scanning electron microscopy (SEM) using a Jeol JSM 6320F instrument (Jeol Ldt., Tokyo, Japan). The nanoneedle probe was used with a spring constant of 6 N/m, and tip radius and angle were estimated from SEM (see Figure 1A,B) to be ∼200 nm and ∼0°, respectively. For both probes, the scan rates varied from 0.2 to 1 Hz, the area mapped with the force volume (FV) routine was 80 μm $\times$ 80 μm, and the probed Z-distance was 27 μm (i.e., the retraction distance after reaching target force value). If the target force value was not reached, the probe would continue to extend to the maximal distance, which was 40 μm (for further details, see Supporting Information, S1). FV maps consisting of force−distance (deflection of probe vs the Z-distance) data were collected in 2D grids at the region of interest. Probes were rinsed in ethanol and Milli-Q water prior to use, and an MFP-3D atomic force microscope (Asylum Research, Santa Barbara, CA, US) was used with measurements done in contact mode. Both probes were fully submerged in the water at all times. An internal camera gave low-resolution microscopy images of the probed aperture area.

Analysis. *Igor Pro 6.03A* (Wavemetrics, Lake Oswego, OR, US) was used together with custom-made software that automated the calculation of adhesion energy, distance to the hard surface, and the initial attraction force when the probe makes contact with the surface (snap-in force) in the analysis of the FV maps. The adhesion energy was calculated as the area delimited by the retraction force curve, and a virtual line going from the point where the retraction force curve crossed the baseline to the point where the probe loses contact with the surface and jumps away from the surface (the snap-back point). The hard surface distance was determined as the distance at which the targeted deflection (4−100 nN) was reached and the snap-in force was calculated as the force by which the probe was pulled down by the surface at initial contact.

(21) Yazdanpanah, M. M.; Hosseini, Pabba, S.; Berry, S. M.; Dobrokhotov, V. V.; Safir, A.; Keynton, R. S.; Cohn, R. W. *Langmuir* **2008**, *24*, 13753.

(22) Yazdanpanah, M. M.; Harfenist, S. A.; Safir, A.; Cohn, R. W. *J. Appl. Phys.* **2005**, *98*, 073510.

(23) Hansen, J. S.; Perry, M.; Vogel, J.; Hansen, C. R.; Geschke, O.; Emnéus, J.; Nielsen, C. H. *J. Micromech. Microeng.* **2009**, *19*, 025014.

(24) Vogel, J.; Perry, M.; Hansen, J. S.; Bolinger, P.-Y.; Nielsen, C. H.; Geschke, O. *J. Micromech. Microeng.* **2009**, *19*, 025026.
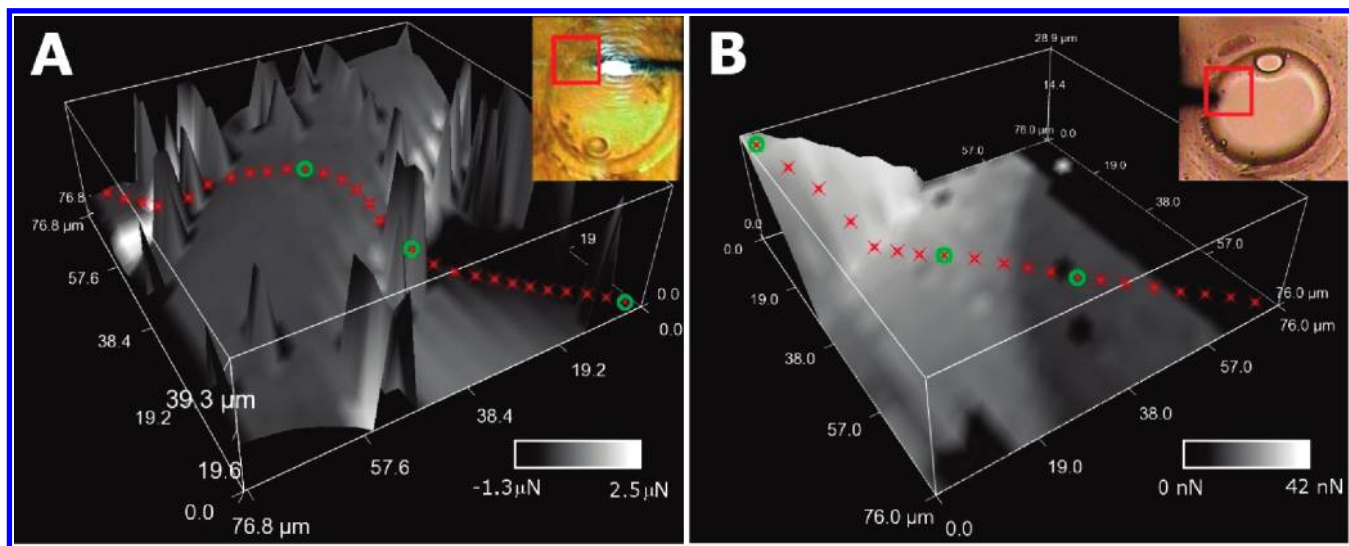
Figure 2. Topographic maps with a gray-scale overlay of the snap-in forces calculated from FV data of the fluid block copolymer membrane probed with the AC240TS probe (A) and with the nanoneedle probe (B). Inserts show optical images of the probed membrane systems where the red squares delimit the areas measured by AFM. In B, the dark gray area in the right-hand part of the box reflects a change in snap-in force indicating a change in structure compared to the light gray areas. Notice the increase in snap-in force sensitivity for the nanoneedle. Representative data points marked by green circles and red crosses along radial lines are analyzed in more detail in Figures 3 and 4, respectively.

Manual cross-section analysis was done by selecting force−distance curves along a radial line across the membrane having a minimum of artifacts in the FV map. By marking the separation values when the deflection change (relative to baseline) reached the targeted values described in Supporting Information (SI 2), it was possible to construct a hard surface (steep positive deflection), a soft surface (snap-in point, negative deflection), and a release surface (snap-back point, deflection returns to zero).

Results and Discussion

The quality of the custom-made nanoneedle probe was verified by SEM (see Figure 1A,B). The total length of the nanoneedle was ∼40 μm, and the width of the crystal on the tip was ∼400 nm. Earlier experiments with the probe had confirmed its robustness when forces in the micronewton range were exerted on it. The quality of the AC240TS probe was not tested before use.

According to earlier experiments,[9] the polymer membrane was expected to be surrounded by a Plateau-Gibbs border that would function as a reservoir of polymer units and cosolvent for the thin polymer membrane in the central region. When probed, the higher aspect ratio of the nanoneedle allowed not only for a more precise control of the probed area, but also for the possibility of probing membrane areas recessed in the aperture.

From the topography maps, the hard ETFE surface could easily be observed (see Figure 2). The torus-surrounded polymeric membrane, which was visible on the optical images (see inserts), was not readily detectable with the AC240TS probe (see Figure 2A), whereas the nanoneedle probe revealed some structure in the aperture region (see Figure 2B).

A snap-in force overlay (gray-scale) added on top of the 3D images in Figure 2 reveals that for the AC240TS probe (see Figure 2A) it is difficult to identify the precise transition between the torus and the central membrane region, although a region with high snap-in force is observable on the sides of the rim indicating the presence of polymer membrane material. For the image made by the nanoneedle probe (Figure 2B), we observe a sharp transition between the torus region and the thin central membrane region.

Both membrane bending and stretching during the many nanoindentations on the thin membrane region make thickness determination difficult. However, previous studies have proved that free-standing $PMOXA_{15}$-$PDMS_{68}$-$PMOXA_{15}$ polymer membranes in the same solvent have a thickness of about 10 nm[25] and are capable of insertion of ionchannels.[8] The PDMS segment in the polymer used in this study consists of 60 units (compared to 68 units used in the previous studies), and therefore, 10 nm is likely to be the upper limit for the membrane thickness.

In order to investigate this further, we selected points across the FV maps (red crosses) arranged radially relative to the aperture center. Three of these points (green circles) in each image were selected to illustrate the probed behavior of the membrane in the three distinct regions—the aperture rim, the toroidal region, and the thin membrane region. The two probes have a large difference in the deflection sensitivity. For the AC240TS probe, both the thin membrane and the thicker torus regions cause strong (off-scale) attraction forces at (and after) the snap-in point in some regions. This appears in the generated 3D topographic map of the hard surface as artificial spikes.

Representative force−distance curves (see Figure 3A,B), corresponding to the green circles in Figure 2) show that the nanoneedle probe is able not only to detect soft surface interactions more precisely than the AC240TS probe, but also to indent thin fluid membranes without rupture as illustrated by the sequence in Figure 3C. Due to the constant small diameter of the nanoneedle, the circumferential surface line interface between probe and the sample remains constant and small, which is in contrast to the AC240TS probe. Upon complete penetration of the fluid membrane, the two surface interactions along the nanoneedle will almost cancel each other out (except for a small drag force), while the AC240TS probe will be buried all the way up to the cantilever leading to imprecise probing. Retracting the nanoneedle will lead to measured force similar to those of measured upon extension, while the AC240TS probe will deflect to extreme degrees before snapping off the surface. The three nanoneedle indentation positions for the thin membrane are marked in Figure 3C.

(25) Nardin, C.; Winterhalter, M.; Meier, W. *Langmuir* **2000**, *16*, 7712.
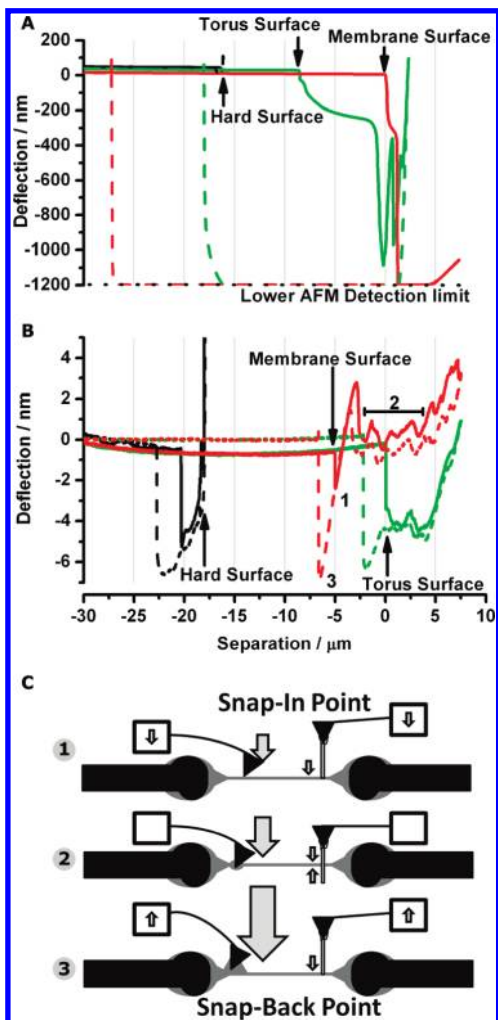
Figure 3. Selected force–distance curves from the green circle data points in Figure 2. (A) AC240TS probe. (B) Nanoneedle probe. Black curves are from the rim, green from the torus, and red is from the thin membrane. Solid lines are extension curves (going left to right), and dashed lines are retraction curves (going right to left). As can be seen, the sensitivity of both probes is similar when a hard surface (i.e., the ETFE scaffold rim) is probed. For soft surface nanoindentations (i.e., in the torus and free-standing membrane regions), only the nanoneedle probe is capable of measuring the interactions without going off-scale. The nanoneedle probe gives reproducible force curves for both extension and retraction through a thin, free-standing membrane similar to previous observations at liquid interfaces.[21] Also, the deflection spike between 1 and 2 is similar to what has previously been observed for cell membrane penetration.[19] (C) Schematic illustration of the system between the snap-in and snap-back events of the probes. The probing method with the AC240TS is shown at the left, and the nanoneedle is shown at the right. The fluid copolymer membrane (gray) spans the aperture in the ETFE scaffold (black). Boxed arrows show cantilever movements, while the other arrows illustrate the size and direction of the forces exerted by the membrane on the probe tip. Sequence numbers refer to positions in B.

Figure 3A illustrates the challenge of deducting the topography of a fluid surface where the point-of-contact leads to out-of-scale attractive interaction forces (corresponding to negative deflections) with the probe. This is in contrast to probing hard surfaces where the point-of-contact leads to repulsive interaction forces (corresponding to positive deflections). Since contact with the soft polymeric surface resulted in only negative deflection forces, we analyzed its topography by measuring the positions at
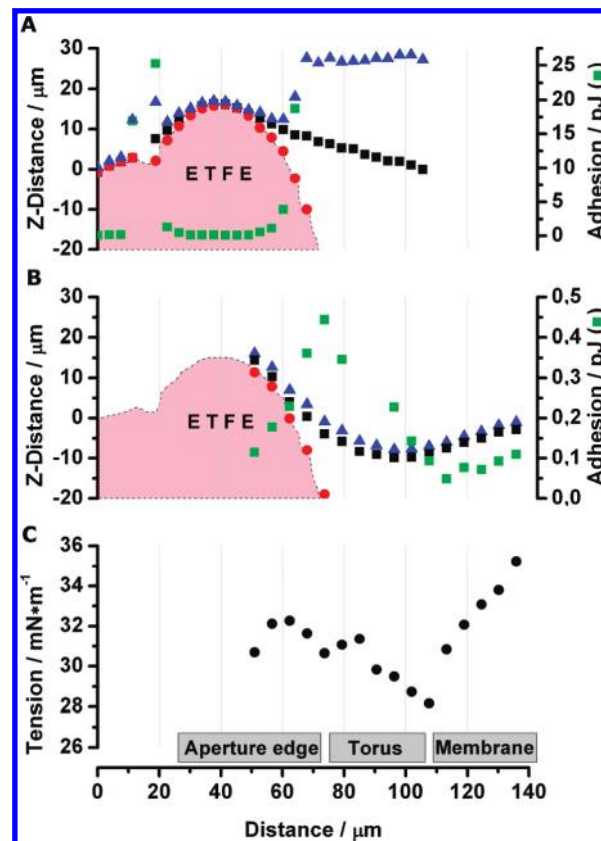

Figure 4. Cross sections of the FV maps made with the AC240TS (A) and the nanoneedle probes (B) at the data points depicted by red ×'s in Figure 2A,B. Black squares: Z-distance of the soft surface (the snap-in point in the force curves; see Figure 3). Red circles: Z-distance of the hard surface (a positive deflection where the target force is reached). Blue triangles: Z-distance of the release surface (the snap-back point in the force curves). Green squares: adhesion energy. Origin of the scales is set to the level of the scaffold far away from the aperture and curves in B are offset such that the hard surfaces are aligned and used as reference. For visual guidance, a light red shading representing the ETFE scaffold (hard surface) is show in both A and B. Adhesion energy data points for the AC240TS probes between 62 and 110 μm are omitted due to off-scale artifacts (see Figure 3A). The points in (C) represent the surface tension at each point in B between the polymer and the aqueous environment calculated from $\gamma = F_r/(2\pi r)$.

which the probe measures the initial negative deflection—the snap-in point. By plotting the snap-in points, the surface of the fluid polymer could be reconstructed and compared to the position of the hard surface. The adhesion energy deducted from each force–distance curve shows a significantly higher sensitivity for the nanoneedle probe compared to that of the AC240TS probe (compare with Figure 3A and B).

The selected data points from the FV images were manually read out and artifacts discarded. The final result is shown in Figure 4. Notice that the adhesion energy is plotted on a much smaller scale for the nanoneedle compared to that of the AC240TS probe.

The experiments show a similar increase in adhesion energy in the region containing the steep inner surface of the aperture. The high adhesion energy for the AC240TS probe, even in the thin membrane region, is likely caused by two types of interactions. One type of interaction occurs when the tetrahedral tip dips into the polymer material. Here, the circumferential interface line length d between tip and sample surface is related to tip penetration as $d = ((z - z_0) \cdot \tan(35°) + 5 \text{ nm})2\pi$, where $(z - z_0)$ is the

penetration depth of the probe tip. Thus, for example when $(z - z_0) = 5 \, \mu$m $d = 22 \, \mu$m. Another type of interaction occurs when the cantilever itself comes into contact with the polymer material. In contrast, for the nanoneedle probe, the circumferential interface line length is almost constant, since it is determined by the nanoneedle cylinder circumference, and thus, $d = \pi 400$ nm $= 1.3 \, \mu$m. As the line tension energy is proportional to line length, the nanoneedle has a significanty lower (and constant) adhesion energy compared to the AC240TS probe. In addition, since the length of the nanoneedle under the tetrahedral tip is about 40 μm, undesirable interactions between cantilever and polymer material (e.g., the torus/rim region) can be avoided.

As a consequence, the attractive force is constant, while the tip is inside the torus (only one interface line) as seen when nanoneedle probes are used to study a continuous fluid medium.[21] The backside of the thick torus layer is reached when the deflection of the nanoneedle probe returns to the baseline (see Figure 3B), and by using this method, an idea of the shape of the torus backside can be found. When probing the thin membrane region, the nanoneedle probe quickly penetrates the membrane without any significant attraction/deflection forces involved, but with a slight drag effect (small deflection on approach and attraction on retraction). The reproducible "ripple" features (in region 2 in Figure 3B) seen in the deflection−separation curve while the thin membrane is penetrated by the nanoneedle are likely caused by small adhesive differences or/and features along the nanoneedle surface.[21]

The difference in probing behavior between the two types of probes is also observed at the "releasing surface", i.e., the surface created above the unperturbed soft surface at the distance (snap-back point) where the polymer releases the probe, For the AC240TS probe, the Z-position of the releasing surface is significantly higher compared to that detected with the nanoneedle probe. This is consistent with the differences in length and form of the probes leading to differences in adhesion between probe and membrane.

The surface tension (Figure 4C) of the biomimetic membrane system probed with the nanoneedle probe can be calculated at each representative data point (same points as used for Figure 4B) by using an equation published for the same probe geometry:[21] $\gamma = F_r/(2\pi r)$, where F_r is the snap-back force and r is the radius of the nanoneedle. The surface tension at the aperture edge is around

31 mN/m, decreasing to about 28 mN/m in the toroidal region, then showing an increasing trend reaching values > 36 mN/m in the central membrane region. This reflects transition from the solvent-containing toroidal region to the central region solventless biomimetic polymer membrane.

Conclusion

The nanoneedle indentation method makes it possible to map micrometer-squared area regions of fluid polymer biomimetic membranes having nanometer-scale thickness. The membranes are stable toward hundreds of these nanoindentations, and the force−distance curves indicate both a torus containing excess membrane material (solvent and amphiphiles) as well as a central thin membrane region. Even though the cantilever is kept ∼40 μm away from the probed surface, it is possible to obtain subnanometer deflection sensitivity on and below the fluid surface with the nanoneedle. In contrast, conventional tetrahedrally shaped tips have much lower force resolution due to their susceptibility to much stronger attraction forces caused by their more bulky probe geometry. The use of nanoneedle-elongated AFM probes significantly reduces the amount of measurement artifacts and increases the precision of the probing allowing for refined structural and functional studies of biomimetic membranes.

Supporting Information Available: Parameters used for the FV experiments (SI 1) and parameters used for making the cross-section analysis (SI 2). The material is available free of charge via the Internet at http://pubs.acs.org.

Paper II

Available online at: OMICS Publishing Group (www.omicsonline.com)

Membrane
Science & Technology

Research Article   **Open Access**

Surface Modifications of Support Partitions for Stabilizing Biomimetic Membrane Arrays

Mark Perry, Jesper S. Hansenz, Karin Stibius, Thomas Vissing, Kamila Pszon-Bartosz, Christian Rein, Bahram Eshtehardi, Maike Benter and Claus Hélix-Nielsen*

Aquaporin A/S, Ole Maaløes Vej 3, DK-2200 Copenhagen, Denmark
DTU Nanotech, Technical University of Denmark, DK-2800 Lyngby, Denmark
NanoScience Center, Copenhagen University, Universitetsparken 5, DK-2100 Copenhagen Ø, Denmark
Nanon A/S, Priorparken 878, 2605 Brøndby, Denmark
DTU Physics,Technical University of Denmark, DK-2800 Lyngby, Denmark

Abstract

Black lipid membrane (BLM) formation across apertures in an ethylene tetra-fluoroethylene (ETFE) partition separating two aqueous compartments is an established technique for the creation of biomimetic membranes. Recently multi-aperture BLM arrays have attracted interest and in order to increase BLM array stability we studied the effect of covalently modifying the partition substrate using surface plasma polymerization with hydrophobic *n*-hexene, 1-decene and hexamethyldisiloxane (HMDSO) as modification groups. Average lifetimes across single-sided HMDSO modified partitions and formed using 1-decene modified partitions were similar and significantly lower than for arrays formed using untreated ETFE partitions. For single side *n*-hexene modification average membrane array lifetimes were not significantly changed compared to untreated ETFE. Double-sided *n*-hexene modification greatly improved average membrane array lifetimes compared to membrane arrays formed across untreated ETFE partitions. *n*-hexene modifications resulted in BLM membrane arrays which over time developed significantly lower conductance (G_m) and higher capacitance (C_m) values compared to the other membranes with the strongest effect for double sided modification. *n*-hexene modification is evident as a change in surface energy whereas the surface roughness does not change significantly. The concomitant low G_m and high C_m values for BLM arrays formed using double-sided *n*-hexene modification enable transmembrane ionic current recordings with a high signal-to-noise (*s/n*) ratio. We demonstrated this by reconstituting gA and α-hemolysin (α-HL) into BLM arrays. The improvement in membrane array lifetime and *s/n* ratio demonstrate that surface plasma polymerization of the supporting partition can be used to increase the stability of biomimetic membrane arrays.

Abbreviations: α-Hemolysin: α-HL; AFM: Atomic Force Microscopy; BLM: Black Lipid Membrane; DPHPC: 1,2-Diphytanoyl-sn-Glycero-3-Phosphocholine; ETFE: Ethylene Tetrafluoroethylene; HMDSO: Hexamethyldisiloxane

Introduction

Biomimetic membranes with embedded proteins are increasingly attracting attention because of their properties as model cell membranes, which can be employed in a variety of fundamental biological studies and medical and technological devices [15,16]. The latter have both scientific and practical interest because of their potential applications in the field of biosensors, drug screening, tissue engineering, and medical implants [12]. Amongst the general challenges in biomimetic membrane design is to scale up membrane effective areas, to create stable (addressable) membrane arrays with long (>days) lifetimes [6]. Specifically, it is important to ensure that the membranes have low ionic permeability as evidenced by a low value for the electrical conductance (G_m) in particular for sensors based on ion channels embedded in biomimetic membrane arrays. Also, a high value for the membrane capacitance (C_m) is desirable in sensors based on detecting changes in membrane impedance. Generally, the formation, stability, and electrical properties of large stable membranes are critically dependent on the coupling between the membrane and its supporting scaffold [8,22,23]. In the development of biomimetic membranes it therefore becomes important to ensure good coupling/adhesion at the interface between the biomimetic membrane and its surrounding scaffold.

Black lipid membrane (BLM) formation across apertures in a hydrophobic scaffold or partition, typically ethylene tetra-fluoroethylene (ETFE), separating two aqueous compartments is

an established technique for the creation of biomimetic membranes [19]. BLMs can be established principally by two basic techniques; the Mueller-Rudin painting technique [16] and the Montal-Mueller folding technique (Montal and Mueller 1972), respectively. Painted BLMs are formed by depositing a solvent (hydrocarbon) containing lipid solution across a partition aperture of up to 1 mm in diameter and then allow the solution to thin out (as evidenced by an increase in C_m) so that a lipid bilayer is formed surrounded by a solvent containing torus. Folded BLMs are formed by spreading lipid monolayers at the air-water interface in each compartment and then raising the aqueous solution resulting in a BLM formed across the partition aperture with typical diameters of 50–100 µm.

Common for both the painting and folding technique for establishing BLMs is the requirement for a partition pretreatment step before stable lipid bilayers with low G_m values – i.e. tight membranes – and high C_m values – i.e. large effective bilayer areas – can be created across the partition aperture. The pretreatment typically consists of applying a hydrocarbon solvent to the partition, which is subsequently

allowed to dry onto it prior to filling the chamber compartments with the electrolyte solution [22]. The partition pretreatment step provides a proper interaction of the lipid molecules around the aperture edge which ensures stabilization of the lipid bilayer. A high degree of stabilization is directly reflected in a low value of G_m and the pretreatment step creates essential conditions for establishing stable biomimetic membranes [19].

Recently, multi-aperture BLM arrays have attracted interest as a method to scale up the effective area of biomimetic membranes [8]. Functional biomimetic membranes formed across multiple apertures requires a high degree of stability and production reproducibility and both parameters are strongly influenced by the partition material properties. Previously we described the development of an automation technique for establishing BLMs in arrays and we showed that variations in the pretreatment of the ETFE partition was a major determining factor for the ability to reproducible establish lipid bilayers [8]. The reproducibility could however be increased significantly by developing a controllable airbrush pretreatment technique. Although a high reproducibility was achieved with the automation technique for establishing lipid bilayers, the low leak currents of established bilayers could only be maintained for approximately 100 min, meaning that membrane lifetimes were not increased concomitantly.

In this study we addressed the stability of painted BLMs as a function of changing the chemical composition of the surface of the partition substrate – mimicking the traditional prepainting. Plasma polymerization is a well-known technique for changing the chemical properties of the top 10-100 nm of a substrate surface while maintaining the bulk physio-chemical substrate properties [24]. Previous studies have shown that plasma polymerization can be used to modify the otherwise chemically inert surface of ETFE and be used to introduce covalently bound surface functionalities onto substrates [9-11,17]. We employed plasma polymerization (see Figure 1A) to add hydrophobic groups to the ETFE substrate material mimicking the traditional prepainting step and evaluated the effects of surface modification on lipid bilayer stability and reproducibility.

We investigated three different monomers for surface modification: hexamethyldisiloxane (HDMSO) 1-decene and *n*-hexene (see Figure 1B-D). HDMSO was chosen because of its ability to form hydrophobic layers on polymeric films by plasma polymerization [2,26], The olefins 1-decene and *n*-hexene were chosen as a mimic to traditional prepainting using a low molecular weight hydrocarbon [8].

We demonstrate that by using double-sided plasma polymerization with *n*-hexene it is possible to obtain stable (i.e. long lived) biomimetic lipid membrane arrays with high C_m values (large effective areas) and good adhesion as reflected by low G_m values. We suggest that plasma polymerization may provide an efficient method to create substrates suitable for establishing reproducible and long-lived bilayer lipid membranes. Moreover, the surface modification can be tailor made for specific membrane forming solutions.

Experimental

Reagents and materials

Tefzel ethylene tetrafluoroethylene (ETFE) LZ200 fluoropolymer for the fabrication of multi aperture partitions were from DuPont Fluoropolymers (Detroit, U.S.A). Sheets of regenerated cellulose (DSS-RC70PP) were purchased from Alfa Laval (Nakskov, Denmark). Round glass cover slips (30 mm) were from VWR – Bie & Berntsen (Herlev, Denmark). *n*-hexene from Fluka, purity ≥ 96 %, hexamethyldisiloxane

(HMDSO) from ABCR purity 98 %, and 1-decene from Aldrich, purity ≥ 94 % were used for plasma polymerization and were purchased from Sigma-Aldrich Denmark (Brøndby, Denmark). Diphytanoyl-*sn*-Glycero-3-Phosphocholine was from Avanti Polar Lipids Inc. (Alabaster, U.S.A). *Bacillus brevis* gAA (gA) (Sigma), *Staphylococcus aureus* α-Hemolysin (Sigma), 99% ethanol, *n*-heptane and *n*-decane (Fluka) were purchased from Sigma-Aldrich Denmark (Brøndby, Denmark). All other chemicals were of analytical grade and purchased from commercial sources.

Micro structuring and surface modification of ETFE partitions

ETFE LZ200 film (50.8 μm thickness) was laser structured to produce partition aperture arrays as previously described [6]. Partitions produced were multi-aperture partitions rectangular with 8 × 8 arrays of apertures with 300 μm aperture diameters and nominal centre–to–centre distances of 400 μm.

Surface plasma polymerization and characterization

Surfaces of ETFE were plasma polymerized with HMDSO, 1-decene, and *n*-hexene in a custom built plasma chamber with a chamber volume of 30 L using argon (Ar) as activation and carrier gas for a sketch of the chamber set up see Figure 1A) and for a general reference please refer to (Yasuda 1985.). The parameters for the plasma treatments are tabulated in the appendix. All surfaces of ETFE

Figure 1: Plasma chamber sketch and monomer structures. A): Diagram of the plasma chamber. The chamber (black outline) is evacuated by a vaccum line (green) where a pump is connected via a trap to collect residual monomers. Electric fields are generated using a generator and antenna in the chamber (blue system). Monomers are supplied as a flow with Ar as carrier gas (red system). B): Hexamethyldisiloxane (HDMSO) monomer. C): 1-decene monomer. D): *n*-hexene monomers.

Figure 2: Principle for establishment of BLM arrays. The aqueous electrolyte solution (is filled up to the cut glass cover slip (A) and the BFS (red) is applied from the top (B). The aqueous electrolyte solution is then slowly applied to the *cis* chamber thereby raising the BFS across the 8×8 aperture partition (green) to form an array of lipid bilayers (C-D).

were cleaned with ethanol (EtOH) and MilliQ water prior to plasma treatment. The Softplasma™ technique for treating ETFE partitions can be divided into an activation step an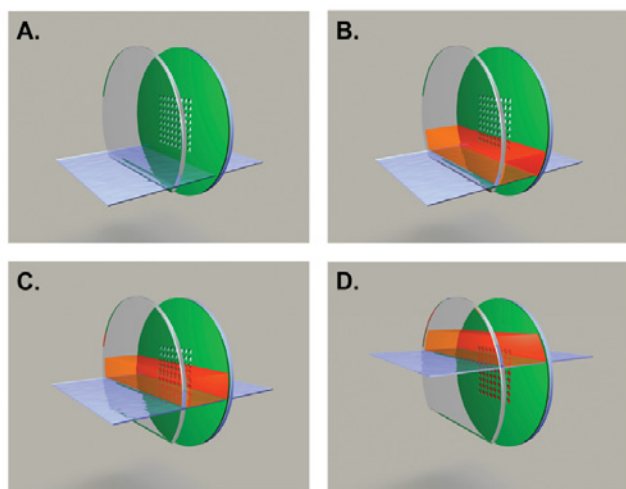d polymerisation step. In the activation step, a 40kHz radio frequency (RF) or 50Hz Argon plasma is created in the plasma chamber at a medium vacuum between 5 and 15Pa. Both the partial pressure and activation time are lower during the activation step as compared to the polymerisation step.

Upon surface activation, the monomer in its gaseous phase is pumped into the plasma chamber. For the surface treatment of our model ETFE partitions a polymerisation time of 7-12 minutes has been found to produce a monomer thickness that renders our samples resistant to our cleaning procedures. After polymerisation the plasma is broken by switching of the power and any non-reacted monomer is pumped out of the chamber. Finally the vacuum is broken by letting air into the plasma chamber. Throughout the procedure mass flow controllers are used to measure Argon and monomer flow. For single-sided treatments the samples were laid out on a glass surface in the chamber, whereas for the double-sided treatments the partitions were mounted in a small grooved aluminum block.

Following plasma polymerization treatment, the water contact angle of the samples was measured using DataPhysics OCA 15 (Filderstedt, Germany) and the samples were characterised using Fourier Transform Infrared/Attenuated Total Reflection (FTIR/ATR) spectroscopy using Thermo Nicolet Nexus 470 Spectrometer (Thermo Scientific Denmark, Copenhagen, Denmark). The spectra were obtained by ATR on a Ge-mirror. The solvent stability of the plasma coatings were tested by analyzing water contact angles and FTIR spectral features before and after rinsing the surface modified samples in three successive rinsing cycles of 60:40 v/v EtOH:water, *n*-heptane, and MilliQ water.

n-hexene modified ETFE partitions were examined using atomic force microscopy (AFM). For comparative measurements a ´half´ *n*-hexene treated surface was prepared by *n*-hexene treating an ETFE partition while protecting part of the surface by a glass slide during plasma modification. The sample was then glued with epoxy to a silicon wafer base. Measurements were made on samples in MilliQ water with an Asylum Research MFP-3D AFM instrument (Asylum Research,

Santa Barbara, CA, US) using a hexadecanethiol modified Au-coated Bio-Lever probe (Olympus Denmark, Ballerup, Denmark) with a nominal tip radius of curvature of 30 nm. The probe was stored in 0.1 MM hexadecanethiol/EtOH for two weeks. Initial stress of the probe was released by allowing it to equalize for 1 hour before measurements. Adhesion energy value maps were calculated by integrating force-distance curves (contact mode) for each pixel (1.56μm × 1.56μm) using an algorithm provided by Asylum Research. The probe was calibrated on the silicon wafer base (Olympus Denmark, Ballerup, Denmark) with contact angle ~40°, and a reference force volume (FV) map was made.

Preparation of lipid solutions and formation of BLM arrays

The bilayer forming solution (BFS) consisted of 1, 2-Diphytanoyl-*sn*-Glycero-3-Phosphocholine (DPhPC) in *n*-decane (50 mg/ml). The lipid solution was prepared the day before, and stored at −20°C until use. Planar lipid bilayers were established across the surface modified ETFE partition arrays by the lipid bilayer automation technique as previously described [8], see Figure 2. Briefly, the two-cell lipid bilayer chamber was assembled with a surface modified 8×8 multi aperture ETFE partition array and with a circular regenerated cellulose sheet (DSS–RC70PP, Alfa Laval, Nakskov, Denmark). This porous semi-supported bilayer design prevents BFS flow through the apertures from the *trans* to the *cis* chamber upon establishment of lipid bilayers. The *trans* chamber was subsequently filled with 7.5 ml 0.2 M KCl saline solution, whereas the *cis* chamber was added 0.5 ml of the saline solution. The lipid bilayer solution (100 μl) was then carefully added to the *cis* chamber using a Hamilton pipette. The level of the aqueous electrolyte solution in the *cis* chamber was then slowly raised by adding approximately 7 ml of the saline solution using a plastic Pasteur pipette. In this way lipid bilayers were created across all of the 64 apertures of the ETFE partition arrays. The formation of lipid bilayers in the partition aperture arrays was recorded by voltage-clamp measurements of the membrane C_m and G_m values [18].

Voltage–clamp data acquisition and processing

The experimental setup consisted of a Model 2400 Patch Clamp Amplifier with a head stage containing $10G\Omega/10M\Omega$ feedback resistors (A–M Systems, Inc., WA, USA) and a Thurlby Thandar Instruments model TG2000 20MHz DDS function generator (RS Components Ltd, Northants, UK). The Ag/AgCl electrodes were placed in the *trans* and *cis* compartments chamber with the ground electrode positioned in the *trans* compartment. G_m and C_m were determined from responses to rectangular and triangular waveforms (20 mV_{pp} and 50 Hz). The capacitance of the perforated ETFE partition in electrolyte only (i.e. no membranes) is < 100 pF. Data acquisition was done with a combined oscilloscope/analog-digital converter (ADC–212/50, Pico Technology, Cambridgeshire, UK) connected to a laptop computer. Sampling frequency was 50 Hz. Off-line analysis was done using custom made software [18]. For the gAchannel activity measurements the peptide was added from ethanolic stock solution to the BFS to a final protein:lipid ratio of 1:10^7. *Staphylococcus aureus* α-Hemolysin (α-HL) was incorporated by adding 10 μl of a 0.5 mg/ml PBS stock solution to the *cis* chamber. For the gAexperiments the aqueous solution was 1 M HCl and for the α-HL experiments the aqueous solution in the chamber consisted of phosphate buffered saline (PBS). The applied potential across the partition arrays was +60 mV.

Results and Discussion

Plasma funtionalization results in robust partition coatings

All samples were characterized using FTIR/ATR and the results

Figure 3: FTIR/ATR spectra of the plasma-treated samples. A): 1-decene treated samples immediately after processing (dark blue), after a single ethanol wash (light green), after a single heptane wash (red) and after three ethanol+heptane washing cycles (light blue). Also shown is reference non-processed ETFE (dark green) and reference ETFE after three ethanol+heptane washing cycles (purple). B): HMDSO treated samples immediately after processing (red) and after three ethanol+heptane washing cycles (green), and reference non-processed ETFE (blue). C): n-hexene treated samples immediately after processing (red) and after three ethanol+heptane washing cycles (green), and reference non-processed ETFE (blue).

are presented in Figure 3. For the 1-decene treated sample (Figure 3A) peaks appear in the 3000 to 2800 cm^{-1} region which are not present in the non-treated ETFE sample shown as dark green (reference) and purple (after 3 ethanol+heptane washing cycles). The dark blue spectrum shows ETFE directly after plasma treatment. The changes are clear, indicating that hydrocarbon groups are on the surface. After washing steps (light green (single ethanol wash), red (single heptane wash) and light blue (three cycles of ethanol+heptane washes) the peaks persist indicating that the chemical structures formed are stable consistent with a covalent modification of the ETFE surface.

The HMDSO treated sample spectra are shown in Figure 3B. The non-treated ETFE (blue) is shown with HMDSO treated (red) and HMDSO treated after three cycles of ethanol+heptane washings). The peaks of the HMDSO interfere with the C-F peaks from ETFE but when low density polyethylene (PE) (Dupont , Geneva, Switzerland) is used as reference instead of ETFE distinct washing cycle resistant peaks at 1230, 1260 and 800 cm^{-1} appear (results not shown) indicating formation of bonded interactions with the substrate.

Figure 3C shows the n-hexene treated samples directly after treatment (red) and after three cycles of ethanol+heptane washings (green) together with the untreated reference (blue). After treatment peaks indicated by asterisks emerge at 2970, 2926, and 2870 cm^{-1} corresponding to CH$_3$ and CH$_2$ groups. The broad peak about 1710 cm^{-1} corresponds to a partial oxidation of the monomer and perhaps some remaining C=C double bonds. Although it is not possible to estimate from FTIR the quantity of the different chemical groups, the spectrum does not change after three washing cycles indicating formation of a stable coating.

The interactions between monomers and the ETFE surface are very complex and simplistic pictures may not adequately describe the interaction. Generally Argon plasma activation will result in defluorination and dehydrogenation of the ETFE and monomers respectively. The resulting free monomer radicals subsequently binds to the ETFE surface as evidenced by FTIR analysis, where spectral features emerging after treatment are resistant to washing procedures indicating formation of stable bonding. Presumably also crossliking between monomers linked to the ETFE also occurs resulting in a bound crosslinked film on the surface.
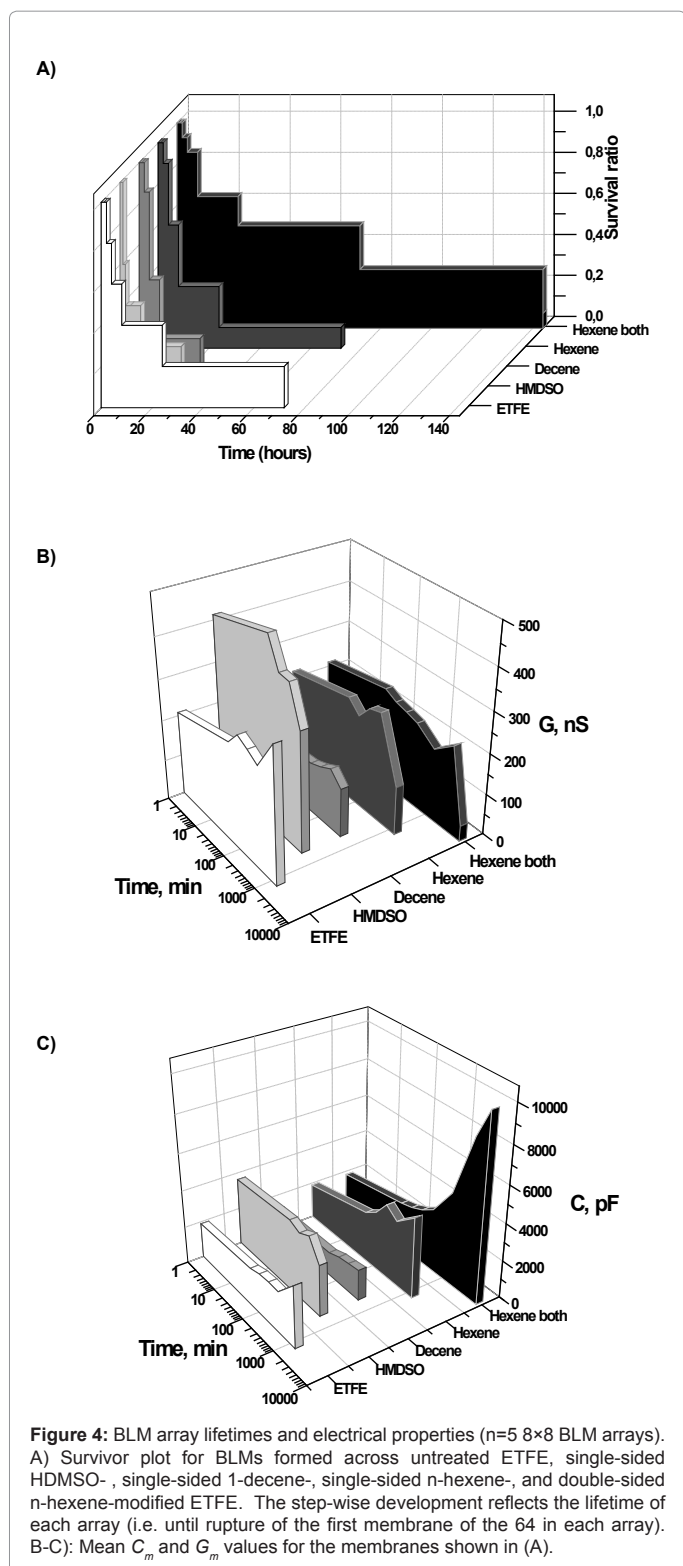
Partition surface modification affects BLM array maximal lifetime

We then tested the BLM array average lifetime for membranes formed using partitions modified with the three modification groups. Lipid bilayers were established with the previously described lipid bilayer automation technique (where the bilayer forming solution is applied from the *cis* side, see Figure 2) [7]. The results are summarized in Figure 4a (*n*=5-12 for each type of modification).

All plasma-treated samples were used after three washing cycles. The 'untreated' ETFE partitions were prepainted with the bilayer forming solution (BFS) according to an 'airbrush' procedure where a thin layer of BFS was deposited on the ETFE surface [8]. With prepainted ETFE partitions we obtained maximal lifetimes just above 70h for 8×8 BLM arrays. We then investigated single side surface modification mimicking the traditional prepainting with a hydrocarbon solvent. Thus in the assembled bilayer chamber the modified surface always faced the *cis* compartment. Lifetimes for BLM arrays formed across single-sided HMDSO modified partitions and BLMs formed using 1-decene modified partitions were similar with a maximal lifetime less than 30h – significantly lower than for BLM arrays formed across untreated ETFE partitions. For single side *n*-hexene modification maximal membrane array lifetimes were not significantly changed compared to untreated ETFE. However, single-sided *n*-hexene modification resulted in membranes that over time developed higher C$_m$ values and concomitant low G$_m$ values compared to all other conditions (see below). This led us to speculate whether we may be able to improve BLM array lifetime induced by *n*-hexene modification by employing modification on both sides of the partitions. Indeed double sided *n*-hexene surface modification greatly improved average membrane array lifetimes, where we obtained a maximal lifetime of 6 days.

Surface modification affects BLM array electrical properties

We assessed the quality of the BML arrays by characterizing their electrical properties, specifically G$_m$ and C$_m$ and the results are presented in Figure 4B and 4C. The G$_m$ and C$_m$ values for each experimental condition represent the average values as a function of time T for the fraction of membranes that have survived until T. Membranes formed

Figure 4: BLM array lifetimes and electrical properties (n=5 8×8 BLM arrays). A) Survivor plot for BLMs formed across untreated ETFE, single-sided HDMSO- , single-sided 1-decene-, single-sided n-hexene-, and double-sided n-hexene-modified ETFE. The step-wise development reflects the lifetime of each array (i.e. until rupture of the first membrane of the 64 in each array). B-C): Mean C_m and G_m values for the membranes shown in (A).

in HMDSO coated partitions have significantly higher G_m values indicating a higher ionic leak. Lower G_m values are seen for membranes formed in the 1-decene coated partitions however this should be seen together with the very low C_m values which indicated that the effective bilayer membrane area for membranes formed in 1-decene coated

partitions is significantly smaller. For the *n*-hexene coated partitions the G_m values are comparable to the values found for membranes formed in the untreated ETFE partitions, however over time the G_m values are reduced significantly indicating that ionic leaks through the membrane is reduced. Comparing G_m in Figure. 4B with C_m in Figure. 4C it is clear, that the trend for G_m follows the trend for C_m over time for membranes formed in ETFE, HMDSO, and 1-decene coated partitions. This is in contrast to the observations when using *n*-hexene coated partitions. Here a significant increase in C_m over time is accompanied with a decrease in G_m. This indicates that for membranes formed in untreated ETFE partitions, HMDSO, and 1-decene coated partitions an increase in membrane area (capacitance) is concomitant with an increase in ionic leak across the membrane. Membranes formed in the *n*-hexene coated partitions show the opposite trend where an increase in membrane area over time is concomitant with a decrease in ionic leak.

Membranes formed in partitions modified on both sides with *n*-hexene evolve from G_m=210 nS and C_m=1800 pF immediately after membrane formation to G_m = 40 nS and C_m= 8640 pF after 140 h. Taking the specific capacitance value of a decane containing lipid bilayer to be 0.4 μF/cm² (Benz et al. 1975), the final conductance of the membrane in double-sided *n*-hexene coated partition corresponds to a bilayer membrane area of 0.02 cm² which is roughly 50% of the available aperture area.
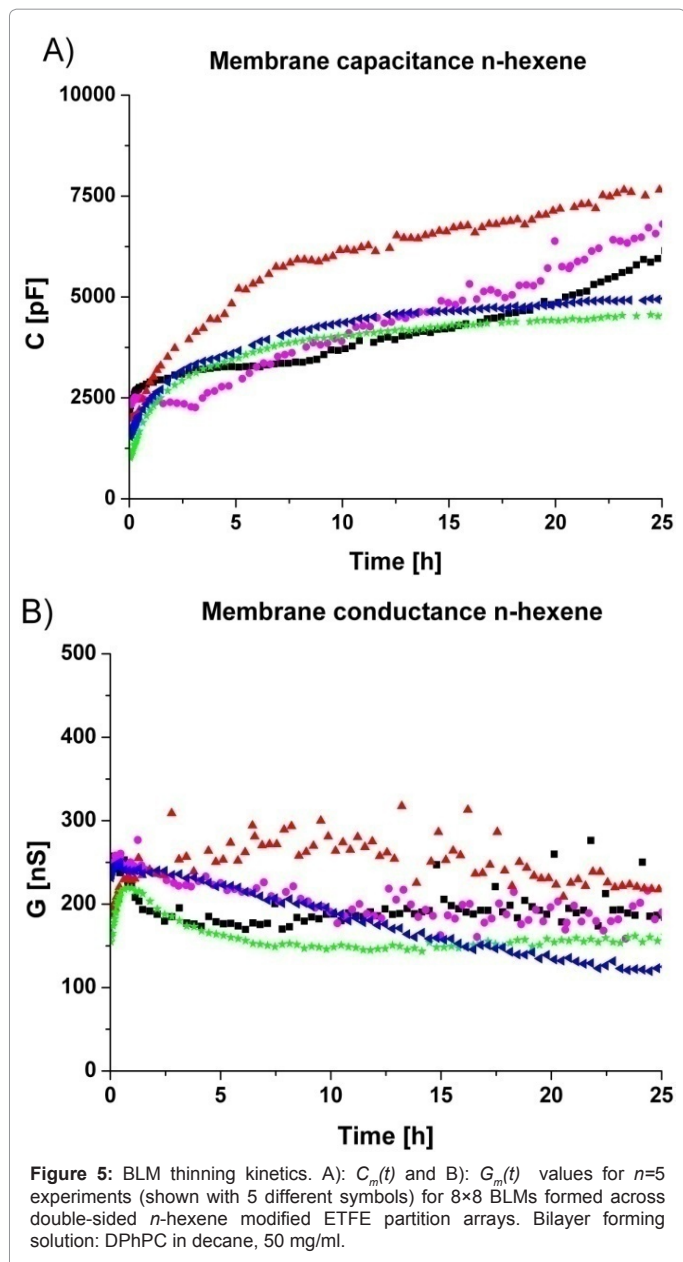
In the early phase (<24h after formation) for double-sided *n*-hexene modified partitions, C_m is around 1800 pF which could suggest that just a BSF 'glob'is formed. However solvent containing membranes generally undergo a 'thinning' process evidenced as an increase in C_m over time while G_m remains constant. We found that double sided modification with *n*-hexene resulted in thinning kinetics in the early phase consistent with the formation of (small) BLM areas in the film, see Figure 5. Thus *n*-hexene wetting of both front and back surfaces is important for BLM array stability – consistent with BLM stabilization originating from the stability of the Plateau-Gibbs border between the BLM and the surrounding hydrocarbon solvent-containing torus [21]. The torus is formed so it contacts both sides of the partition at the rim of each aperture. This is consistent with our observation that only double-sided hexene treatment significantly enhances stability (i.e. slowest release of solvent from the torus) – as none of the single-sided treatments performed here improves stability relative to the case for prepained but otherwise untreated ETFE.

The capacitance increases after about 500 min, but we also note that this increase is over a time period approaching 10.000 min (cf Figure 2C). Thus the apparent dramatic increase is likely to represent (slow) exclusion of decane from the toruses over time so that the effective bilayer area is increasing.

The stabilizing effect of n-hexene is not related to macroscopic hydrophobicity *per se*

n-hexene is a hydrophobic molecule and one might expect that surface hydrophobicity *per se* is responsible for the increased BLM stability and electrical properties. Thus lipid acyl-chains may orient themselves towards the hydrophobic surface creating a lipid mono-layer on the partition surface. In order to obtain insight into the mechanism by which surface modification affected BLM array stability and electrical properties we measured the macroscopic surface hydrophobicity by water contact angle measurements.

None of the hydrophobic monomers applied resulted in an increased hydrophobicity of the ETFE surface. Water contact angles

Figure 5: BLM thinning kinetics. A): $C_m(t)$ and B): $G_m(t)$ values for n=5 experiments (shown with 5 different symbols) for 8×8 BLMs formed across double-sided n-hexene modified ETFE partition arrays. Bilayer forming solution: DPhPC in decane, 50 mg/ml.

Figure 6: AFM imaging of a n-hexene modified partition surface where a triangular area in the lower right corner has been shielded during plasma treatment leaving an unmodified ETFE surface. A): Topographic map. B): Force-distance curves for untreated (black) and n-hexene modified (red) partition surface interacting with a hydrophobic (hexadecane coated) AFM tip. Solid lines represent approach while dashed lines represent retraction. C): 50×50 pixel force volume (FV) map generated from force-distance curves (B) for each pixel for the area shown in A. For the untreated surface area the average adhesion energy W_{ad} = 665±152 aJ (average of 251 FV measurements), while for the n-hexene modified surface W_{ad} = 345±90 aJ (average of 902 FV measurements). For the silicon wafer (natural oxide layer) mounting surface W_{ad} = 122±21 aJ (average of 100 FV measurements).

were reduced by the treatments from 106±2° for pure ETFE to 102±2° for HMDSO, 98±2 ° for 1-decene, and 90±2° for n-hexene. After cleaning with a sequential wash in 60:40 v/v EtOH:water, n-heptane, and MilliQ water the contact angle values for the modified surfaces decreased slightly to 98±2° (HMDSO), 98±2° (1-decene), and 89±2° (n-hexene) respectively. The large difference in electrical properties (G_m and C_m) observed for BLM arrays formed using HMDSO and 1-decene modified partitions is not reflected in the contact angle value which is the same (98°) for both cleaned surfaces. In fact the strongest stabilizing effect was obtained with n-hexene which has the lowest contact angle value (89°).

Quantification of n-hexene modification induced changes in partition surface energy

In order to investigate whether the stabilizing effect of n-hexene was related to changes in nano-scale surface roughness we characterized the
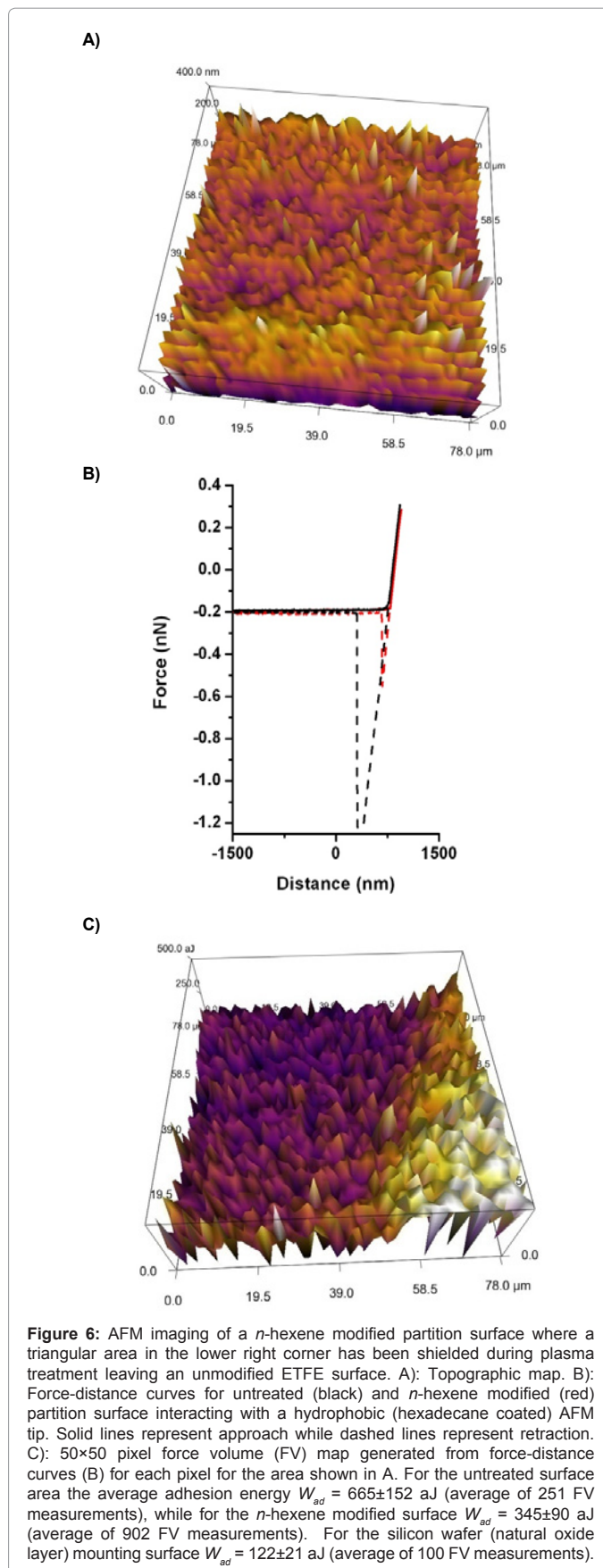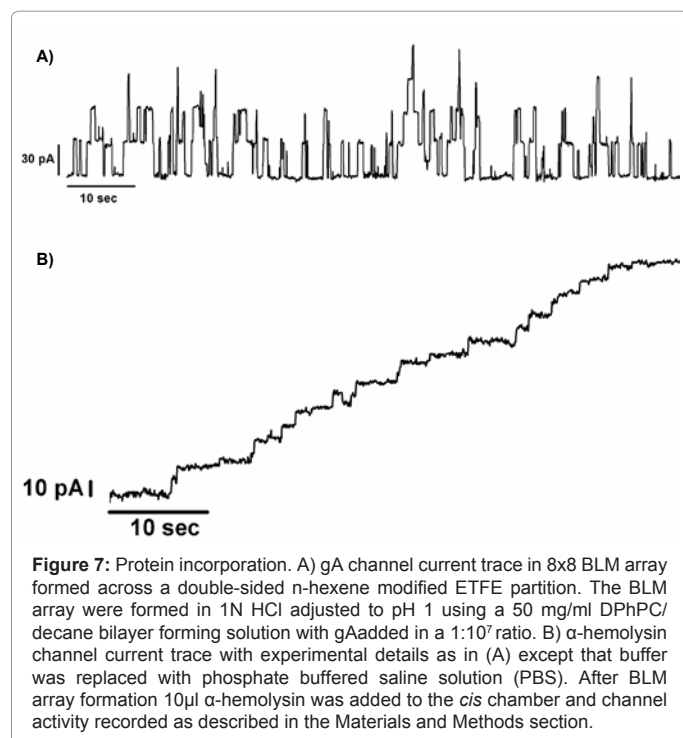
Figure 7: Protein incorporation. A) gA channel current trace in 8x8 BLM array formed across a double-sided n-hexene modified ETFE partition. The BLM array were formed in 1N HCl adjusted to pH 1 using a 50 mg/ml DPhPC/decane bilayer forming solution with gAadded in a 1:10^7 ratio. B) α-hemolysin channel current trace with experimental details as in (A) except that buffer was replaced with phosphate buffered saline solution (PBS). After BLM array formation 10µl α-hemolysin was added to the *cis* chamber and channel activity recorded as described in the Materials and Methods section.

Surface	Water contact angle Pre wash	Water contact angle Post wash
Untreated ETFE	106°	106°
HMDSO	102°	98°
1-decene	98°	98°
n-hexene	90°	89°

Table 1:

surface topography and of non-treated versus *n*-hexene modified ETFE partition surfaces using atomic force microscopy (AFM) topographical measurements. The results are shown in Figure 6A. Wure found no structural difference between normal and *n*-hexene plasma treated surfaces (see Figure 6A). We then investigated the adhesion energies W_{ad} between a hexadecane functionalized AFM tip (mimicking the lipid molecule acyl chains) and the surfaces by measuring force-distance relations (see Figure 6B) and obtained a force-volume (FV) map of the ETFE and n-hexene modified surface (see Figure 6C). The corresponding W_{ad} values (*mean±s.d.*) were 665±152 aJ (*n*=251 FV measurements) for the untreated surface and 345±90 aJ (*n*=902 FV measurements) for the *n*-hexene treated surface. For comparison for the silicon wafer (natural oxide layer) W_{ad} = 122±21 aJ (*n*=100 FV measurements). Thus the decrease in contact angle from 106º to 89º corresponds to an almost 50% decrease in adhesion energy probed with a hexadecane coated surface. The W_{ad} values reflect both the interactions between the interfaces (hexadecane/*n*-hexene, hexadecane/ETFE, or hexadecane/silicon) and the entropic cost of re-wetting both interfaces upon tip withdrawal.

In general high adhesion energies coincide with high hydrophobicity which is consistent with surface thermodynamics. However the stabilizing effect of *n*-hexene is not due to an increase in hydrophobicity *per se*; 1-decene modified surfaces which have a higher contact angles in fact results in less stable BLMs. This suggests that the energetics of the interaction between modified surfaces and a lipid/hydrocarbon phase not only relates to macroscopic hydrophobic wetting but also involves contributions due to the amphiphilic nature

of the lipids. The stabilizing effect may thus be related to the molecular structure of hexene beyond a mere hydrophobic/ mesoscopic surface topography based mechanism. Since torus stability is related to effective 'sealing' with lipid monolayers interfacing the hydrocarbon containing torus with the aqueous phase, our results suggest that the hexene moieties provides a more favorable interaction with the lipid acyl chains than the other monomers tested.

n-hexene modified ETFE partitions provides BLM arrays with a high current *s/n* ratio

To demonstrate that *n*-hexene modified partition aperture arrays combined with the BLM automation technique design are able to support functional incorporation of membrane proteins we reconstituted the peptide gA from *B. brevis* into a BLM array 24h after membrane formation. The pentadecapeptide subunits residing in each monolayer of the lipid bilayer form a cation-selective dimer channel resulting in channel activity as shown in Figure 7A, for a general gA review see [1]. To further demonstrate protein incorporation we established α-HL into 8×8 BLM arrays. The pore of α-HL is created in the lipid bilayer upon assembly of seven 33 kDa monomeric polypeptides on the membrane surface (Dinges et al. 2000; Fink et al. 1989). Figure 7B shows a current trace after addition of α-HL demonstrating the formation of α-HL pores.

A G_m value of 40 nS observed for membranes established on double sided n-hexene treated partitions corresponds to a resistance of 25 MΩ for the entire 64 aperture array. The discrepancy between 25 MΩ and the giga Ohm resistance usually recorded for lipid membranes is attributed to the presence of a leak current in our chamber setup. We have previously determined the leak current to be around 50-100nS (data not shown). In other words, when our membrane arrays are completely sealed in all 64 apertures, the current detected by our set-up is the leak current in our system. As soon as a single aperture membrane breaks, ions can freely flow across the partition separating the *cis* and *trans* chambers in our set-up and we observe a dramatic increase in the detected current between said chambers. The combination of a sufficiently stable leak current with GΩ membrane seals still enables us to perform transmembrane ionic current recordings with a high current amplitude signal-to-noise (*s/n*) ratio.

This suggests that the established BLM arrays may be developed into biosensor arrays where the sensor readout is based on e.g. the activity of single ligand-gated ion channels.

Conclusion

In this study, we were able to increase the reproducibility and stability of BLM arrays by forming the arrays across ETFE partitions modified using double-sided *n*-hexene plasma polymerization. This demonstrates that the adhesion between the lipid and substrate is an important factor for establishing stable planar lipid bilayer membranes. The bilayer stabilizing adhesion induced by *n*-hexene is not correlated with macroscopic hydrophobicity. The shorter *n*-hexene monomers have a stronger stabilizing effect than the longer more acyl-chain like 1-decene monomer. This suggests that the stabilizing effect is not only determined by hydrophobic wetting, but also by the amphiphilic nature of the lipid molecules. The concomitant low G_m and high C_m values for bilayers formed using double-sided *n*-hexene modification enable recordings of transmembrane ionic currents with a high s/n ratio. Thus *n*-hexene modification can be used to stabilize large arrays of biomimetic membranes and still enable current recordings with single channel resolution. In conclusion, plasma polymerization

may be employed to create surface modified scaffolds with improved stability performance for biomimetic membranes. The general versatility in surface modification implies that it can be tailored to meet specific requirements dictated by the choice of biomimetic membrane components.

Acknowledgments

References

1. Andersen OS, Kopppe II RE, Roux B (2007) Gramicidin channels: Versatile tools. In: Chung SH, Andersen OS, Krishnamurthy V (eds) Biological Membrane Ion Channels. Springer, New York, pp 33-80

2. Behnisch J, Tyczkowski J, Gazicki M, Pela I, Holländer A et al. (1998) Formation of hydrophobic layers on biologically degradable polymeric foils by plasma polymerization. Surface and Coatings Technology 98:872-874

3. Benz R, Fröhlich O, Läuger P, Montal M (1975) Electrical capacity of black lipid films and of lipid bilayers made from monolayers. Biochim. Biophys. Acta 394:323-334

4. Dinges MM, Orwin PM, Schlievert PM (2000) Exotoxins of Staphylococcus aureus. Clin Microbiol Rev 13:16-34

5. Fink D, Contreras ML, Lelkes PI, Lazarovici P (1989) Staphylococcus aureus alpha-toxin activates phospholipases and induces a Ca2+ influx in PC12 cells. Cell Signal 1:387-93

6. Hansen JS, Perry M, Vogel J, Groth J, Vissing T et al. Bohr H, Nielsen CH (2009a) Large scale biomimetic membrane arrays. Anal Bioanal Chem 395:719-727

7. Hansen JS, Perry M, Vogel J, Vissing T, Ibragimova S et al.(2009b) Development of Novel Biomimetic Membrane Design. Biophysical Society Meeting Abstracts. Biophysical Journal, Supplement 2009:635a

8. Hansen JS, Perry M, Vogel J, Vissing T, Geschke O et al.(2009c) Development of an automation technique for the establishment of functional lipid bilayer arrays. J. Micromech. Microeng. 19:025014

9. Inagaki N, Narushima K, Amano T (2006) Introduction of carboxylic groups on ethylene-co-tetra fluoroethylene (ETFE) film surfaces by CO2 plasma. J. Adhes. Sci. Technol. 20:1443-1462

10. Inagaki N, Narushima K, Kuwabara T, Tamura K (2005) Introduction of amino functionalities on ethylene-co-tetrafluoroethylene film surfaces by HN3 plasmas. J. Adhes. Sci. Technol. 19:1189-1205

11. Inagaki N, Narushima K, Lim SK, Park YW, Ikeda Y (2002) Surface modifications of ethylene-co-tetrafluoroethylene films by remote plasma. J. Polym. Sci. B. 40:2871-2882

12. Martin DK (2007) Nanobiotechnology of Biomimetic Membranes. Springer Verlag, New York, pp 173

13. Montal M, Mueller P (1972) Formation of bimolecular membranes from lipid monolayers and a study of their electrical properties. Proc Natl Acad Sci U S A 69:3561-6

14. Mueller P, Rudin DO (1969) Translocators in bimolecular lipid membranes: their role in dissipative and conservative bioenergetic transduction. Curr Topics Bioenergetics 3:157–249

15. Nielsen CH (2009a) Biomimetic membranes for sensor and separation applications. Anal Bioanal Chem 395:697-718

16. Nielsen CH (2009b) Major Intrinsic Proteins in Biomimetic Membranes. In: Jahn TP, Bienert GP (eds) Major Intrinsic proteins and their role in the exchange of metalloids. Landes Bioscience Publishers, Austin, TX, pp 127-145

17. Park YW, Inagaki N (2004) A new approach for selective surface modification of fluoropolymers by remote plasmas. J. Appl. Polym. Sci. 93:1012-1020

18. Perry M, Vissing T, Boesen TP, Hansen JS, Emneus J, Nielsen CH (2009) Automated sampling and data processing derived from biomimetic membranes. Bioinspir. Biomim. 4:44001

19. Tien HT, Ottova-Leitmannova A (2003) Planar lipid bilayers (BLMs) and their applications Membrane Science and Technology Series. Elsevier, Amsterdam, pp 1034

20. Vogel J, Perry M, Hansen JS, Bolinger PY, Nielsen CH, Geschke O (2009) A support structure for biomimetic applications. Journal of Micromechanics and Microengineering 19:025026

21. White SH (1972) Analysis of the torus surrounding planar lipid bilayer membranes. Biophys J 12:432-45

22. White SH, Petersen DC, Simon S, Yafuso M (1976) Formation of planar bilayer membranes from lipid monolayers. A critique. Biophys J 16:481-9

23. White SH, Thompson TE (1973) Capacitance, area, and thickness variations in thin lipid films. Biochim Biophys Acta 323:7-22

24. Yasuda H (1977) Modification of polymers by plasma treatment and by plasma polymerization. Radiat Phys Chem 9:805-817

25. Yasuda H (1985.) Plasma Polymerization. . Academic Press, Inc. , Orlando, Fl:

26. Zanini S, Riccardi C, Orlandi M, Esena P, Tontini M. et al.(2005) Surface properties of HDMSO plasma treated polyethylene terephathalate. Surface and Coatings Technology 200:953-957.

Paper III

Automated and closed microfluidic formation and regeneration of highly stable biomimetic membrane arrays

K Pszon-Bartosz[1,2], M Perry[1], J S Hansen[1,2], J Vogel[1,2], C Hélix-Nielsen[1,3], J Emnéus[2] and O Geschke[1,2]

[1]Aquaporin A/S, Ole Maaløes Vej 3, 2200 Copenhagen N, Denmark

[2]Technical University of Denmark, Department of Micro- and Nanotechnology, DTU Nanotech building 345   east, DK-2800 Kongens Lyngby, Denmark

[3]Technical University of Denmark, Department of Physics, DTU Physics 309, DK-2800 Kongens Lyngby, Denmark

E-mail: Kamila.Pszon@nanotech.dtu.dk

Abstract

Biochemical analysis of membrane proteins is still a difficult task and requires a method for formation of stable and long lasting lipid membranes; the natural platform to sustain protein functionality. A fully automated and closed microfluidic device for the formation, regeneration and investigation of an array of planar lipid membranes was developed using CO_2 laser ablation. The device comprised five layers clamped together, rendering the device cleanable and reusable. By voltage clamp measurements, it was shown that the device allowed the formation and regeneration of an array of lipid bilayers across a perforated (8 x 8 apertures) ETFE partition and that microfluidic pumping enabled thinning of the thick lipid-solvent to form the lipid bilayer. Voltage clamp measurements showed moreover that the pore-forming heptameric α-HL membrane protein could successfully be reconstituted into the bilayer lipid array by simple injection into the microfluidic system.

Abbreviations

α-HL   α-Hemolysin

BFS   Bilayer Forming Solution

BLM   Black Lipid Membrane

DPhPC   1,2-Diphytanoyl-*sn*-Glycero-3-Phosphocholine

ETFE   Ethylene Tetrafluoroethylene

NBD-PC   1-Oleoyl-2-[6-[(7-nitro-2–1,3-benzoxadiazol-4-yl)amino]hexanoyl]-*sn*-
                glycero-3-phosphocholine

PMMA   Poly(methyl methacrylate)

PTFE   Polytetrafluoroethylene

1.Introduction

There is a growing interest in trying to mimic biological membranes by creating artificial lipid bilayers (biomimetic membranes), which can be used in sensor and separation devices [1]. However, there are still many difficulties to be overcome; amongst these are the inherent fragility of lipid membranes and the challenge of up-scaling the effective membrane area. Various methods for the formation of membrane arrays with long lifetimes (>days) have recently been investigated [2, 3].

Conventionally, lipid membranes are formed across apertures in a hydrophobic material separating two aqueous compartments. In principle they can be established by two different methods; the Mueller-Rudin painting method [4] and the Montal-Mueller folding method [5]. In the folding method, a lipid monolayer is spread at the air-water interface in each compartment. Raising the aqueous solution results in membrane formation across the aperture. In the painting method, lipid membranes are formed by self-assembly of an initially thick lipid-solvent film spread over one side of an aperture submerged in aqueous solution. The lipid layer gradually thins down to form a bilayer. However, this spontaneous process is rather slow and several ways to induce the thinning process have been presented [3, 6-13] Some of them have been performed in microfluidic systems, the motivation being that it enables rapid exchange of electrolytes, use of small quantities of materials, rapid transport of material to and from the lipid membranes and finally the possibility for automation [11, 14]. Automated formation of lipid bilayers in a microfluidic system was proposed by Malmstadt et al. [6] and by Funakoshi et al. [15]. However, in both cases the bilayers were formed inside the microfluidic channels perpendicular to the channel wall and therefore electrolyte exchange was not possible. Several studies on membrane formation in a microfluidic system, enabling liquid exchange on both sides of the membrane, have been presented with a microfluidic channel on one side of the membrane, leaving the top compartment of the device

open. Open systems like this may however lead to problems with solvent evaporation and limited membrane stability. Therefore, closed devices with flow possibilities on each side of the membrane have recently attracted researchers' attention. Mach et al. [14] designed a microfluidic device for automated formation of a single lipid bilayer by giant liposome adsorption across a micron-sized aperture in a glass slide, sandwiched between two polydimethylsiloxane (PDMS) channels, allowing fast perfusion on each side of the membrane. Suzuki et al. [16] presented an automated and closed double-layered channel device for one lipid bilayer formation. Sandison et al. [11] proposed a closed system fully accessible via microfluidic channels on both sides of the membrane and also showed that they were able to form a single lipid bilayer membrane by spontaneous thinning of the lipid solution, encouraged by buffer agitation in both channels.

Whereas creation of a single biomimetic membrane across an aperture is a well-established technique, creation of biomimetic membranes in arrays is not straightforward. Microfluidic help in that matter was suggested by Suzuki et al. [16] and Sandison et al. [11]. These authors mentioned the possibility for up-scaling the effective membrane area by producing many apertures along the channel and arrays of apertures in polymer partition, respectively. However, due to the stability problem of a micrometer-sized membrane made in a device with upper and lower flow channels the up-scaling approaches have only been established in the configuration with microfluidic channels on one side of the membranes [17].

Here, we presented a new way of increasing micrometer-sized BLM stability in a closed and automated microfluidic device by using an array of micropores. This is an alternative to reported by Kawano et al. BLM stability improvement by forming a lipid membrane across a nanopore instead [18]. The hypothesis that is should be possible to create bilayers by microfluidic pumping of a lipid solution across an array of micro-meter sized apertures in a fully automated horizontal device, where a subsequent pumping of electrolyte would induce lipid film thinning was based on our earlier work. We have already shown that the process of multiple bilayer formation could be established by manual raising the aqueous electrolyte solution leading to the raising of the bilayer-forming solution across an array of apertures in a vertical device [19]. Moreover we showed that scaling up the membrane area led to an increase in membrane lifetime [3].

Here, we developed a microfluidic system in order to enable continuous formation, thinning, and regeneration of an array of micrometer-sized bilayer lipid membranes in a fully closed and automated microfluidic device, as well as the automated reconstitution of a membrane protein inside the BLMs. The device was entirely fabricated by the CO_2 laser ablation in ETFE, PMMA and Viton® materials, which is a quick and inexpensive alternative to existing technologies like micro milling, casting or silicon technology for microarray based device production. The device provides an environment for the reconstitution of proteins that is

similar to their native one, with the bilayer membrane surrounded by water on both sides, and with the possibility for control of electrolytes on both sides of the membrane and fast and precise exchange/regeneration of the membrane itself.

The device fabrication time and the material costs are very important parameters to ensure that biomimetic membrane based arrays are made economically feasible for example for creating commercially available equipment for biochemical studies of proteins and for the development of future sensor arrays and separation technologies. Therefore, preferred biomimetic membrane designs comprise single-use chambers or microarray devices that are based on low-cost materials and are easy to produce.

2. Materials and methods

2.1. Reagent and materials

Poly(methyl methacrylate) (PMMA) raw material was used (Nordisk Plast A/S, Denmark) in various plate thicknesses: (1.5, 1.75 and 4) mm. Ethylene tetrafluoroethylene (ETFE) Tefzel LZ200 fluoropolymer for the fabrication of multi-aperture partitions, and Viton® A fluoroelastomer for the production of microchannels were both from DuPont Fluoropolymers (Detroit, U.S.A.). Double adhesive acrylic tape (ARcare® 90819, Adhesives Research, Ireland) was used for the production of device sealing parts. A conventional laboratory oven (Memmert GmbH, Schwabach, Germany) was used for the annealing process of PMMA plates in order to avoid stress cracks.

Ethanol [analytical grade, 97%] was purchased from Merck KGaA (Darmstadt, Germany). A 5 mg/ml lipid-solvent solutions of 1,2-diphytanoyl-sn-glycero-3-phosphocholine (Avanti Polar Lipids, USA) in n-decane, doped with 1 mol% 1-oleoyl-2-[6-[(7-nitro-2-1,3-benzoxadiazol-4-yl)amino]hexanoyl]-*sn*-glycero-3-phosphocholine (Avanti Polar Lipids, USA), was used for membrane formation. Staphylococcus aureus α-Hemolysin (Sigma), n-decane (Fluka) and potassium chloride powder were purchased from Sigma-Aldrich Denmark (Brøndby, Denmark). All electrolyte solutions were prepared using Milli-Q water.

2.2. CO_2 laser setup

The laser micromachining was carried out using a Synrad Inc. (Mukilteo, WA, USA) 48-5S Duo Lase carbon dioxide laser. A computer aided design program WinMark Pro® version 4 from Synrad Inc. (Mukilteo, WA, USA) was used to set the movements of the laser beam, number of laser beam passes over a given design, laser beam speed and laser output power. The laser had a maximum output power of 65 W, which could be varied linearly. The laser system was equipped with a marking head containing a field lens and two swivel-mounted mirrors. The lens was able to focus the laser beam to a 290 µm diameter spot at a focal

distance of 190 mm. The mirrors allowed the placement of the focused laser beam anywhere on a 110 by 110 mm large working area. The maximum speed of the beam was 1000 mm s^{-1}.

2.3. Device design, fabrication and assembly

The microfluidic device design is depicted in Figure 1. Each part (including tape and holders) was fabricated using CO_2 laser technology. Laser settings (number of laser beam passes, laser power and velocity) were adjusted individually to each microfluidic device part. Microchannels were fabricated in two 1 mm thick fluoroelastomeric (Viton®) parts (47 mm x 32 mm), which were then sandwiched with double adhesive tapes on both sides of a 50 µm ETFE partition (47 mm x 32 mm). The sandwich was then covered on both sides with 1.75 mm thick PMMA plates (47 mm x 32 mm), each sealed by tape and then clamped with 4 mm thick PMMA holders (48 mm x 48 mm), using four screws. The two Viton® parts had square chambers in the middle (10 mm x 10 mm) connected to the microchannels, enabling liquid injection and removal. The microchannel system is presented in Figure 1b and the typical Gaussian profile of the cross-section of one of the Viton® channels is shown in Figure 1c. The central 50 µm thick ETFE partition, with an array of 8 x 8 apertures (300 µm in diameter, 400 µm - centre-centre distance between neighbouring apertures), was laser micromachined as previously described [20]. The ETFE surface was covalently modified by plasma treatment with lower-carbon-chain-length alkanes, predominantly hexanes, resulting in a hydrophobic surface coating. This surface modification was applied to provide a molecular anchoring for establishing the lipid membranes across the micro-structured arrays.

Prior to alignment and assembly the different parts were cleaned by flushing or sonication with ethanol and water. The most crucial step was the sealing of the Viton® parts with the ETFE partition, since placing the double adhesive tapes around the microchannel edges required high precision. To enable connection of the Viton® microchannels to the outer world, prior to sealing, 10 µl Eppendorf tips (Eppendorf Nordic, Denmark) were put into holes made by 0.7 mm in diameter needles on two sides of the Viton® material. The plastic tips provided flexible but stable interconnection between the Viton® microchannels and PTFE tubing with an inner diameter of 0.8 mm and an outer diameter of 1.6 mm (Bohlender GmbH, Germany). In order to improve fluidic sealing, 5 mm thick PMMA plates were used to clamp the device together.

2.4. Characterization of Viton® micro-channels

To characterize the black non-transparent Viton® fluoroelastomeric material optical microscopy was used. The channel depth and width were measured by taking pictures of the channel cross-section using a Leica DML optical microscope and a built-on Canon Power Shot S40. The pictures were analysed using the freeware software ImageJ. The channel depth

and width were measured using a built-in measurement function, relating the acquired length in pixels to a scale.

2.5. Connection with injector, pumps and electrical set up

The microfluidic system set-up, with pumps, injector, syringe barrels and electrodes is illustrated in Figure 2. The device consisted of two compartments, each one with its own inlet and outlet. The inlet of the top and bottom compartment was connected to each a syringe pump (1 and 3) (model: 540060, TSE system GmbH, Germany). The bottom compartment was in addition connected to a six-valve rotary injector (2) (IDEX Health & Science, Germany) equipped with a 40 µl injection loop for injection of small quantities of different liquids. Both outlets were further connected to Ag/AgCl electrodes inserted in two syringe barrels (4 and 5) with the same level of liquid to minimize the pressure difference on each side of the ETFE partition.

The microfluidic device, injector and syringe pumps were placed in an in-house manufactured Faraday cage in which Voltage clamp measurements were performed. The electrical setup consisted of a headstage (HS-2A, Eastern Scientific LLC), an amplifier (PICOAMP-300, Eastern Scientific LLC), and an oscilloscope (IDS710, ISO-TECH). Data acquisition was performed with a combined oscilloscope/analogue-digital converter (ADC-212, Pico technology). A 200 mM or 1 M KCl solution served as an electrolyte for membrane and protein incorporation characterisation, respectively. By applying triangular and rectangular voltage clamp wave forms across the BLMs, and measuring the resulting responses, the capacitance and conductance of the membrane array could be calculated respectively, as previously described [21]. To measure protein incorporation electrically, a potential of 60 mV was applied, and the resulting membrane output current was filtered through 1 kHz on the amplifier and subsequently further filtered through a low-pass Bessel filter with 50 Hz cut-off (Frequency Devices, IL, USA) before data acquisition.

2.6. Flow rate tests

Different flow rates with either electrolyte or n-decane were tested through the upper and bottom compartments to ensure that no leakage took place in the system. Pumping was carried out at increasing flow rates from 5 to 50 µl/min − with increments of 5 µl/min, until leakage was observed or for 10 min if the device was not leaking.

2.7. Preparation of lipid solutions for BLM experiments

The bilayer forming solution (BFS) consisted of 1,2-diphytanoyl-*sn*-glycero-3-phosphocholine (DPhPC) in n-decane (5 mg/ml), doped with 1 mol% 1-oleoyl-2-[6-[(7-nitro-2-1,3-benzoxadiazol-4-yl)amino]hexanoyl]-*sn*-glycero-3-phosphocholine (NBD-PC) to

enable visual inspection of the BFS. The BFS was prepared the day before, and stored at −20 °C until use.

2.8. *Procedure for bilayer membrane formation*

Planar lipid membranes were established across the laser microfabricated ETFE partition array by a modification of the lipid bilayer painting method [4]. The main difference was that the lipid bilayer was automatically formed and thinned aided by microfluidics. The procedure is illustrated in Figure 3: (a) the electrolyte was pumped at a flow rate of 50 µl/min, through both compartments of the microfluidic device, (b) 40 µl of the BFS was then injected into the bottom compartment. As the BFS passes the ETFE partition, it is painted onto the array, (c) the excess BFS is removed and the membrane thinning process induced by the continuous flow of electrolyte through the top and bottom compartments, (d) finally, electrical measurements on the formed bilayer lipid membranes were performed.

2.9. *Reconstitution of transmembrane protein*

S. aureus α-hemolysin (α-HL) was reconstituted into the 8×8 bilayer membrane array by injecting 40 µl of a 10 µg/ml stock solution in 1.0 M KCl into the bottom chamber of the microfluidic system. In this case the aqueous solution pumped through the microfluidic compartments was 1.0 M KCl.

3. Results and discussion

A closed microfluidic device for automated formation, regeneration and subsequent investigation of an array of planar lipid membranes, incorporating reconstituted protein inside, was developed and investigated. The device was entirely fabricated by cheap and fast CO_2 laser ablation in ETFE, PMMA and Viton® materials making it economically feasible for the production of commercially available equipment. The device consisted of two compartments separated by a perforated ETFE partition, across which bilayer lipid membranes were formed. Fast injection and removal of liquids above and below the ETFE partition was possible using continuous pumping of electrolyte and injection of the bilayer forming solution followed by the protein solution. The lipid membrane thinning process was induced by the microfluidic process. Since the microchannels were created in a fluoroelastomer material (Viton®), which is chemically resistant to hydrocarbons, n-decane containing bilayer forming solutions were not detrimental to the system.

Conventional painting methods for lipid bilayer formation are slow and require that a thick bulky membrane spontaneously thins into a bilayer membrane. Current methods for lipid bilayer formation also usually require manual application of the BFS across the membrane support. The creation of biomimetic membranes in arrays is even more difficult. So far

utilization of a microfluidic system with a fully closed chamber for automated formation and regeneration of an array of bilayer lipid membranes, as well as reconstitution of protein therein, has to our knowledge not yet been implemented.

3.1. *Establishment of long-life biomimetic membranes in the microfluidic device by pumping induced thinning process*

The procedure for bilayer membrane formation in the microfluidic device is shown in figure 3. A pre-defined volume of the BFS was injected into the lower compartment of the device, covering the entire membrane support; a process that could be repeated many times (1st, 2nd 3rd generation membrane). Continuous monitoring of membrane capacitance and conductance over time indicated whether the BFS thinned into lipid bilayers in the ETFE partition using microfluidic pumping. By continuously pumping electrolyte into the two compartments of the device, excess BFS was removed and the thinning process was electrically studied. For the most stable lipid bilayer arrays; after a first portion of BFS was injected, an increase in membrane capacitance was observed after approximately 25 min (increase in effective bilayer area) while the membrane conductance remained at the same level (indicating a tight membrane) (figure 4, 1st generation membrane). Further pumping resulted in membrane leakage, which finally resulted in breakage of the membrane (an increase in membrane capacitance was concomitant with an increase in membrane conductance indicating an increase in ionic leak across the membrane). A 2nd generation membrane was created by injecting a new portion of BFS. As seen in figure 4, the same behaviour of capacitance and conductance over time was observed as for the 1st generation membrane. When injecting a 3rd BFS portion (figure 5), it can be seen that membrane life time (3rd generation membrane) was significantly increased, however, the effective membrane area did not change (the same capacitance value as for the 1st and 2nd generation membranes). Successful formation of the 3rd generation membrane was thus likely enabled by the pre-painting (1st and 2nd generation membranes) of the ETFE partition by the BFS, similarly as previously described [19]. The most stable lipid bilayer arrays established under these conditions had a lifetime of ~42 h and exhibited capacitance and conductance values of ~4300 pF and ~250 nS, respectively. The capacitance for formed lipid bilayers on 8x8 array with apertures with average diameters of 300 μm and literature values of the specific capacitance of 0.4 μF cm^{-2} for the solvent containing lipid bilayers [22] was expected to be ~18100 pF. This indicates that the lipid bilayers were established and the area of the most stable membranes constituted around ~24 % of the total area of the array.

The lifetime of the first, second and third generation membranes created in the microfluidic device was around 5 to 45 min (n = 5), 10 to 180 min (n = 6) and 25 to 42 hours (n = 2),

respectively, while their capacitance value was around 1000 to 3300 pF (n = 5), 1700 to 4800 pF (n = 6) and 4300 to 4500 pF (n = 2), respectively.

Our microfluidic device induced the thinning process of the thick lipid-solvent to form highly stable lipid bilayers in an array. Kawano et al. [18] reported that a BLM formed in a micropore was unstable in a device with upper and lower flow channels and they improved stability by forming a lipid membrane across a nanopore. Our results demonstrate another approach of increasing BLM stability in a closed microfluidic device; by using an array of micropores. This may be attributed to a self-repairing process of the membranes by the surrounding reservoirs. We have previously shown that scaling up the membrane area led to an increase in membrane lifetime: 8×8 membrane arrays (an average lifetime 1 h) vs. 64×64 membranes array (an average lifetime 16 h), [3].

A future optimisation of the microfluidic system could prove important in order to obtain a uniform lipid flow through the device and to have a better control of the pressure applied to the system; in this way possibly increasing the effective lipid bilayer area.

3.2. Incorporation of the pore-forming heptameric α-HL membrane protein demonstrates that functional lipid bilayers were established

To evaluate if functional lipid bilayers were established in the microfluidic device, additionally to membrane capacitance and conductance measurements, the pore-forming heptameric α-HL membrane protein was reconstituted into the lipid bilayer membrane array. The membrane pore of α-HL can be created in a lipid bilayer upon assembly of seven 33 kDa monomeric polypeptides on the membrane surface [23, 24]. The α-HL membrane protein was injected into the bottom compartment of the microfluidic system incorporating pre-formed bilayer lipid membrane arrays, and the obtained current trace recorded (Figure 6). Stepwise current increases could be observed and compared with previously presented results [25]. Knowing that ionic current through a single α-HL pore as a function of voltage yields a linear dependence [26] we scaled the literature single channel incorporation current value [~35 pA; 1M KCl, 30 mV] [25] to our experimental conditions [~70 pA; 1M KCl, 60 mV], our results demonstrate that several α-HL pores were inserted into a lipid bilayer at the time. This electrical recording together with membrane capacitance and conductance measurements (figure 4 and 5) confirmed that functional lipid bilayers were established in the microfluidic device.

4. Conclusion

A fully automated and closed microfluidic device for the formation, regeneration and investigation of an array of planar lipid membranes with reconstituted α-HL membrane protein was described. The benefits of this automated and closed microfluidic device include

controlled deposition of lipid solution into the apertures, thick lipid film thinning facilitated by microfluidic pumping, improvement of the membrane stability and lifetime (42 hours), and solution exchange on both sides of the membrane. The device was entirely fabricated by CO_2 laser technology, which is a quick and inexpensive alternative to existing technologies. The system provides an environment for reconstituting proteins that is similar to their native one, having the bilayer surrounded on both sides by water, thus providing the possibility of fast and precise measurement of exchange of analytes and ligands through transmembrane protein pores and channels. The developed system shows the potential for formation of biomimetic membrane arrays that could be useful for biochemical studies of proteins and for the development of future sensor arrays and separation technologies.

5.Acknowledgments

6. References

[1] Nielsen CH. Biomimetic membranes for sensor and separation applications. Analytical and Bioanalytical Chemistry. 2009;395[3]:697-718.

[2] Zagnoni M, Sandison ME, Morgan H. Microfluidic array platform for simultaneous lipid bilayer membrane formation. Biosensors and Bioelectronics. 2009;24[5]:1235-40.

[3] Hansen JS, Perry M, Vogel J, Groth JS, Vissing T, Larsen MS, et al. Large scale biomimetic membrane arrays. Analytical and Bioanalytical Chemistry. 2009;395[3]:719-27.

[4] Mueller P, Rudin Do. Bi molecular lipid membranes techniques of formation study of electrical properties and induction of ionic gating phenomena. 1969:141-56.

[5] Montal M, Mueller P. Formation of bimolecular membranes from lipid monolayers and a study of their electrical properties. Proc Natl Acad Sci U S A. 1972;69[12]:3561-6.

[6] Malmstadt N, Nash MA, Purnell RF, Schmidt JJ. Automated formation of lipid-bilayer membranes in a microfluidic device. Nano Letters. 2006;6[9]:1961-5.

[7] Suzuki H, Tabata KV, Noji H, Takeuchi S. Highly reproducible method of planar lipid bilayer reconstitution in polymethyl methacrylate microfluidic chip. Langmuir. 2006;22[4]:1937-42.

[8] Ide T, Ichikawa T. A novel method for artificial lipid-bilayer formation. Biosensors and Bioelectronics. 2006;21[4]:672.

[9] Suzuki H, Tabata KV, Noji H, Takeuchi S. Electrophysiological recordings of single ion channels in planar lipid bilayers using a polymethyl methacrylate microfluidic chip. Biosensors and Bioelectronics. 2007;22[6]:1111-5.

[10] Sandison ME, Zagnoni M, Abu-Hantash M, Morgan H. Micromachined glass apertures for artificial lipid bilayer formation in a microfluidic system. J Micromech Microengineering. 2007;17[7]:S189-96.

[11] Sandison ME, Morgan H. Rapid fabrication of polymer microfluidic systems for the production of artificial lipid bilayers. J Micromech Microengineering. 2005;15[7]:S139-44.

[12] Sandison ME, Zagnoni M, Morgan H. Air-exposure technique for the formation of artificial lipid bilayers in microsystems. Langmuir. 2007;23[15]:8277-84.

[13] Zagnoni, Sandison, Marius, Lee, Morgan. Controlled delivery of proteins into bilayer lipid membranes on chip. Lab on a Chip. 2007;7[9]:1176-83.

[14] Mach T, Chimerel C, Fritz J, Fertig N, Winterhalter M, Futterer C. Miniaturized planar lipid bilayer: Increased stability, low electric noise and fast fluid perfusion. Analytical and Bioanalytical Chemistry. 2008;390[3]:841-6.

[15] Funakoshi K, Suzuki H, Takeuchi S. Lipid bilayer formation by contacting monolayers in a microfluidic device for membrane protein analysis. Anal Chem. 2006;78[24]:8169-74.

[16] Suzuki H, Tabata K, Kato-Yamada Y, Noji H and Takeuchi S. Planar lipid bilayer reconstitution with a micro-fluidic system. Lab Chip. 2004; 4: 502–505.

[17] Suzuki H, Le Pioufle B, Takeuhci S. Ninety-six-well planar lipid bilayer chip for ion channel recording fabricated by hybrid stereolithography.Biomed Microdevices. 2009; 11:17–22.

[18] Kawano R, Osaki T, Sasaki H, and Takeuchi S. A Polymer-Based Nanopore-Integrated Microfluidic Device for Generating Stable Bilayer Lipid Membranes. Small 2010; 6[19]: 2100–2104.

[19] Hansen JS, Perry M, Vogel J, Vissing T, Hansen CR, Geschke O, et al. Development of an automation technique for the establishment of functional lipid bilayer arrays. J Micromech Microengineering. 2009;19[2]:025014.

[20] Vogel J, Perry M, Hansen JS, Bolinger P, Nielsen CH, Geschke O. A support structure for biomimetic applications. J Micromech Microengineering. 2009;19[2]:025026.

[21] Perry M, Vissing T, Boesen TP, Hansen JS, Emneus J, Nielsen CH. Automated sampling and data processing derived from biomimetic membranes. Bioinspiration. 2009;4[4]:044001.

[22] Benz R, Janko K. Voltage-induced capacitance relaxation of lipid bilayer membranes effects of membrane composition. Biochimica et Biophysica Acta [BBA]/Biomembranes. 1976;455[3]:721-38.

[23] Dinges MM, Orwin PM, Schlievert PM. Exotoxins of staphylococcusaureus. Clin Microbiol Rev. 2000;13[1]:16-34.

[24] Fink D, Contreras ML, Lelkes PI, Lazarovici P. Staphylococcus aureus α-toxin activates phospholipases and induces a Ca2+ influx in PC12 cells. Cell Signal. 1989;1[4]:387-93.

[25] Hemmler, Bose, Wagner, Peters. Nanopore unitary permeability measured by electrochemical and optical single transporter recording. Biophys J. 2005;88[6]:4000-7.

[26] Meller A, Branton D. Single molecule measurements of DNA transport through a nanopore. ELECTROPHORESIS. 2002;23[16]:2583-2591.
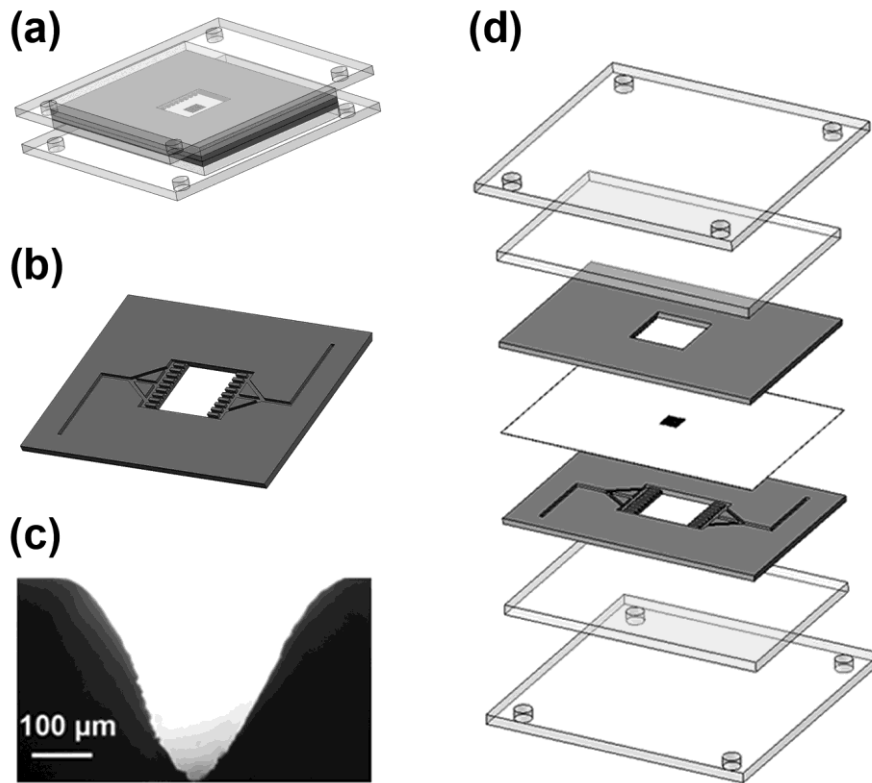
Figures

Figure 1 Schematics of the microfluidic device; (a) an assembled device, (b) a Viton® with microchannels system, (c) a cross-section of a Viton® microchannel in an optical microscope, (d) exploded view of the device. The component order of the assembly is from bottom to top: a PMMA clamping holder, a PMMA plate, a Viton® with microchannels, an ETFE partition, a Viton® with microchannels (note that the microchannels contact the ETFE partition and are invisible in the view shown here), a PMMA plate, and a PMMA clamping holder.
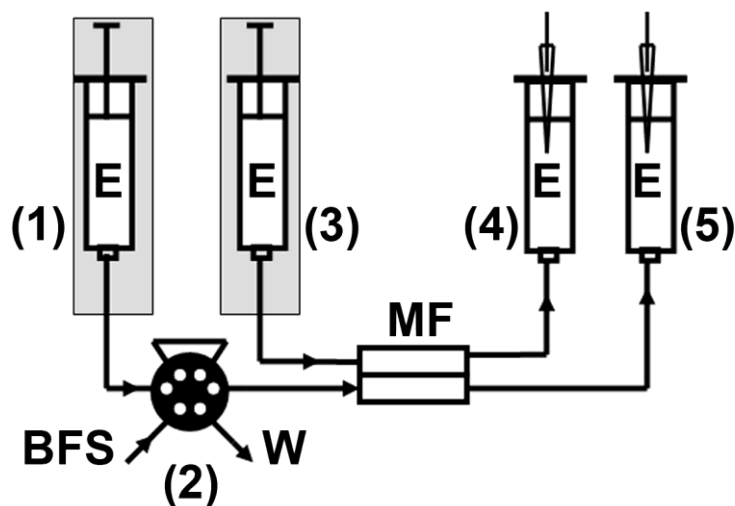
Figure 2 The microfluidic system set-up containing: (1), (3) syringe pumps delivering electrolyte (E) to both microfluidic device compartments; (2) six-valve rotary injector enabling electrolyte (E) and bilayer forming solution (BFS) injection into the bottom compartment and waste (W) removing; (4), (5) syringe barrels collecting liquids from the top and bottom compartments enabling electrical measurements of the lipid membrane formed within the device.
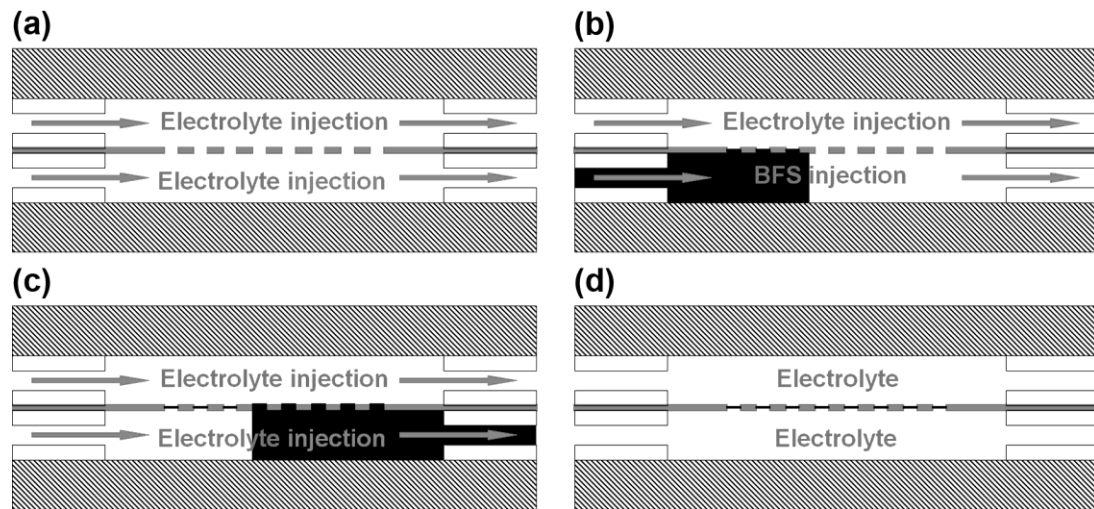
Figure 3 The procedure for bilayer membranes formation in the microfluidic device; (a) the electrolyte is pumped at a flow rate of 50 μl/min, through the Viotn® (white boxes) microchannels and both compartments of the microfluidic device, (b) 40 μl of the BFS (black) is then injected into the bottom compartment, (c) the excess BFS (black) is removed and the membrane thinning process induced by the continuous flow of electrolyte on both sides of the ETFE partition (gray), (d) finally, electrical measurements on the formed bilayer lipid membranes (black) can be performed.
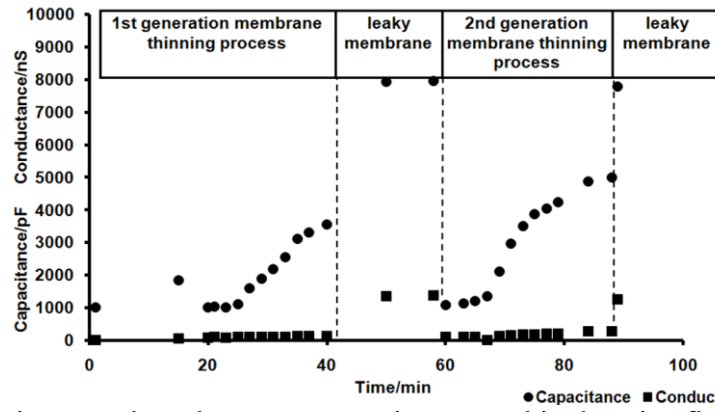
Figure 4 Capacitance and conductance versus time created in the microfluidic device 1st and 2nd generation membranes. Membrane thinning was induced by microfluidic pumping.
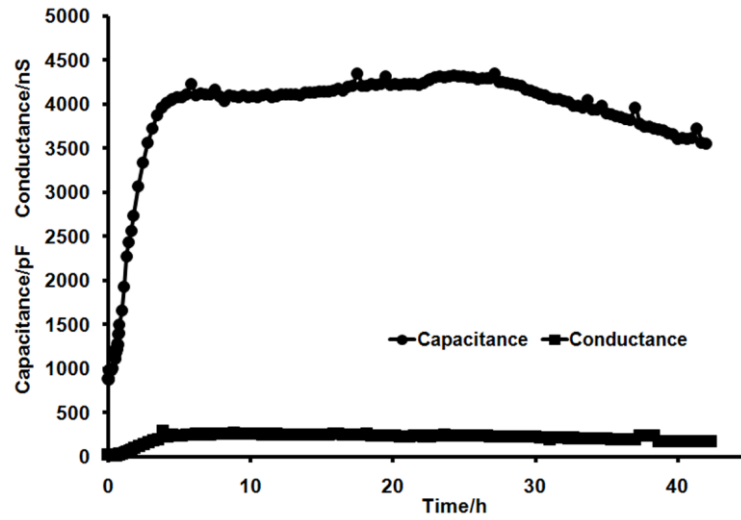
Figure 5 Capacitance and conductance versus time created in the microfluidic device 3rd generation membrane. Membrane thinning was induced by microfluidic pumping.
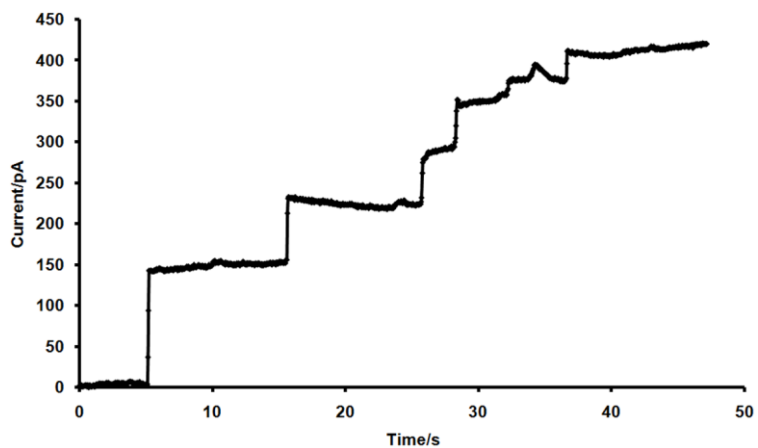
Figure 6 Current trace of the reconstitution of the pore-forming heptameric α-HL membrane protein in established in the microfluidic device 8×8 bilayer arrays.

Paper IV

Assessing the efficacy of vesicle fusion with planar membrane arrays using a mitochondrial porin as reporter

Kamila Pszon-Bartosz [a,b], Jesper S. Hansen [a,b,1], Karin B. Stibius [a,c,1], Jesper S. Groth [a], Jenny Emnéus [b], Oliver Geschke [b], Claus Hélix-Nielsen [a,c,*]

[a] Aquaporin A/S, Ole Maaløes Vej 3, DK-2200 Copenhagen N, Denmark
[b] Technical University of Denmark, Department of Micro- and Nanotechnology, DK-2800 Kongens Lyngby, Denmark
[c] Technical University of Denmark, Department of Physics, DTU Physics, DK-2800 Kongens Lyngby, Denmark

ARTICLE INFO

ABSTRACT

Reconstitution of functionally active membrane protein into artificially made lipid bilayers is a challenge that must be overcome to create a membrane-based biomimetic sensor and separation device. In this study we address the efficacy of proteoliposome fusion with planar membrane arrays. We establish a protein incorporation efficacy assay using the major non-specific porin of *Fusobacterium nucleatum* (FomA) as reporter. We use electrical conductance measurements and fluorescence microscopy to characterize proteoliposome fusion with an array of planar membranes. We show that protein reconstitution in biomimetic membrane arrays may be quantified using the developed FomA assay. Specifically, we show that FomA vesicles are inherently fusigenic. Optimal FomA incorporation is obtained with a proteoliposome lipid-to-protein molar ratio (LPR) = 50 more than 10^5 FomA proteins could be incorporated in a bilayer array with a total membrane area of 2 mm^2 within 20 min. This novel assay for quantifying protein delivery into lipid bilayers may be a useful tool in developing biomimetic membrane applications.

1. Introduction

There is a growing interest in mimicking biological membranes and create membrane-based sensor and separation devices. However, there are many challenges that must be overcome in order to build biomimetic membrane devices for industrial applications. One of the challenges is to ensure sufficient delivery of functional protein to the lipid matrix [1]. Fusion of lipid vesicles containing proteins (proteoliposomes) with a planar membrane has been used for many years and it is a powerful technique to incorporate membrane proteins into planar lipid bilayers [2,3]. In particular this method has been valuable for studies were incorporation of only few proteins (or even single proteins) is sufficient. However, large scale systems based on lipid bilayers will often require substantial amounts of incorporated proteins. It therefore is of interest to evaluate the up-scaling potential of vesicle based protein delivery.

Optimization of proteoliposomes fusion with biomimetic membranes depends on increasing proteoliposome fusogenicity. Theoretical studies indicate that the early stages of fusion involve formation of a fusion pore—or intermediate, a neck-like connection between two bilayers, with an initial size of about 10 nm [4,5]. The fusion time scale has not been measured experimentally, but patch-clamp electrophysiology [6] and ultrafast optical microscopy of giant vesicles [7] indicate that the fusion pore can be formed in less than 100 μs.

Fusogenicity may be increased by lowering the energetic barriers for formation of fusion intermediates. Vesicle fusion may be induced by lipids having opposite charges in vesicle and receiving planar membrane, respectively [8,9]. Another strategy involves the use of fusogenic peptides in the two fusing membranes as demonstrated by the use of soluble *N*-ethylmaleimide-sensitive factor attachment protein (SNAP) and associated (SNARE) receptor

---

leading to the formation of SNAP–SNARE complexes and vesicle fusion [10,11]. Fusion can also be driven solely by osmotic gradients across the planar receiving membrane provided that the vesicles are permeable to solute [12]. The latter has been demonstrated using vesicles with the antibiotic nystatin and ergosterol [2,3,13]. Nystatin–ergosterol channel complexes are weakly anion-selective and thus render the vesicle solute permeable. Upon fusion with an ergosterol-free planar membrane fusion events are evident as ion current transients reflecting the dissolution of the nystatin–ergosterol channel complexes.

The nystatin–ergosterol method is a powerful technique for protein incorporation but as the single-channel conductance for the nystatin–ergosterol complex is not a well-defined entity one cannot determine quantitatively the amount of protein delivered to the planar membrane.

However, by using ion channels that remain open after incorporation into the planar membrane one may asses the amount of inserted protein by detecting the increase in bilayer macroscopic conductance G after transfer of ion channels from the vesicle membrane to the bilayer. When the single-channel conductance g is known one may use the ratio G/g to estimate the total number of (ion channel) proteins that has been incorporated by fusion during this process (the fusion efficacy). This method has been demonstrated by using the voltage dependent anion channel (VDAC) [14,15]. With this method about ∼100 fusion events corresponding to the insertion of about 500 VDACs in 10 min per mm^2 membrane area could be obtained. Still VDAC incorporation has to be driven by applying an osmotic gradient across the planar membrane and by addition of divalent cations.

Here we speculated if one could use the major outer membrane protein of *Fusobacterium nucleatum* (FomA) as a reporter for vesicle fusion with planar membranes—even in the absence of a transmembrane osmotic gradient. The rationale behind this comes from the suggestion that FomA participates in coaggregation between periodontal *F. nucleatum* and *Streptococcus sanguis* bacteria by direct binding [16]. FomA forms trimeric β-barrels where each barrel is predicted to consist of 14 β-strands [17] and the single-channel conductance is known [18]. Thus it should be possible to quantify proteoliposome fusion with planar membranes via the G/g ratio. Since porins can be tailored to specific functions [19] vesicles with fusigenic engineered FomA porins could also constitute building blocks for functional planar biomimetic membranes *per se*. In this study we assessed FomA vesicle fusogenicity as quantified by G/g and how FomA incorporation into planar membranes depends on proteoliposome lipid-to-protein ratio (LPR) and incubation time.

2. Materials and methods

2.1. Reagent and materials

Tefzel ETFE LZ200 Fluoropolymer for the fabrication of multi-aperture partitions, and Viton A Fluoroelastomer for the production of rubber chamber sealing rings were from DuPont Fluoropolymers (Detroit, USA). Uncoated 35- and 50-mm glass-bottom culture dishes were purchased from MatTek Corporation (Ashland, MA, US). The lipids 1,2-diphytanoyl-*sn*-glycero-3-phosphocholine (DPhPC), 1,2-dioleoyl-*sn*-glycero-3-phosphocholine (DOPC), and 1-oleoyl-2-[6-[(7-nitro-2-1,3-benzoxadiazol-4-yl)amino]hexanoyl]-*sn*-glycero-3-phosphocholine (NBD-PC) were from Avanti Polar Lipids Inc. (Alabaster, AL, USA). *n*-Decane (Fluka) was purchased from Sigma–Aldrich Denmark (Brøndby, Denmark). The *F. nucleatum* outer membrane protein A (FomA) was kindly provided by Dr. Jörg H. Kleinschmidt (Universität Konstanz, Konstanz,

Germany). All other chemicals were of analytical grade and purchased from commercial sources.

2.2. Preparation of bilayers forming solution (BFS) and proteoliposome suspensions

The lipid bilayer forming solution (BFS) consisted of DPhPC in *n*-decane (25 mg/ml) doped with 1 mol% NBD-PC. The lipid solutions were prepared the day before the experiment, and stored at −20 °C until use.

Liposomes were prepared from thin film of DOPC lipids dissolved in PBS containing 1 wt% OG (octyl-β-D-glucopyranoside) (Anatrace, Affymetrix Europe, High Wycombe, UK) to a final lipid concentration of 10 mg/ml. The lipid solution was sonicated for 1 min and subjected to five then freeze–thaw cycles. After 1 min of sonication, the lipid solution was extruded 12 times through a barrel extruder (Lipex™ Extruder, Northern Lipids Inc., Burnaby, Canada) with two polycarbonate filters (Whatman, Maidstone, UK) with 200 nm pore sizes at 20 bar pressure. FomA dissolved in 10 mM borate buffer (9.6 mg/ml, pH 10 with 2 mM EDTA) was refolded in *N*-lauryl-*N,N*-dimethylammonium-N-oxide (LDAO) micelles (LDAO/FomA mol:mol ratio = 1000). Before mixing with liposomes the protein was labeled with Texas Red® (Sigma–Aldrich Denmark, Brøndby, Denmark) with a substitution degree of 0.4 mol dye/mol protein. Liposomes were mixed with the protein solution and dialyzed in Spectra/Por® MicroDialyzers (Spectrum Laboratories Inc., Breda, The Netherlands) for 24 h against PBS to remove the detergent. Samples with LPR = 25, 50, 100 and 200 were prepared and diluted with PBS to a final lipid concentration of 0.16 mg/ml.

2.3. Liposomes and proteoliposomes characterization

Size distribution analyses of liposomes and proteoliposomes were performed with NanoSight LM10 and NTA 2.0 Analytical software (NanoSight Ltd., Amesbury, UK). Around 1 ml of 0.001 mg/ml sample was needed to perform each measurement three times. The samples were measured for 90 s with manual shutter and gain adjustments. Mean and standard deviation values were obtained from mono-modal model fittings using the nanoparticle tracking analysis (NTA) 2.0 software.

2.4. BLM array formation and characterization

Planar horizontal lipid bilayers were established across microstructured ETFE partition arrays as previously described [20,21]. Briefly, ∼0.5 μl of the BFS was deposited onto the partition array. To thin the membranes into bilayers, a sterile plastic inoculation loop with a 1 μl loop capacity (Sarstedt Nümbrecht, Germany) was used. The thinning process was carried out by gently sweeping the inoculation loop across the entire BLM array prior to addition of proteoliposomes.

Automated voltage-clamp measurements and data processing were carried out as previously described [22]. Fluorescent imaging was performed on a Zeiss Axiovert 200 M epifluorescence microscope (Carl Zeiss, Jena, Germany) equipped with a monochrome Deltapix DP450 CCD camera (Deltapix, Maalov, Denmark). Images were acquired using Deltapix DpxView Pro Acquisition software (Deltapix, Maalov, Denmark). Objectives used were air-corrected Plan-Neofluar 2.5×/0.075 Numerical Aperture (NA) and 10×/0.25 NA, respectively.

Incorporation of proteoliposomes with different LPR values into an array of planar membranes was established by adding 2 μl of proteoliposomes with 0.16 mg/ml lipid concentration in close proximity to the lipid bilayer. The aqueous chamber solution

consisted of PBS buffer. The applied potential across the partition arrays was 60 mV.

3. Results and discussion

3.1. FomA proteoliposomes insert spontaneously into planar membranes

We first characterized FomA DOPC proteoliposome fusion with an array of planar membranes and assessed protein functional activity by voltage-clamp recordings of bilayers formed from (DPhPC)/decane solutions separating two aqueous compartments containing PBS. Stepwise increases of the current across the bilayer were observed when FomA proteoliposomes were applied in close proximity of the membrane (Fig. 1a, upper current trace). No transmembrane currents were observed for the DPhPC bilayer alone (Fig. 1a, middle current trace) or when protein-free DOPC liposomes were applied in close proximity of the DPhPC membrane (Fig 1a, lower current trace). The conductance amplitude histogram reveals a broad distribution with mean value of 0.07 nS for a total of 139 fusion events. This value can be compared with the 1.17 nS measured for FomA trimeric channel conductance in 1 M KCl [18]. Scaling the 1 M KCl FomA conductance value according to the conductivity ratio between PBS and 1 M KCl conductivity the scaled conductance value is 0.08 nS in good agreement with our data. These results demonstrate that functionally active FomA

was successfully reconstituted into an array of planar membranes at physiologically relevant electrolyte concentrations. Fusion occurred spontaneously when FomA proteoliposomes were placed close to the membrane array in the absence of osmotic gradients across the membrane needed in other fusion methods, e.g. [3].

3.2. FomA proteoliposomes have an upper limit LPR

In order to evaluate the influence of the protein content of the proteoliposomes we performed fusion experiments with proteoliposomes prepared with different LPRs and this is shown in Fig. 2a. The highest fusion efficacy (measured as G/g) was achieved with LPR 50 (see Table 1). Fusion efficacy increases when the LPR value decreases from 200 to 50. However, with LPR = 25 functional protein incorporation is close to that observed for LPR = 200. A reason for the low efficacy at low LPR may due to the fact that an LPR = 25 corresponds to a protein area coverage of 64%. This may be the upper limit for FomA protein reconstitution in proteoliposomes before protein precipitation occurs. It may thus be that only small amounts of protein were reconstituted into proteoliposomes at the nominal LPR = 25 leading to concomitant low protein incorporation with the planar membranes. There were no significant size differences between protein-free liposomes and proteoliposomes with nominal LPR = 200, 100 and 50 as evidenced by nanoparticle tracking analysis (see Fig. 2b). Proteoliposomes with nominal LPR = 25 has a mean diameter of 200 nm which is significantly different from the observed liposome diameter of 150 nm. Although we do not know the reason for the apparent size difference it may be related to the very high protein concentration (and potential precipitation) during the mixing and dialysis steps in proteoliposome production.

3.3. Proteoliposome fusion kinetics and membrane stability

In order to assess how proteoliposome LPR is related to fusion kinetics and membrane stability we analyzed membrane currents I ($I \sim G/g$) over time with the two LPR values giving the highest efficacy (LPR = 50 and 100) and this is presented in Fig. 3a. After
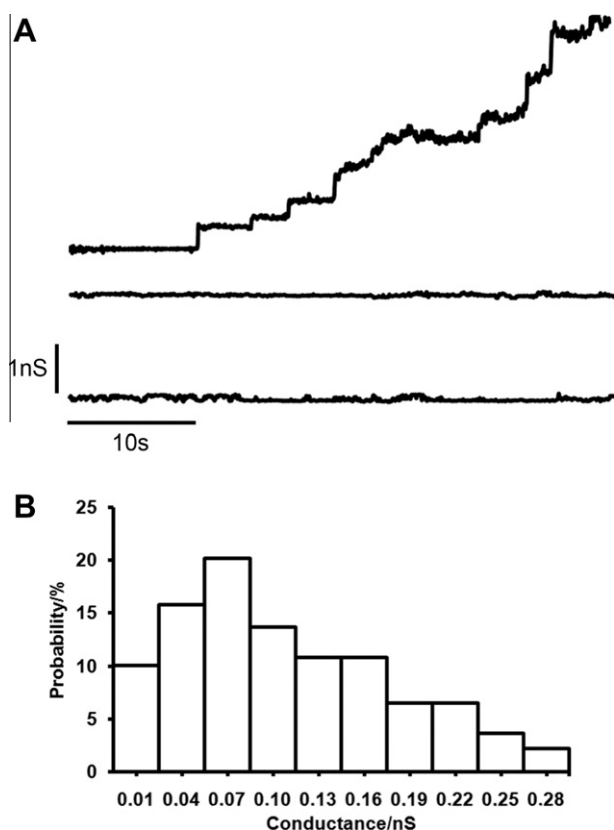
Fig. 1. FomA channels recordings demonstrate proteoliposomes fusion into an array of planar membranes. (A) Conductance across: an array of DPhPC membranes in PBS buffer after addition of DOPC–FomA proteoliposomes (upper trace), an array of DPhPC membranes alone in PBS buffer (middle trace), and after addition of FomA free liposomes (lower trace). (B) Histogram of the probability of the occurrence of a given conductivity unit (139 fusion events were recorded) during DOPC–FomA proteoliposomes, with LPR 200, fusion into 8 × 8 array of DPhPC planar membranes. The applied potential across the partition arrays was +60 mV. The conductance of single FomA channel in PBS was in the range 0.01–0.28 nS with a maximum probability for a conductance of 0.07 nS.

Fig. 2. (A) Maximal FomA proteoliposomes fusion into an array of planar membranes. The applied potential across the partition arrays was +60 mV. (B) Liposome/proteoliposome diameters. Mean values are based on mono-modal model fittings applied to the experimental data by NTA (nanoparticle tracking analysis) software (error bars represent SD, $n = 3$).

Table 1
Proteoliposome fusion efficacy.

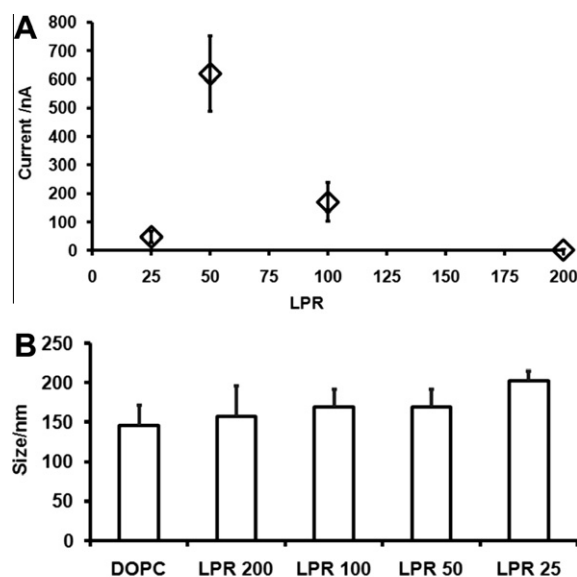| LPR[a]	Proteoliposome FomA coverage[b] (%)	Number of FomA proteins per proteoliposome[c]	Maximal fusion efficacy G/g[d]
25	64	5146 ± 933	11,429 ± 4343
50	47	2682 ± 971	147,619 ± 31,527
100	31	1754 ± 635	40,417 ± 16,020
200	18	934 ± 618	524 ± 179

[a] Lipid to protein molar ratio at the step of proteoliposomes preparation.
[b] Assuming 0.72 nm^2 lipid polar head surface and 16 nm^2 FomA monomer area.
[c] Calculation based on the nominal LPR and the size of proteoliposomes determined by NTA measurements.
[d] Assuming single FomA conductance = 0.07 nS.
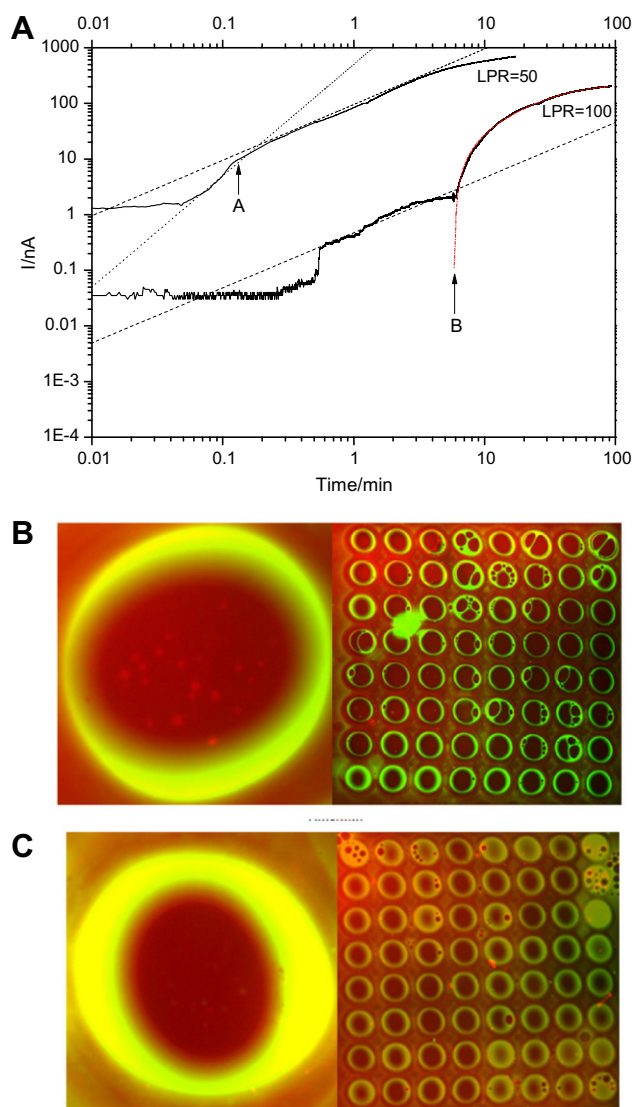
Fig. 3. Characterization of proteoliposome fusion into planar membranes. (A) Total membrane current I versus time t for proteoliposome LPR = 50 and 100. Straight (guiding) lines indicate first order ($I \sim t$) (dashed lines) and second order ($I \sim t^2$) (dotted lines) proportionality, respectively. Arrow A indicates transition from second to first-order kinetics and arrow B indicates onset of exponential kinetics: $I \sim A \cdot (1 - \exp(-t/\tau))$. Dashed-dot line (red) represents a fit to the exponential kinetics equation with $\tau = 30.1$ min. (B) Combined fluorescent images of FomA (red) proteoliposomes with LPR = 50 fused into planar membranes (left: single aperture; right: the 8 × 8 bilayer array). (C) As in (B) with LPR = 100. Images were acquired with a 20× (B and C, left) and 2.5× (B and C, right) air-corrected objective. Average ± SD outer aperture diameter for the 8 × 8 array is 300 ± 5 μm. (For interpretation of references to color in this figure legend, the reader is referred to the web version of this article.)

addition of 2 μl proteoliposomes (0.16 mg/ml) with LPR = 50 fusion efficacy showed an initial lag phase followed by a second order rise phase ($I \sim t^2$) within the first 6 s. This is followed by a longer first order ($I \sim t$) rise phase and finally I is levelling off approaching a saturating level. For LPR = 100 the initial lag phase is shorter and followed by a longer first order rise phase until 6 min (the jumps just after 0.53 min reflect insertion of multiple FomA proteins, cf. Fig 1a). At 6 min an inoculation loop was swept across the entire membrane array. The induced stirring causes the incorporation to follows an exponential time course until a saturating level is reached after 90 min. In cases where some membranes in the array broke during the first order rise phase they could be recreated by careful local application of the inoculation loop and the efficacy level resulting in current levels returning to the level just prior to membrane breakage. Although LPR = 100 results in free-standing membranes reaching saturating incorporation levels, fusion with proteoliposomes having LPR = 50 reach several fold higher levels within 10 min.

Thus one may use either slow first-order kinetics corresponding to passive diffusion of the proteoliposomes up to the membrane, or use stirring for rapid delivery of vesicles to the receiving membrane. The two different kinetic schemes may be considered as part of a microfluidic design where flow conduits and rates may be adjusted for various types of flow, e.g. turbulent flows for creating efficient stirring of the membrane interfacial regions. Subsequently membranes may be stabilized, e.g. via hydrogel encapsulation [23].

Table 1 shows the maximal fusion efficacy (G/g) corresponding to the effective number of trimeric FomA channels incorporated. For LPR = 100 the total membrane conductance corresponds to about 40,000 FomA trimers whereas for LPR = 50 a total of 150,000 FomA trimers appears to have been inserted. With the theoretical numbers for single proteoliposome conductances based on their LPRs this corresponds to insertion of about 54 and 22 proteoliposomes, respectively. However, this is under the assumption that all proteoliposomes have functional protein content corresponding to their LPR and that all proteins retain their functionality after insertion. This may not be the case, and there may be non-functional protein material inserted the membrane together with the functional FomA channels. However, we note that the membrane conductance levels off with time for both LPR = 50 and 100 approaching a steady state. If the membrane stability was generally compromised due to the presence of non-functional (mis-folded) protein this would be manifest in large conductance fluctuations and membrane rupture. We do not see evidence of this and conclude that the receiving membrane may contain non-functional protein but that this does not compromise membrane overall integrity.

In order to further characterize proteoliposome fusion into planar membranes we simultaneously monitored the membrane array optically and electrically. Using the fluorescent lipid analog NBD-PC (1 mol%) in the membrane bilayer forming solution and Texas Red® labeled FomA we could observe bilayers formation and protein incorporation and this is shown in Fig. 3b. For both LPR = 50 and 100 we observed high-intensity dots in some membranes in the array moving within the membrane area delimited by the Plateau–Gibbs border. This heterogeneity may reflect that the incorporated protein aggregate in the membrane or that proteoliposomes (or proteins) aggregate on the membrane surface. The heterogeneity is most pronounced for LPR = 50 which may reflect the high protein concentration (and possible precipitation) for LPR = 50 proteoliposomes.

In summary, we established an outer membrane porin fusion efficacy assay and used this to quantify proteoliposomes fusion with an array of planar membranes. We showed the influence of LPR on FomA proteoliposomes reconstitution yield. Maximal fusion obtained was almost 150,000 porin insertions during 20 min with

proteoliposomes prepared with LPR = 50. Incorporation could be established as a process with either first order or exponential kinetics. This may be of interest to microfluidic designs involving protein delivery to biomimetic membranes developed for sensor and separation applications.

Acknowledgments

References

[1] C.H. Nielsen, Biomimetic membranes for sensor and separation applications, Anal. Bioanal. Chem. 395 (2009) 697–718.
[2] D.J. Woodbury, C. Miller, Nystatin-induced liposome fusion. A versatile approach to ion channel reconstitution into planar bilayers, Biophys. J. 58 (1990) 833–839.
[3] D.J. Woodbury, Nystatin/ergosterol method for reconstituting ion channels into planar lipid bilayers, Methods Enzymol. 294 (1999) 319–339.
[4] A. Grafmulller, J. Shillcock, R. Lipowsky, Pathway of membrane fusion with two tension-dependent energy barriers, Phys. Rev. Lett. 98 (2007) 218101.
[5] J.C. Shillcock, R. Lipowsky, Tension-induced fusion of bilayer membranes and vesicles, Nat. Mater. 4 (2005) 225–228.
[6] M. Lindau, G. Alvarez de Toledo, The fusion pore, Biochim. Biophys. Acta 1641 (2003) 167–173.
[7] C.K. Haluska, K.A. Riske, V.R. Marchi-Artzner, J.-M. Lehn, R. Lipowsky, R. Dimova, Time scales of membrane fusion revealed by direct imaging of vesicle fusion with high temporal resolution, Proc. Natl. Acad. Sci. USA 103 (2006) 15841–15846.
[8] D. Simberg, S. Weisman, Y. Talmon, Y. Barenholz, DOTAP (and other cationic lipids): chemistry, biophysics, and transfection, Crit. Rev. Ther. Drug Carrier Syst. 21 (2004) 257–317.
[9] L. Stamatatos, R. Leventis, M.J. Zuckermann, J.R. Silvius, Interactions of cationic lipid vesicles with negatively charged phospholipid vesicles and biological membranes, Biochemistry 27 (1988) 3917–3925.
[10] W. Nickel, T. Weber, J.A. McNew, F. Parlati, T.H. Sollner, J.E. Rothman, Content mixing and membrane integrity during membrane fusion driven by pairing of isolated v-SNAREs and t-SNAREs, Proc. Natl. Acad. Sci. USA 96 (1999) 12571–12576.
[11] F. Parlati, T. Weber, J.A. McNew, B. Westermann, T.H. Sollner, J.E. Rothman, Rapid and efficient fusion of phospholipid vesicles by the alpha-helical core of a SNARE complex in the absence of an N-terminal regulatory domain, Proc. Natl. Acad. Sci. USA 96 (1999) 12565–12570.
[12] F.S. Cohen, M.H. Akabas, A. Finkelstein, Osmotic swelling of phospholipid vesicles causes them to fuse with a planar phospholipid bilayer membrane, Science 217 (1982) 458–460.
[13] M.R. de Planque, G.P. Mendes, M. Zagnoni, M.E. Sandison, K.H. Fisher, R.M. Berry, A. Watts, H. Morgan, Controlled delivery of membrane proteins to artificial lipid bilayers by nystatin–ergosterol modulated vesicle fusion, IEE Proc. Nanobiotechnol. 153 (2006) 21–30.
[14] F.S. Cohen, J. Zimmerberg, A. Finkelstein, Fusion of phospholipid vesicles with planar phospholipid bilayer membranes: II. Incorporation of a vesicular membrane marker into the planar membrane, J. Gen. Physiol. 75 (1980) 251–270.
[15] J. Zimmerberg, F.S. Cohen, A. Finkelstein, Fusion of phospholipid vesicles with planar phospholipid bilayer membranes: I. Discharge of vesicular contents across the planar membrane, J. Gen. Physiol. 75 (1980) 241–250.
[16] J. Kaufman, J.M. DiRienzo, Isolation of a corncob (coaggregation) receptor polypeptide from Fusobacterium nucleatum, Infect. Immun. 57 (1989) 331–337.
[17] P. Puntervoll, M. Ruud, L.J. Bruseth, H. Kleivdal, B.T. Hogh, R. Benz, H.B. Jensen, Structural characterization of the fusobacterial non-specific porin FomA suggests a 14-stranded topology, unlike the classical porins, Microbiology 148 (2002) 3395–3403.
[18] H. Kleivdal, R. Benz, H.B. Jensen, The Fusobacterium nucleatum major outer-membrane protein (FomA) forms trimeric, water-filled channels in lipid bilayer membranes, Eur. J. Biochem. 233 (1995) 310–316.
[19] M. Vrouenraets, J. Wierenga, W. Meijberg, H. Miedema, Chemical modification of the bacterial porin OmpF: gain of selectivity by volume reduction, Biophys. J. 90 (2006) 1202–1211.
[20] J. Vogel, M.E. Perry, J.S. Hansen, P.-Y. Bollinger, C.H. Nielsen, O. Geschke, Support structure for biomimetic applications, J. Micromech. Microeng. 19 (2009) 025026.
[21] J.S. Hansen, M. Perry, J. Vogel, J. Groth, T. Vissing, M. Larsen, O. Geschke, J. Emneus, H. Bohr, C.H. Nielsen, Large scale biomimetic membrane arrays, Anal. Bioanal. Chem. 395 (2009) 719–727.
[22] M. Perry, T. Vissing, T.P. Boesen, J.S. Hansen, J. Emneus, C.H. Nielsen, Automated sampling and data processing derived from biomimetic membranes, Bioinspir. Biomim. 4 (2009) 44001.
[23] S. Ibragimova, K.B. Stibius, P. Szewczykowski, M. Perry, H. Bohr, C.H. Nielsen, Hydrogels for in situ encapsulation of biomimetic membrane arrays, Polym. Adv. Technol., in press, doi:10.1002/pat1850.

Book Chapter

13. Strategies for integrating membrane proteins in biomembranes

Jesper S. Hansen[†,§,*], Inés Plasencia[‡] and Kamila Pszon-Bartosz[†,§]

[†]Aquaporin A/S, DK-2200 Copenhagen, Denmark. [§]DTU Nanotech, Technical University of Denmark, DK-2800 Kgs. Lyngby, Denmark. [‡]MEMPHYS-Center for Biomembrane Physics. Department of Physics and Chemistry. University of Southern Denmark. DK-5230 Odense, Denmark. [*]E-mail address: jsh@aquaporin.dk

Abstract Correct integration of membrane proteins with biomimetic membranes is crucial for designing novel sensor and separation technologies based on the functionality of membrane proteins. Membrane proteins are generally delicate molecules and care need to be taken in order to retain protein structure and function during handling and reconstitution into model membranes. This chapter will give a detailed overview of available and novel membrane protein reconstitution strategies in both vesicular and planar model membrane designs.

13.1 Protein reconstitution

Membrane proteins function among others as receptors, ion channels, transporters and pore formers. They carry out important cellular functions in many physiologic processes in normal physiology, and may cause or contribute to several disease states. For the same reason membrane proteins are key targets for therapeutic intervention (Fang et al. 2003). Membrane proteins can moreover be chemically modified or genetically engineered, giving unprecedented control over membrane binding and transport properties (Castellana and Cremer 2006). Therefore, membrane proteins, either in native forms or modified versions, may give rise to the creation of novel protein-based biosensors, biomedical screening platforms and novel separation technologies.

Reconstitution of membrane proteins into artificially made lipid bilayers represent a powerful technique to study and functionally work with membrane proteins under controlled experimental conditions (Woodbury 1999). However, membrane protein reconstitution is not a trivial process. Here we will give a practical approach to the strategies and considerations for functionally reconstituting membrane proteins into vesicular and planar model membranes. The requirements for protein reconstitution yield in sensor or separation applications may not be the same. Reconstitution approaches and considerations to meet the requirements of reconstitution yield in sensor or separation technologies are also discussed here.

13.2 Reconstitution in vesicles

Vesicles are spherical shells of lipid bilayers and represent one of the most widely used methods for reconstituting membrane proteins into biomimetic model membranes. When lipids are the principal component of the vesicles, they may also be called liposomes. Polymerosomes on the other hand refers to vesicles formed by synthetic polymers (Lorenceau et al. 2005; Rastogi et al. 2009; Rosenkranz et al. 2009).

There are presently several methods available for reconstituting membrane proteins into vesicles. The protein purification conditions will be an initial parameter defining the reconstitution methodology to choose. Although few membranes proteins can be extracted by organic solvents, e.g. pulmonary surfactant proteins SP-B and SP-C (Curstedt et al. 1988; Johansson et al. 1988), most membrane protein purification protocols rely on solubilizing the cell membrane to obtain an aqueous detergent-solubilized protein state that subsequently may be reconstituted into model membranes.

13.2.1 Preparation of liposomes and proteoliposomes

Various techniques exist for preparing liposomes, and the method of choice may result in different types of liposomes. The types of liposomes may be classified on the basis of size and number of bilayers forming the vesicles (Szoka and Papahadjopoulos 1980; Deamer and Uster 1983). The classifications used for the different types of liposomes are often divided into:

1. *Multilamellar vesicles (MLV)*. This type of vesicles contains multiple lipid bilayer vesicles inside each other. They vary in size, internal volume (Singer et al. 1990) and osmotic activity (Yoshikawa et al. 1983). This can make liposome analysis and results interpretation difficult.
2. *Small unilamellar vesicles (SUV)*. SUVs consist of a single lipid bilayer and the vesicle sizes are between 4 –20 nm. These vesicles are very small, resembling the sizes of biological vesicles carrying neurotransmitters in the nerve synapses.
3. *Large unilamellar vesicles (LUV)*. These vesicles also consist of a single lipid bilayer and are defined by having sizes between 50 nm and up to 10 μm. These vesicles are often the preferred type for protein reconstitution.
4. *Giant Unilamellar vesicles (GUV)*. They are also known as cell-size unilamellar vesicles, because their size approximately mimics biological living cell sizes. GUVs are defined by having a size of ≥10 μm.

Vesicle size will not be the only parameter affected by the preparation method, the polydispersity, surface potential, degree of ionization, thermotropic phase behavior, permeability and physical stability will also be affected (Szoka and Papahadjopoulos 1980; Angelova et al. 1992; Joannic et al. 1997; Feitosa et al. 2000). Many applications of vesicles rely on a narrow size distribution and a concomitant high stability during a long time period (Fendler 1987). When natural or synthetic long–tailed phospholipids are dispersed in aqueous solution, they form large multilamellar structures (Gabriel and Roberts 1984).

There are several methods to form unilamellar vesicles from multilamellar. This is relevant for creating vesicles suitable for reliable and reproducible protein reconstitution and may also be of importance in many analytical techniques. A straightforward method to create unilamellar vesicles from multilamellar vesicles is sonication. However, it does not produce a uniform size distribution and moreover the method may potentially cause metal contamination, lipid degradation and generation of heat and aerosols (Maguire et al. 2003). Another method is mechanical extrusion of multilammelar vesicles through a filter membrane with a defined pore size, resulting in unilamellar vesicles with a narrow size distribution (often monodisperse). Vesicle extrusion may be carried out by small inexpensive handheld extruders or with nitrogen pressurized barrel extruders. The latter can range in capacities from 1 ml, 10 ml and up to industrial scale (many liters/h). Generally, we have good experience with both hand-held and pressurized barrel extruders. However, hand-held extruders tend to produce a slightly more polydisperse vesicle solution and vesicles produced in this manner also tend to be slightly more instable compared to the barrel extruded vesicles (higher tendency of vesicle-vesicle fusions).

An important consideration in protein reconstitution is which strategy to choose for delivering membrane proteins into model membranes. As mentioned the majority of membrane protein reconstitution procedures involve the use of a detergent. The detergent play a dual role for membrane proteins in solution: i) the solubilization of the native membrane to release the contained membrane spanning protein into solution and ii) maintain the protein folded and soluble in an aqueous state (le Maire et al. 2000). Moreover, the physio-chemical properties of the detergent may be important for the integrity and activity of the protein upon reconstitution into model membranes (Paternostre et al. 1988; Rigaud et al. 1988).

To produce protein reconstituted liposomes (proteoliposomes) removal of the detergent is necessary in order to transfer the proteins from an aqueous detergent solubilized state and into the model membrane lipid bilayer. Conventional techniques for removing the detergent include among others dialysis, gel exclusion chromatography and adsorption onto polymeric materials. A detailed description and comparison of the various techniques for detergent removal is reviewed in (Silvius 1992; Ollivon et al. 2000). Generally the choice of detergent removal

technique is often a choice between using dialysis or adsorption onto polymeric materials such as hydrophobic Bio–Beads or a combination of both these techniques. Both methods are straightforward and do not require costly technical equipment. The decision of which method to use for detergent removal is typically based on the nature of the detergent. Detergents with a high critical micelle concentration (cmc) and molecular weight micelles of <10,000 Da can be dialyzed away, whereas dialysis is not an appropriate technique for detergent removal if the opposite is the case (Table 1). Table 1 gives a brief overview of some of the more commonly used non-denaturing detergents for membrane protein reconstitution and also indicates whether the detergent is dialyzable.

Table 1. Non-denaturing detergents commonly used for membrane protein reconstitution.

Type	Detergent	Mw micelle (Da)	CMC (mM)	Dialyzable
Anionic	Sodium cholate	900-1,300	9-15	Yes
	Sodium deoxycholate	1,200-5,000	2-6	Yes
Cationic	CTAB	62,000	1	Yes
Zwitterionic	CHAPS	6,150	6-10	Yes
	CHAPSO	7,000	8	Yes
	LDAO	ND	1	Yes
Nonionic	OG	25,000	20-25	Yes
	OTG	ND	9	Yes
	Triton X-100	90,000	0.24	No
	C12E8	65,000	0.09	No
	DDM	50,000	0.15	No
	Digitonin	70,000	0.5	No
	MEGA-9	ND	6-7	Yes
	MEGA-10	ND	19-25	Yes

[1]Abbreviations: CTAB: Hexadecyltrimethylammonium bromide; LDAO: Lauryldimethylamine N-oxide; OG: Octyl-β-glycopyranoside; OTG: Octyl β-D-thioglucopyranoside; C12E8: Dodecyl octaethylene glycol ether; DDM: n-Dodecyl β-D-maltoside.
[2]ND indicates that the detergent molecular weight micelles have not or cannot be determined.
[3]CMC changes with temperature and salt concentration.

Another parameter to consider before carrying out the protein reconstitution process is the lipid-to-protein ratio (LPR). The LPR is the mol of lipids per mol protein to be reconstituted into the vesicles. There is an upper limit of how much protein that physically can be incorporated into a defined amount of lipid (or polymer). This limit depends on the surface area of the protein and the area of the lipid. The area per lipid of phosphatidylcholines has for example been characterized by NMR spectroscopy and may provide useful information in LPR calculations (Petrache et al. 2000). Since the lipid membrane exists as a bimolecular structure, lipid molecules are needed in both bilayers to cover a single transmembrane pro-

tein. Similarly the crystal structure has been determined for various membrane proteins from which the protein monomer surface has been published. The spinach aquaporin SoPIP2;1 is just one example (Tornroth-Horsefield et al. 2006). Alternatively the protein surface area may be determined from the crystal structure. Thus, based on the area values of the lipid and protein a minimum mol/mol ratio of lipid molecules to protein may be estimated. It is often necessary to test different LPRs (e.g. LPR 200, 100, 50, 25, etc) to find the optimal protein reconstitution conditions.

In our laboratory we work with aquaporins which are tetrameric α-helical water channel forming membrane proteins. We have good experience with octyl-β-glycopyranoside (OG) and generally use this detergent for protein solubilization and reconstitution. Since OG is dialyzable the preferred detergent removal technique is dialysis (Table 1). To ensure complete detergent removal a second (optional) Bio-Beads step may be included. Our scheme for protein reconstitution into liposomes to produce proteoliposomes is:

1. *Preparation of detergent containing MLVs.* The MLVs are prepared either by drying down the lipid from a chloroform phase or directly dissolving lyophilized lipids in resuspension buffer. The resuspension buffer is usually matched to that of the protein.
2. *Formation of detergent containing LUVs.* LUVs are generally prepared by extrusion using a pressurized barrel extruder with 100, 200 or 400 nm filters depending on the desired proteoliposomes size.
3. *Mixing of detergent LUVs with detergent solublized protein.* Detergent solubilized protein is mixed with the formed detergent containing LUVs to the desired LPR (e.g. 200, 100 or 50).
4. *Detergent removal.* To remove the detergent dialysis is applied. An efficient way is to use dynamic dialysis where a continuous flow of the detergent-free dialysate buffer passes the dialysis tubing containing the lipid-protein-detergent sample (with flow rates 2–10 ml dialysate/min).
5. *Optionally second detergent removal step.* To ensure that all detergent has been removed from the formed proteoliposomes absorption Bio-Beads may be added to the proteoliposomes sample. This may be relevant for carrying out stopped-flow permeability measurements of aquaporin function. Following the additional detergent removal step the supernatant is collected and used (the proteoliposomes).

Our simplified scheme represented above for reconstitution aquaporins into model membrane vesicles is in many aspects a general methodology and may be followed as a flow diagram for preparing proteoliposomes using a dialyzable detergent. Parameters such as the detergent, detergent concentration, dialysis times, the optimal LPR and buffer composition may vary from protein to protein. Various protein isoforms may often require different buffer conditions.

13.2.2 How lipid composition may affect protein folding

A stable integration of a protein into a lipid membrane will be affected among other factors by the hydrophobic interactions of the hydrophobic protein segment(s) with the acyl chains of the lipids. The difference between the hydrophobic length of an membrane integral protein and the hydrophobic thickness of the membrane is known as hydrophobic mismatch. In order to avoid unfavorable exposition of the protein to the hydrophilic environment the length of the hydrophobic thickness of the membrane and the hydrophobic segment of the protein are expected to be matched so they are approximately equal.

Elastic properties of the lipid bilayer are vital to the folding and function of membrane proteins (Booth 2005). Membrane proteins have a percentage of apolar residues that is much higher than for their water soluble counterparts (Samatey et al. 1995; Hong et al. 2009). However, membrane proteins cannot bury all the hydrophobic residues in a hydrophobic core. Therefore, the membrane proteins associate with lipid bilayers both *in vivo* (Van den Berg et al. 2004; Osborne et al. 2005) and *in vitro* (Seddon et al. 2004) and tend to aggregate in aqueous solutions in order to escape the hydrophilic environments. The bilayer thickness is determined by several factors, where some of them for example are the lipid chain length and the degree of saturation of the lipid acyl chains (Rawicz et al. 2000), cholesterol content (Mouritsen and Zuckermann 2004) and the membrane proteins themselves (Mitra et al. 2004). When the lipids forming the model membrane constitute a hydrophobic environment shorter than the hydrophobic protein segment the protein usually tend to aggregate or oligomerize to minimize the exposed hydrophobic areas. Alternatively they can change the conformation or induce a tilt of the protein in the membrane. In the opposite situation, where the protein chain length is longer than the hydrophobic protein segment the mismatch can result in protein aggregation.

Membrane proteins may also have specific requirements of phospholipids and sterols which may be essential for folding, oligomerization and/or activity. Moreover, the lipid composition of biological membranes varies, so it may be a good idea to consider what the origin of the protein in question is and in which host organism the protein have been expressed and purified from. A detailed review of specific lipid requirements of selected membrane proteins as well as the lipid composition of various biological membranes are given by Opekarová and Tanner (2003) (Opekarova and Tanner 2003). A good starting point, however, for membrane protein reconstitution is to use total lipid extracts such as soybean asolectin or *E. coli* total lipid extract. These lipid mixtures are total extracts and therefore contain all the natural components of a biological membrane. They also generally tend to result in good protein reconstitution yield.

13.3 Reconstitution in planar membranes

Planar biomimetic membranes constitute an important platform for studying membrane protein function and protein-lipid interactions. The planar membrane design creates a possibility to study the transport processes of a membrane protein across the lipid bilayer (Janshoff and Steinem 2006). Techniques available to study processes across planar artificially made membranes include among others eletrophysical measurements (Mueller and Rudin 1969; Montal and Mueller 1972) and optical techniques such a fluorescence microscopy or a combination (Hemmler et al. 2005; Wilburn et al. 2006; Hansen et al. 2009a). The structural and dynamic processes of proteins in the membrane may also be studied by surface sensitive techniques (Goennenwein et al. 2003; Buzhynskyy et al. 2007a; Buzhynskyy et al. 2007b).

The potential biotechnological applications of planar membrane designs are large and include both sensor and separation technologies. The creation of membrane protein microarrays for high-throughput screening of protein-drug interactions has attracted much attention (Fang et al. 2002; Majd and Mayer 2008). Designs that fit into modern plate readers are attractive in the development of high-throughput membrane protein assays for the pharmaceutical industry (Fang et al. 2006; Le Pioufle et al. 2008; Suzuki et al. 2009). Provided that the effective functional membrane area can be scaled up sufficiently, planar biomimetic membranes may also be suitable for novel separation technologies using membrane protein channels (Nielsen 2009).

Small fusiogenic pepsipeptides or peptides such as valinomycin, gramicidin or alamethicin, respectively, spontaneously self-insert into pre-established membranes (Zagnoni et al. 2007). These membrane spanning molecules are therefore well-characterized and due to the ease of reconstitution they are often applied to demonstrate the functionality of artificially made lipid membranes (Hansen, Perry et al. 2009a; Hansen et al. 2009b). In contrast, medium to large membrane proteins (35-500 kDa) do generally not reliable self-insert into pre-established membranes (Zagnoni, Sandison et al. 2007). An exception is the heptameric α-hemolysin channel pore from *S. aureus* (Suzuki et al. 2007). In addition, several *E. coli* outer membrane porins such as OmpA, OmpF and FomA may be reconstituted into planar membranes directly from a detergent solubilized state (Arora et al. 2000; Pocanschi et al. 2006; Schmitt et al. 2006). It should be noted, however, that although the detergent solubilized proteins can be added in a few microliter aliquots to the lipid bilayer chamber, the detergent present tends to make the established membrane(s) unstable.

In order to study most membrane proteins, reliable and controllable reconstitution methods are required for the delivery of functionally active membrane proteins into planar membranes.

13.3.1 Vesicle fusion with planar lipid bilayers

The conventional technique to deliver membrane proteins to pre-established planar lipid bilayers is by vesicle fusion. The methodology can be viewed as a biomimicry of the ubiquitous biological phenomena of exocytosis. In exocytosis intracellular vesicles fuse with the plasma membrane and subsequently release the extracellular content (Zimmerberg et al. 1980a). This is involved in important biological processes such as neurotransmitter release from nerve synapses and the release of hormones and messenger substances from endocrine and exocrine glands (Zimmerberg, Cohen et al. 1980a). Vesicles fusion with artificially made membranes is inspired by these elegant biological processes in nature, albeit *in vitro* model systems of vesicle fusion with model membranes are greatly simplified compared to the naturally occurring processes.

The approach of vesicle fusion with model membrane systems can be simplified to four discrete steps:

1. *Preparation of proteoliposomes.* Reconstitute the membrane protein of interest into vesicles, usually LUVs, resulting in formation of proteoliposomes (see section 13.2).
2. *Establishment of a planar model membrane.* Planar lipid bilayers are typically created across a Teflon aperture and commonly by using the Müller-Rudin (Mueller and Rudin 1969) or the Montal-Müller technique (Montal and Mueller 1972).
3. *Addition of the proteoliposomes to the planar model membrane.* Aliquots of the prepared proteoliposomes are added (usually) to the *cis* side of the chamber design, which per definition consist of a *cis* and a *trans* side separated by the established membrane.
4. *Induction of fusion of the proteoliposomes with the membrane.* There are various means to stimulate vesicles fusion with the established lipid bilayers. An efficient way to induce fusion events is by the creation of osmotic gradient across the membrane (described in details below).

The reality is often more nuanced than simplified schemes and vesicle fusion with planar membranes is no exception. The fusion efficiency is often influenced by several factors that may be difficult to pinpoint. These may both be related to the applied biomimetic membrane chamber design, the stability of the established

biomimetic membrane and the specific nature of the membrane protein in question.

In general, adding proteoliposomes to a pre-established lipid model membrane results in a low basal rate of fusion. Efficient reconstitution of membrane proteins into the planar membrane thus requires stimulation of the fusion rate. An efficient way to induce fusion events of vesicles to planar membranes is by creating an osmotic gradient across the membrane (Cohen et al. 1980). Creation of an osmotic gradient across the membrane may be established by addition of an osmolyte (i.e. salt or sugar) to the same side of the membrane as the vesicles (*cis* side). An effective way to do this is to add a 3 M KCl solution to the *cis* chamber side to a final concentration in the chamber of around 800-900 mM KCl (Woodbury 1999). The established osmotic gradient across the membrane is believed to result in osmotic swelling of the vesicles which eventually causes them to burst and subsequently fuse to the planar bilayer membrane (Zimmerberg et al. 1980b; Cohen et al. 1982).

In exocytosis calcium ions play a crucial role for biological membrane fusion (Furber et al. 2009). For *in vitro* vesicle fusion to planar membranes divalent cations (i.e. Ca^{2+}, Mg^{2+}, Ba^{2+}) in milli-molar concentrations have been described to enhance vesicle fusion to planar lipid bilayers in the presence of an osmotic gradient (Cohen, Zimmerberg et al. 1980). In contrast, with vesicles derived from brain synapses or proteoliposomes reconstituted with Ca^{2+} binding proteins, only Ca^{2+} specifically stimulates fusion events (not Mg^{2+} or Ba^{2+}) and it does so in micromolar concentrations (Zimmerberg, Cohen et al. 1980b). This indicates that the effect of calcium ions on vesicle fusion events arise from protein interactions rather than lipid interactions. This also fits well with the mechanism of biological exocytosis, where the soluble *N*-ethylmaleimide sensitive factor attachment receptor (SNARE) protein complexes dock the vesicles to the plasma membrane, and a subsequent influx of Ca^{2+} triggers vesicle fusion (Jeremic et al. 2004; Ungermann and Langosch 2005; Carr and Munson 2007). However, although Ca^{2+} has an important role in biological membrane fusion, it may not necessarily be beneficial to include Ca^{2+}, or other divalent cations, for that matter in model membrane systems. In this relation, Woodbury (1999) describes that the vesicles may clump or fuse together prior to reaching the planar membrane, leading to suboptimal fusion conditions (Woodbury 1999). Indeed, we also noticed in our laboratory that Ca^{2+} does not necessarily stimulate vesicle fusion to planar membranes. In support of Woodbury (1999) we also find that Ca^{2+} appears to result in vesicle-vesicle fusions and formation of vesicle aggregation before reaching the planar membrane. That this is the case may be evidenced by dynamic light scattering measurements (Table 2). It is likely that these larger fused vesicle or vesicle aggregates looses the ability to fuse with the established planar membrane. Therefore, it is recommended to carefully test and evaluate whether including Ca^{2+} in model membrane systems are beneficial for stimulating fusion events of the model membrane system in question.

Table 2. Dynamic light scattering measurements of initially 200 nm extruded lipid vesicles under various buffer conditions.

Solution outside vesicles	Vesicle size	PDI
Phosphate buffered saline (PBS)	137 ± 2	0.11
300 mM KCl, PBS	134 ± 0	0.09
10 mM CaCl$_2$, PBS	8253 ± 469	0.63
10 mM CaCl$_2$, 300 mM KCl, PBS	4952 ± 2097	1.00

Vesicles consisted of POPE:POPC:POPS:Ergosterol (2:1:1:1). Results are n = 3 measurements ± standard deviation. PDI is the polydispersity index, where in this case a value of 0 represents a monodisperse, while a value of 1 indicates a completely polydisperse solution. (Ibragimova and Rein unpublished results).

Magnetic stirring of the model membrane system may be important to keep a continuous motion of the vesicles in the chamber (Woodbury 1999). This may increase the likelihood that vesicles come so close to the planar membrane that they can interact and fuse with the planar membrane.

The buoyancy of vesicles may possess a problem for obtaining optimal fusion efficiency with the planar membrane. In biological exocytosis docking of the vesicles to the plasma membrane is a crucial step for fusion, which is mediated by SNARE proteins (Carr and Munson 2007). In model membrane systems, we usually do not have SNAREs, but what we can do is altering the vesicle density. The vesicle density may be increased to ensure that the vesicles sink down on to the planar membrane, thereby ensuring close proximity of the vesicles with the membrane. In principle this should be able to increase the likelihood for membrane fusion. In practice, increasing the density of vesicles may be created by encapsulating 200-300 mM of a sugar, preferably a membrane impermeant sugar such as sorbitol or mannitol, inside the vesicles. This may be done by i) creating the vesicles in a sugar containing buffer and ii) removing the sugar outside the vesicles. Removal of sugar outside the vesicles may essentially be done by the techniques briefly mentioned in section 13.2.1 for removal of detergent during protein reconstitution into vesicles.

A factor that may also be considered for optimizing the fusion efficiency of proteoliposomes with planar membranes is the LPR of the proteoliposomes. We have found that the LPR may affect the fusion efficiency of *F. nucleatum* outer membrane porin A (FomA) with planar membranes in a LPR dependent manner. Our results demonstrate that fusion events with planar membranes are significantly increased with decreasing LPR (200 to 50) with maximal fusion efficiency at LPR 50 (Fig. 1). The theoretical proteoliposome coverage with FomA porins increases from 22 to 89% when LPR value decreases from 200 to 50. However, with LPR 25 the fusion events ceases to a level near that of LPR 200, indicating that at LPR 25 the protein content in the vesicles is too high (Fig. 2). It is simply

not possible to accommodate all protein in proteoliposomes prepared with LPR 25, since the area of the total amount of protein is higher than that of the proteoliposomes themselves. Thus, the maximal fusion capacity that can be achieved for a specific protein varies with the specific molecular size of the protein in question.

In general, it is always advisable to do a theoretical calculation of the protein coverage in vesicles with a chosen LPR (i.e. LPR 50, 100 or 200, etc) prior to protein reconstitution (i.e. incorporation into vesicles or fusion experiments).
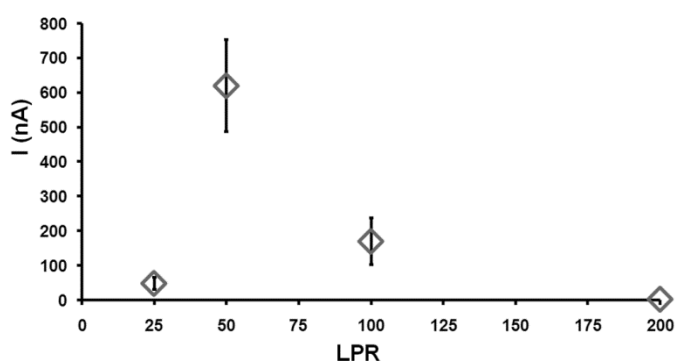

Fig. 1. Dependence of LPR on FomA proteoliposomes fusion with planar lipid membrane arryas. Planar lipid bilayers arrays were established as described by (Hansen, Perry et al. 2009a).

The fusion efficiency of vesicles with planar membranes is influenced by numerous factors as discussed in this section. Clearly creating an osmotic gradient across the established lipid bilayers and having magnetic stirring in the model membrane chamber design are likely the most important parameters for getting started with model membrane vesicle fusion experiments. Subsequently, factors such as including divalent cations in the model membrane buffers, increase vesicle density or adjusting the LPR may be considered to achieve optimal vesicle fusion efficiency.

13.3.2 Addressing vesicle fusion events with planar membranes

How do we address the vesicle fusion efficiency is in our model membrane system? Vesicle fusion with planar membranes is characterized by i) the transfer of vesicular contents across the planar membrane to the *trans* chamber side and ii) the incorporation of vesicular membrane with the planar membrane (Zimmerberg, Cohen et al. 1980b). These two criteria may be utilized to create sensor systems for assessing the degree of vesicle fusion events with planar membranes.

To utilize i) vesicles may be loaded with a fluorescent dye, which upon fusion with the planar membrane is released to the *trans* chamber and following may be quantified (e.g. by fluorescence spectroscopy or microscopy). The water soluble impermeant dye calcein is often used for these purposes. A good feature of calcein is that its fluorescence emission can be quenched, either by self-quenching at high concentrations (≥ 6 mM) or by cobalt ions. Self-quenching may be utilized by encapsulating millimolar calcein concentrations in vesicles, resulting in a low fluorescence emission yield. Upon fusion with the planar membrane calcein is released and diluted, resulting in a high fluorescence emission yield (Perin and MacDonald 1989). To utilize calcein quenching by cobalt ions, the vesicles may be encapsulated with a micromolar calcein concentration, while having cobalt ions in the *trans* chamber buffer. Upon fusion of the calcein-cobalt loaded vesicles the vesicular content is released. This time the cobalt effectively chelates the released calcein and quenches the fluorescence signal (Niles and Cohen 1987; Woodbury and Hall 1988a; Woodbury and Hall 1988b). Alternatively, ethylenediaminetetraacetic acid (EDTA) which is a divalent cation chelating agent may be applied to chelate cobalt. The assay could then be designed encapsulate saturating amounts of cobalt with calcein to create fluorescently quenched calcein-cobalt complexes in vesicles (Kendall and MacDonald 1982). Having included EDTA in the *trans* chamber buffer, results in chelation of cobalt upon release of the calcein-cobalt complexes by vesicle fusion, yielding fluorescent calcein (Kendall and MacDonald 1982).

There are several ways to utilize ii) the incorporation of vesicular membrane with the planar membrane upon membrane fusion:

- *Fluorescent tracer fusion assay*. Fluorescence may be used to label the receiving planar lipid membrane, say green fluorescence, while having a different fluorescence label, say red fluorescence, of the lipid vesicles or a labeled protein reconstituted into the fusiogenic vesicles. In this case vesicle fusion will result in incorporation of the red fluorescent dye of the vesicles or of the labeled proteins reconstituted in the vesicles, respectively, into the planar fluorescently green membrane (Ganesan and Boxer 2009).

- *Nystatin/ergosterol fusion activity assay.* The Nystatin/ergosterol (N/E) fusion activity assay is a very neat way to assess vesicle fusion activity (Woodbury and Miller 1990). Nystatin is a pore-forming antibiotic, which binds to ergosterol and when the ergosterol concentration is high enough, 10 nystatin monomers associate to form a membrane pore (Woodbury 1999). If vesicles are prepared to include both nystatin and ergosterol, the nystatin molecules form functional pores in the lipid vesicles. When the N/E vesicles fuse with the planar membrane functional nystatin pores is being transferred to the planar membrane. The nystatin pore conductance can be measured shortly, because the ergosterol will diffuse into the planar membrane, which in turn causes the nystatin to dissociate into monomers and

the nystatin becomes nonfunctional (Woodbury and Miller 1990). In conductance measurements the fusion event of N/E vesicles will be seen as a "current spike" in voltage clamp measurements (Fig 2A). The number of "spikes" per time can be seen a measure of fusion efficiency. The advantage of this assay is that it can co-include a membrane protein of interest (Woodbury 1999; Zagnoni, Sandison et al. 2007). Since the nystatin becomes nonfunctional upon fusion to the planar membrane most measurements of reconstituted membrane protein using N/E vesicles will not be affected by the presence of nystatin. A disadvantage may be that care has to be taken for interpretation of the N/E fusion events, since it can be hampered by air bubbles that may arise during formation of the planar membrane. If an entrapped air bubble burst in the membrane this may be misinterpreted as a fusion event (our unpublished data). Another disadvantage may also be that the amount of molecules loaded into the planar membrane cannot be directly determined – it only shows if fusion has taken place. To get started with the vesicle N/E fusion activity assay we recommend reading the review by Dixon J. Woodbury (1999) on this topic (Woodbury 1999)

- *Outer membrane porin fusion efficiency assay.* A reporter membrane protein may be used to address the amount of protein that can be reconstituted into a model membrane system with vesicle fusion. As stated in the beginning several *E. coli* outer membrane porins may be reconstituted into planar membranes directly from a detergent solubilized state. However, they may also be reconstituted into vesicles. Many of these β-barrel proteins have a specific conductance that has been well-characterized. Thus, outer membrane porin proteoliposomes may conveniently be used to address fusion efficiency with a model membrane system. The voltage dependent anion channel (VDAC) has in the literature been used as a reporter for vesicle fusion activity with planar membranes (Cohen, Zimmerberg et al. 1980). In our laboratory we use the trimeric *Fusobacterium nucleatum* outer membrane protein A (FomA) as reporter for vesicle fusion efficiency with planar membranes (Fig 2B). In the following we use FomA as example. In voltage clamp measurements FomA porin has a single channel current value of approximately 15 pA in 1.0 M KCl saline solution with an applied potential of ±60 mV (Kleivdal et al. 1995; Pocanschi, Apell et al. 2006). Thus, reconstitution of a single functional FomA porin gives rise to a current increase of approximately 15 pA (Fig 3B). Incorporation of multiple FomA porins is seen as a "ladder-like" increase in the current trace (Fig 2B). Since the current value for a single functional FomA porin is known (15 pA) we can calculate how many porins that did reconstitute with the planar model membrane during vesicle fusion. For further details about voltage clamp measurements we refer to Perry *et al.* 2009 (Perry et al. 2009).
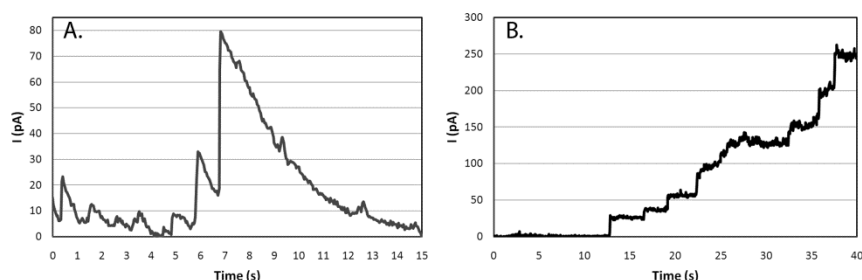
Fig. 2. Vesicle fusion with N/E vesicles and FomA proteoliposomes. A) Current trace of N/E vesicle fusion activity. B) Current trace of FomA proteoliposomes vesicle fusion. Measurements were carried out using voltage clamp technique.

In summary, transfer of vesicular content following vesicle fusion may be used a measure of whether vesicle fusion takes place. The fluorescence calcein assay is an example of a way to address vesicle fusion, by measuring the amount of fluorescent molecules released to the *trans* chamber side. Fluorescence may also be utilized to address transfer of vesicular membrane to the planar membrane, which occurs during membrane fusion. Fluorescent labels may be positioned in the membranes and/or on the membrane protein of interest. Voltage clamp measurements of fusion of N/E vesicles with planar membranes may be utilized to address vesicle fusion activity, whereas reconstitution of outer membrane porin may be used to address vesicle fusion efficiency.

13.3.3 Direct incorporation into planar membranes

A novel strategy for reconstituting membrane proteins into planar membranes is by direct incorporation, which refers to reconstitution of membrane proteins simultaneously with establishing the planar model membrane. Although, a general methodology for direct reconstitution would potentially revolutionize the field of biomimetic membrane research, only a few reports have dealt with the topic of direct reconstitution. Here we will describe the practical approach of direct incorporation described for bR and the nicotinic acetylcholine receptor, respectively, and use these examples to discuss some of the considerations and concerns of this strategy of reconstituting membrane proteins.

A clear advantage of the direct incorporation approach is that the LPR, and thereby also the amount of the protein reconstituted into the model membrane, may be precisely controlled. The ability to incorporate large quantities of protein into model membranes may especially be important for using planar protein-based biomimetic membranes for separation techniques, such as water purification through aquaporin water channel-based biomimetic membranes (Nielsen 2009).

Bamberg *et al.* (1981) reported successful direct reconstitution of the proton-pump bacteriorhodopsin from a proteo-lipid solvent-containing solution (Bamberg et al. 1981). The approach was to solubilize bacteriorhodopsin purple membranes in an aqueous solution and then transfer the protein into an asolectin/*n*-alkane (e.g. *n*-decane) lipid bilayer forming solution. The methodology was to add 100 μL of the bacteriorhodopsin solution (10 mg/ml) to a 1 mL asolectin/n-decane solution (50 mg/mL). The sample was then sonicated and the suspension was subsequently added successive aliquots of CaCl$_2$ (100 μL, 0.1 M) until a clear purple bacteriorhodopsin apolar phase developed. The clear purple apolar phase was then used to successfully create a bacteriorhodopsin-based lipid bilayer membrane while maintaining the functionality of the protein (Bamberg, Dencher et al. 1981). It should be noted however, that bacteriorhodopsin as lyophilized purple membranes can be solubilized in aqueous solutions without the use of detergent. This makes bacteriorhodopsin a somewhat special case that is not general for most other membrane proteins. Beddow *et al.* (2004) reported a similar approach to functionally reconstitute nicotinic acetylcholine receptors into lipid bilayer model membranes (Beddow et al. 2004). The main differences were that the bilayer forming solution consisted of glycerol monooleate and *n*-hexane, the receptor extracts were prepared as vesicles and the bilayer forming solution was emulsified with receptor extract without using CaCl$_2$ (Beddow, Peterson et al. 2004).

Membrane proteins are generally delicate structure especially α-helical proteins whereas β-barrel proteins often are somewhat more stable (Bowie 2001). A concern for the transfer of membrane protein to a solvent containing lipid phase is that the protein structure and function will be affected by the solvent. Several reports have described that membrane proteins can be extracted in a functional state by harsh solvents such as diethyl ether, toluene or chloroform/methanol/water mixtures (Ayala et al. 1985; Ayala et al. 1986; Reiken et al. 1996; Dmitriev et al. 2004). However, it is difficult to predict the long term effects of solvent exposure on protein structure and function. In this context protein functionality has been shown to be affected considerably by solvent exposure and to decrease in a time-dependent manner (Ayala, Nascimento et al. 1985; Beddow, Peterson et al. 2004).

To circumvent the potential deleterious effects of solvent on membrane protein structure and function it may be considered to use a less harmful solvent in the bilayer forming solution. Solventless bilayer forming solutions using squalene, a naturally derived oil, as substitute for *n*-alkanes have been described for formation of planar lipid bilayers (White 1978).

A major issue to be solved for creating a successful general formulation for direct protein incorporation is to make an amphiphilic bilayer forming solution that is sufficiently polar to shield and protect the hydrophilic residues of membrane proteins, while at the same time being hydrophobic enough to make a homogeneous solution that can shield the hydrophobic membrane protein regions and that

can support lipid bilayer formation (Fig. 3). In section 13.2.2 we discussed considerations of hydrophobic matching lipid species to the protein hydrophobic regions for protein reconstitution in vesicles. The same considerations also apply for matching the hydrophobic regions of the protein in a direct protein incorporation formulation.

A likely more demanding challenge is to create an amphiphilic bilayer forming solution that sufficient shield the hydrophilic protein regions, since the extent of the hydrophilic regions varies considerably among membrane proteins (Fig. 3).
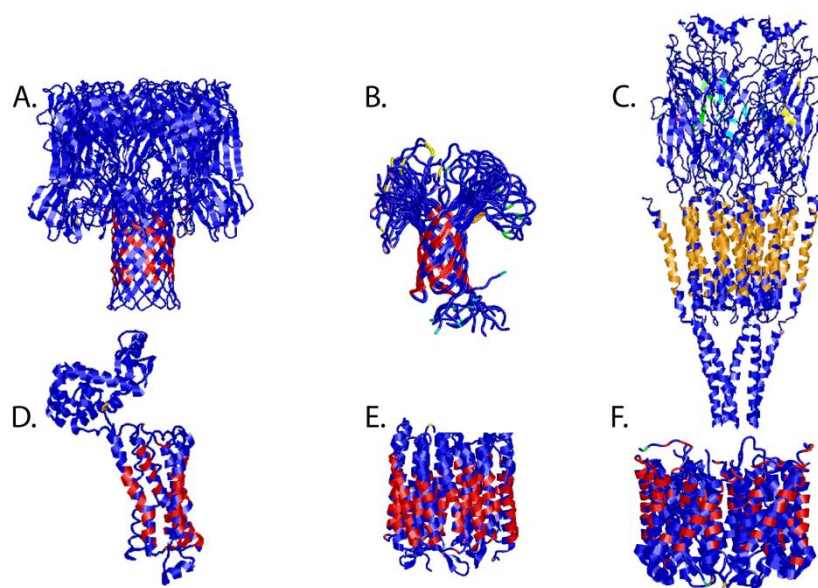

Fig. 3. Hydrophobic and hydrophilic regions of membrane protein surfaces. The extracellular domains of membrane proteins vary. Examples shown are A. α-hemolysin, B. outer membrane porin A (OmpA), C. Nicotinic acetylcholine receptor, D. human B$_2$-adrenergic G protein-coupled receptor, E. Bacteriorhodopsin and F. Spinach aquaporin SoPIP2;1. Analysis of lipid interaction patches (hydrophobicity) was carried out using HotPatch statistical analysis. It is an algorithm-based program for the analysis of protein surface patches (Pettit et al. 2007). Identified (individual) hydrophobic protein surface patches are shown as red, orange, yellow and green, respectively, while blue correspond to hydrophilic surface regions.

For direct protein incorporation it would be advantageous to be able to transfer the protein directly from a detergent-solublized state to the bilayer forming solution. This may be carried out by the use of hydrophobic absorption polymer beads (such as Bio-Beads SM absorbents or similar). In this approach an appropriate amount of the absorption beads (e.g. matching the amount of detergent to be removed) is included to the protein/lipid/solvent dispersion. By placing the protein-

lipid dispersion with bio-beads end-over-end rotation at 4°C over night the protein is transferred to the apolar phase while removing the detergent. Using this approach we have been able to create lipid bilayers reconstituted with spinach aquaporin SoPIP2;1 (our unpublished results). If the detergent was not sufficiently removed during the described procedure it would not be possible to create sealed lipid bilayers.

Direct protein incorporation would be a powerful tool to reconstitute large quantities of membrane protein into model membranes. In this light it is surprising that there are still very limited reports on this subject. Major contributions to biomimetic membrane research may be envisaged provided that attention is directed towards the topic of direct protein incorporation.

13.4 Requirements for protein reconstitution yield

The planar membrane design for protein reconstitution may be suitable for sensor and separation technologies. The protein reconstitution yield into model membrane is almost never addressed, but it makes good sense to include protein reconstitution yield as a biomimetic membrane design criteria. The requirements of the amount of protein to be reconstituted for the different applications may not be the same. Considerations of the protein reconstitution methodology to apply may therefore be of importance in the design criteria for the biomimetic membrane application in question. For sensor applications the reconstitution yield may not be that important per se, instead it may be more important to have an optimized reliable and reproducible protein reconstitution protocol. Sensitive sensor designs may be created with a reasonable low amount of functionally reconstituted protein. Here vesicle fusion with planar membranes may be considered as a first choice reconstitution method.

The maximum protein reconstitution yield that can be reached with vesicle fusion is rather low. Using the outer membrane porin fusion efficiency assay, Cohen *et al*. (1980) showed that the fusion efficiency that could be reached was approximately 513 porin insertions in 10 min into a single bilayer suspended across a 1-mm^2 aperture (Cohen, Zimmerberg et al. 1980). We have addressed the maximum vesicle fusion efficiency of a membrane array consisting of 8×8 apertures with an average aperture diameter of 300 μm. Here the maximal fusion efficiency was approx. 103,333 porin insertions during the vesicle fusion experiment. Although this sounds as a high number of protein insertions it is still only corresponds to around 0.003 ‰ of the total effective membrane area. Therefore it does not make sense to talk in terms of LPR for protein reconstitution using the vesicle fusion strategy. The above mentioned protein reconstitution yields may be sufficient for designing sensor based assays, but clearly the yield is insufficient to create novel separation technologies based on membrane proteins.

Alternative methods for reconstitution membrane proteins in high yield need to be sought.

Direct protein reconstitution may be the novel strategy to consider for obtaining a high protein reconstitution yield into biomimetic membranes. Since the protein and lipid are simultaneously included in a combined bilayer forming solution prior to establishing the biomimetic membranes it may be possible to control the LPR. Thereby it should also be possible to control the amount of protein reconstituted into biomimetic membranes per se.

13.5 Perspectives

To summarize, the following key elements in protein reconstitution should be considered to create novel sensor and separation technologies based on membrane proteins:

- Protein reconstitution into vesicles is the conventional strategy in membrane protein biomimetic designs.
- Proteoliposomes may be applied directly in protein analytical methods or may be further used to reconstitute membrane proteins into planar membrane designs.
- Fluorescence assays, N/E vesicle fusion activity assay or outer membrane porin fusion efficiency assay may be applied to evaluate and optimize protein reconstitution into planar model membranes.
- Direct membrane protein reconstitution may represent a novel strategy to reconstitute large amounts of protein into planar model membranes.
- In both conventional and novel protein reconstitution strategies the LPR and hydrophobic matching of the protein hydrohopbic regions to the model membrane hydrophobic regions are crucial considerations for optimal and functional protein reconstitution.
- Reconstitution yield should be included as a biomimetic membrane design criteria.
- Proteoliposomes fusion with planar membrane may be applied for the creation of novel protein biosensor and drug–screening applications.
- Proteoliposomes fusion efficiency is likely too low to support fabrication of large scale separation technologies based on membrane protein function. Here alternative protein reconstitution strategies need to be explored. Direct protein reconstitution may be a promising approach; albeit technical advances in this protein reconstitution strategy is required.

References

Angelova, M. I., et al. (1992). "Preparation of giant vesicles by external AC electric fields. Kinetics and applications." Prog. Colloid. Polym. Sci. **89**: 127-131.

Arora, A., et al. (2000). "Refolded outer membrane protein A of Escherichia coli forms ion channels with two conductance states in planar lipid bilayers." J Biol Chem **275**(3): 1594-600.

Ayala, G., et al. (1986). "Thermostability of membrane systems in organic solvents." FEBS Lett **203**(1): 41-3.

Ayala, G., et al. (1985). "Extraction of mitochondrial membrane proteins into organic solvents in a functional state." Biochim Biophys Acta **810**(2): 115-22.

Bamberg, E., et al. (1981). "Transmembranous incorporation of photoelectrically active bacteriorhodopsin in planar lipid bilayers." Proc Natl Acad Sci U S A **78**(12): 7502-6.

Beddow, J. A., et al. (2004). "Reconstitution of nicotinic acetylcholine receptors into gel-protected lipid membranes." Anal Chem **76**(8): 2261-5.

Booth, P. J. (2005). "Sane in the membrane: designing systems to modulate membrane proteins." Curr Opin Struct Biol **15**(4): 435-40.

Buzhynskyy, N., et al. (2007a). "Human cataract lens membrane at subnanometer resolution." J Mol Biol **374**(1): 162-9.

Buzhynskyy, N., et al. (2007b). "The supramolecular architecture of junctional microdomains in native lens membranes." EMBO Rep **8**(1): 51-5.

Carr, C. M. and M. Munson (2007). "Tag team action at the synapse." EMBO Rep **8**(9): 834-8.

Castellana, E. T. and P. S. Cremer (2006). "Solid supported lipid bilayers: From biophysical studies to sensor design." Surface Science Reports **61**(10): 429-444.

Cohen, F. S., et al. (1982). "Osmotic swelling of phospholipid vesicles causes them to fuse with a planar phospholipid bilayer membrane." Science **217**(4558): 458-60.

Cohen, F. S., et al. (1980). "Fusion of phospholipid vesicles with planar phospholipid bilayer membranes. II. Incorporation of a vesicular membrane marker into the planar membrane." J Gen Physiol **75**(3): 251-70.

Curstedt, T., et al. (1988). "Low-molecular-mass surfactant protein type 1. The primary structure of a hydrophobic 8-kDa polypeptide with eight half-cystine residues." Eur J Biochem **172**(3): 521-5.

Deamer, D. W. and P. S. Uster (1983). Liposome Preparation: Methods and Mechanism. . Liposomes. E. M.J. Ostro. New York, Marcel Dekker**:** 27-51.

Dmitriev, O. Y., et al. (2004). "Subunit A of the E. coli ATP synthase: reconstitution and high resolution NMR with protein purified in a mixed polarity solvent." FEBS Lett **556**(1-3): 35-8.

Fang, Y., et al. (2002). "Membrane protein microarrays." J Am Chem Soc **124**(11): 2394-5.

Fang, Y., et al. (2006). "Applications of biomembranes in drug discovery." MRS bulletin **31**(7): 5.

Fang, Y., et al. (2003). "G protein-coupled receptor microarrays for drug discovery." Drug Discov Today **8**(16): 755-61.

Feitosa, E., et al. (2000). "Phase transition in dioctadecyldimethylammonium bromide and chloride vesicles prepared by different methods." Chem Phys Lipids **105**(2): 201-13.

Fendler, H. (1987). "Atomic and molecular clusters in membrane mimetic chemistry." Chem. Rev. **87**: 877-899.

Furber, K. L., et al. (2009). "Identifying critical components of native Ca2+-triggered membrane fusion. Integrating studies of proteins and lipids." Ann N Y Acad Sci **1152**: 121-34.

Gabriel, N. E. and M. F. Roberts (1984). "Spontaneous formation of stable unilamellar vesicles." Biochemistry **23**(18): 4011-5.

Ganesan, P. V. and S. G. Boxer (2009). "A membrane interferometer." Proc Natl Acad Sci U S A **106**(14): 5627-32.

Goennenwein, S., et al. (2003). "Functional incorporation of integrins into solid supported membranes on ultrathin films of cellulose: impact on adhesion." Biophys J 85(1): 646-55.

Hansen, J. S., et al. (2009a). "Large scale biomimetic membrane arrays." Anal Bioanal Chem 395(3): 719-27.

Hansen, J. S., et al. (2009b). "Development of an automation technique for the establishment of functional lipid bilayer arrays." Journal of Micromechanics and Microengineering 19(2): 025014.

Hemmler, R., et al. (2005). "Nanopore unitary permeability measured by electrochemical and optical single transporter recording." Biophys J 88(6): 4000-7.

Hong, H., et al. (2009). "Methods for measuring the thermodynamic stability of membrane proteins." Methods Enzymol 455: 213-36.

Janshoff, A. and C. Steinem (2006). "Transport across artificial membranes-an analytical perspective." Anal Bioanal Chem 385(3): 433-51.

Jeremic, A., et al. (2004). "Calcium drives fusion of SNARE-apposed bilayers." Cell Biol Int 28(1): 19-31.

Joannic, R., et al. (1997). "Monodisperse Vesicles Stabilized by Grafted Polymers." Phys. Rev. Lett. 78: 3402-3405.

Johansson, J., et al. (1988). "Size and structure of the hydrophobic low molecular weight surfactant-associated polypeptide." Biochemistry 27(10): 3544-7.

Kendall, D. A. and R. C. MacDonald (1982). "A fluorescence assay to monitor vesicle fusion and lysis." J Biol Chem 257(23): 13892-5.

Kleivdal, H., et al. (1995). "The Fusobacterium nucleatum major outer-membrane protein (FomA) forms trimeric, water-filled channels in lipid bilayer membranes." Eur J Biochem 233(1): 310-6.

le Maire, M., et al. (2000). "Interaction of membrane proteins and lipids with solubilizing detergents. ." Biochim. Biophys. Acta Reviews on Biomembranes 1508: 86-111.

22

Le Pioufle, B., et al. (2008). "Lipid bilayer microarray for parallel recording of transmembrane ion currents." Anal Chem **80**(1): 328-32.

Lorenceau, E., et al. (2005). "Generation of polymerosomes from double-emulsions." Langmuir **21**(20): 9183-6.

Maguire, L. A., et al. (2003). "Preparation of small unilamellar vesicles (SUV) and biophysical characterization of their complexes with poly-l-lysine-condensed plasmid DNA." Biotechnol Appl Biochem **37**(Pt 1): 73-81.

Majd, S. and M. Mayer (2008). "Generating arrays with high content and minimal consumption of functional membrane proteins." J Am Chem Soc **130**(47): 16060-4.

Mitra, K., et al. (2004). "Modulation of the bilayer thickness of exocytic pathway membranes by membrane proteins rather than cholesterol." Proc Natl Acad Sci U S A **101**(12): 4083-8.

Montal, M. and P. Mueller (1972). "Formation of bimolecular membranes from lipid monolayers and a study of their electrical properties." Proc Natl Acad Sci U S A **69**(12): 3561-6.

Mouritsen, O. G. and M. J. Zuckermann (2004). "What's so special about cholesterol?" Lipids **39**(11): 1101-13.

Mueller, P. and D. O. Rudin (1969). "Translocators in bimolecular lipid membranes: their role in dissipative and conservative bioenergetic transduction." Curr Topics Bioenergetics **3**: 157–249.

Nielsen, C. H. (2009). "Biomimetic membranes for sensor and separation applications." Anal Bioanal Chem **395**(3): 697-718.

Niles, W. D. and F. S. Cohen (1987). "Video fluorescence microscopy studies of phospholipid vesicle fusion with a planar phospholipid membrane. Nature of membrane-membrane interactions and detection of release of contents." J Gen Physiol **90**(5): 703-35.

Ollivon, M., et al. (2000). "Vesicle reconstitution from lipid-detergent mixed micelles." Biochim Biophys Acta **1508**(1-2): 34-50.

Opekarova, M. and W. Tanner (2003). "Specific lipid requirements of membrane proteins--a putative bottleneck in heterologous expression." Biochim Biophys Acta **1610**(1): 11-22.

Osborne, A. R., et al. (2005). "Protein translocation by the Sec61/SecY channel." Annu Rev Cell Dev Biol **21**: 529-50.

Paternostre, M. T., et al. (1988). "Mechanisms of membrane protein insertion into liposomes during reconstitution procedures involving the use of detergents. 1. Solubilization of large unilamellar liposomes (prepared by reverse-phase evaporation) by triton X-100, octyl glucoside, and sodium cholate." Biochemistry **27**(8): 2668-77.

Perin, M. S. and R. C. MacDonald (1989). "Fusion of synaptic vesicle membranes with planar bilayer membranes." Biophys J **55**(5): 973-86.

Perry, M., et al. (2009). "Automated sampling and data processing derived from biomimetic membranes." Bioinspir Biomim **4**(4): 044001.

Petrache, H. I., et al. (2000). "Area per lipid and acyl length distributions in fluid phosphatidylcholines determined by (2)H NMR spectroscopy." Biophys J **79**(6): 3172-92.

Pettit, F. K., et al. (2007). "HotPatch: a statistical approach to finding biologically relevant features on protein surfaces." J Mol Biol **369**(3): 863-79.

Pocanschi, C. L., et al. (2006). "The major outer membrane protein of Fusobacterium nucleatum (FomA) folds and inserts into lipid bilayers via parallel folding pathways." J Mol Biol **355**(3): 548-61.

Rastogi, R., et al. (2009). "Flexible polymerosomes--an alternative vehicle for topical delivery." Colloids Surf B Biointerfaces **72**(1): 161-6.

Rawicz, W., et al. (2000). "Effect of chain length and unsaturation on elasticity of lipid bilayers." Biophys J **79**(1): 328-39.

Reiken, S. R., et al. (1996). "Bispecific antibody modification of nicotinic acetylcholine receptors for biosensing." Biosens Bioelectron **11**(1-2): 91-102.

24

Rigaud, J. L., et al. (1988). "Mechanisms of membrane protein insertion into liposomes during reconstitution procedures involving the use of detergents. 2. Incorporation of the light-driven proton pump bacteriorhodopsin." Biochemistry **27**: 2677-2688.

Rosenkranz, T., et al. (2009). "Observing proteins as single molecules encapsulated in surface-tethered polymeric nanocontainers." Chembiochem **10**(4): 702-9.

Samatey, F. A., et al. (1995). "On the distribution of amino acid residues in transmembrane alpha-helix bundles." Proc Natl Acad Sci U S A **92**(10): 4577-81.

Schmitt, E. K., et al. (2006). "Channel activity of OmpF monitored in nano-BLMs." Biophys J **91**(6): 2163-71.

Seddon, A. M., et al. (2004). "Membrane proteins, lipids and detergents: not just a soap opera." Biochim Biophys Acta **1666**(1-2): 105-17.

Silvius, J. R. (1992). "Solubilization and functional reconstitution of biomembrane components." Annu Rev Biophys Biomol Struct **21**: 323-48.

Singer, M. A., et al. (1990). "The formation of multilamellar vesicles from saturated phosphatidylcholines and phosphatidylethanolamines: morphology and quasi-elastic light scattering measurements." Chem Phys Lipids **54**(2): 131-46.

Suzuki, H., et al. (2009). "Ninety-six-well planar lipid bilayer chip for ion channel recording fabricated by hybrid stereolithography." Biomed Microdevices **11**(1): 17-22.

Suzuki, H., et al. (2007). "Electrophysiological recordings of single ion channels in planar lipid bilayers using a polymethyl methacrylate microfluidic chip." Biosens Bioelectron **22**(6): 1111-5.

Szoka, F., Jr. and D. Papahadjopoulos (1980). "Comparative properties and methods of preparation of lipid vesicles (liposomes)." Annu Rev Biophys Bioeng **9**: 467-508.

Tornroth-Horsefield, S., et al. (2006). "Structural mechanism of plant aquaporin gating." Nature **439**(7077): 688-94.

Ungermann, C. and D. Langosch (2005). "Functions of SNAREs in intracellular membrane fusion and lipid bilayer mixing." J Cell Sci **118**(Pt 17): 3819-28.

Van den Berg, B., et al. (2004). "X-ray structure of a protein-conducting channel." Nature **427**(6969): 36-44.

White, S. H. (1978). "Formation of "solvent-free" black lipid bilayer membranes from glyceryl monooleate dispersed in squalene." Biophys J **23**(3): 337-47.

Wilburn, J. P., et al. (2006). "Imaging of voltage-gated alamethicin pores in a reconstituted bilayer lipid membrane via scanning electrochemical microscopy." Analyst **131**(2): 311-6.

Woodbury, D. J. (1999). "Nystatin/ergosterol method for reconstituting ion channels into planar lipid bilayers." Methods Enzymol **294**: 319-39.

Woodbury, D. J. and J. E. Hall (1988a). "Role of channels in the fusion of vesicles with a planar bilayer." Biophys J **54**(6): 1053-63.

Woodbury, D. J. and J. E. Hall (1988b). "Vesicle-membrane fusion. Observation of simultaneous membrane incorporation and content release." Biophys J **54**(2): 345-9.

Woodbury, D. J. and C. Miller (1990). "Nystatin-induced liposome fusion. A versatile approach to ion channel reconstitution into planar bilayers." Biophys J **58**(4): 833-9.

Yoshikawa, W., et al. (1983). "Light-scaterring properties of osmotically active liposomes." Biochim. Biophys. Acta **735**: 397-406.

Zagnoni, M., et al. (2007). "Controlled delivery of proteins into bilayer lipid membranes on chip." Lab Chip **7**(9): 1176-83.

Zimmerberg, J., et al. (1980a). "Fusion of phospholipid vesicles with planar phospholipid bilayer membranes. I. Discharge of vesicular contents across the planar membrane." J Gen Physiol **75**(3): 241-50.

Zimmerberg, J., et al. (1980b). "Micromolar Ca^{2+} Stimulates Fusion of Lipid Vesicles with Planar Bilayers Containing a Calcium-Binding Protein." Science **210**(4472): 906-908.